UNIVERSITÀ DEGLI STUDI DI MILANO

PhD Course in Molecular and Cellular Biology

XXXII Cycle

Design of chimeric ion channels to monitor cAMP-induced conformational changes and dynamics

Bianca Introini

PhD Thesis

Scientific tutor: Prof. Anna Moroni

Academic year: 2018/2019

SSD:BIO/11, BIO/18, BIO/19

Thesis performed at the Dipartimento di Bioscienze, Università degli Studi di Milano.

Table of contents

Summary

Hyperpolarization-activated cyclic nucleotide-gated (HCN1-4) channels are the molecular correlate of I_h (or I_f) current, which plays a key role in the control of neuronal and cardiac rhythmicity. HCNs are activated by the hyperpolarization of the membrane potential and further regulated by the direct binding of cyclic AMP (cAMP) to the cytoplasmic Cyclic Nucleotide Binding Domain (CNBD). cAMP binding determines the removal of the autoinhibitory action exerted by the CNBD on the pore opening and causes conformational changes that propagate from the CNBD to the pore through the C-linker, increasing channel open probability and speeding activation kinetics.

cAMP modulation of HCN controls rhythmicity and excitability at cardiac and neuronal level and pain perception. Thus, in order to understand several physiological functions, as well as diseases affecting both the cardiac and neuronal system, a detailed description of the cAMP-induced conformational changes is required. Moreover, functional studies indicate that cAMP binding to the CNBD induces the transition of the C-terminal domains, from dimer of dimer to tetramer and that this transition is driven by the movements of the C-linker.

The goal of this work is to describe the propagation of the movements through the C-linker to the pore. To this end, I have applied spectroscopic techniques, such as Electron Paramagnetic Resonance (EPR) and Double Electron-Electron Resonance (DEER) to study dynamic changes in the structure of the purified and labelled protein. First, I constructed a chimeric channel by fusing the C-linker/CNBD of human HCN4 to the prokaryotic pore domain of KcsA. This protein has the advantage that can be produced and easily purified in *E. coli*. Isothermal Titration Calorimetry (ITC) and Differential Scanning Calorimetry (DSC) measurements demonstrated that the purified chimera is able to bind cAMP. Particularly, ITC gave a Kd value of 1.7 μM, which agrees with the one previously published for the isolated C-linker/CNBD fragment of HCN4. Moreover, the rescue of a K^+-uptake deficient *E. coli* strain demonstrated that the chimeric channel is able to conduct a K^+ ions flow.

EPR-DEER experiments performed on the chimera revealed that the binding of cAMP to the CNBD domain causes clear conformational changes in the C-terminal region, which transits from a dimer of dimers conformation to a 4-fold symmetrical gating ring. These data confirm previous biochemical and functional indication obtained on the full-length channel and give further details on the direction and the extent of subunit displacement occurring during the conformational transition.

The transition of the channel from a dimer of dimer to a tetrameric configuration of the cytosolic domain might reflect a pre-conditioning state for cAMP action on channel gating and partly explains the agonist activity exerted by cAMP on channel kinetics and open probability.

Riassunto

I canali HCN (Hyperpolarization-activated Cyclic Nucleotide-gated) conducono una corrente entrante cationica (I_h o I_f) che riveste un ruolo fondamentale nel controllo della ritmicità neuronale e cardiaca. I canali HCN sono attivati dall'iperpolarizzazione del potenziale di membrana e la loro attività elettrica è ulteriormente regolata dal legame del nucleotide ciclico adenosina ciclica monofosfato (cAMP) al loro dominio citoplasmatico C-terminale, il CNBD (Cyclic Nucleotide Binding Domain). Il legame del cAMP abolisce l'azione autoinibitoria esercitata dal CNBD sull'apertura del poro del canale e innesca dei cambiamenti conformazionali che si propagano dal CNBD sino al poro attraverso il C-linker. L'interazione con cAMP determina l'aumento della probabilità di apertura del canale e ne accelera la cinetica di attivazione. La modulazione da parte del cAMP dell'attività dei canali HCN controlla la ritmicità e l'eccitabilità a livello cardiaco e neuronale ed è inoltre coinvolta nella percezione del dolore. Pertanto, per poter comprendere i meccanismi alla base delle sopracitate funzioni fisiologiche e delle malattie che colpiscono sia il sistema cardiaco che neuronale, è necessaria una descrizione dettagliata dei cambiamenti conformazionali indotti dal cAMP.

Inoltre, studi funzionali suggeriscono che il legame del nucleotide ciclico al CNBD induce una transizione dei domini C-terminali da dimero di dimero a tetramero. In particolare, questa transizione è guidata dai movimenti del C-linker.

L'obiettivo di questo progetto è quello di descrivere come avviene la propagazione dei movimenti indotti da cAMP attraverso il dominio del C-linker fino al poro del canale. A questo scopo, ho utilizzato tecniche spettroscopiche, quali l'EPR (Electron Paramagnetic Resonance) e il DEER (Double Electron Electron Resonance). Queste tecniche, infatti, permettono di studiare i cambiamenti dinamici che caratterizzano la struttura della proteina, una volta che quest'ultima è stata purificata e marcata con sonde paramagnetiche. A tale scopo, ho ingegnerizzato un canale ionico chimerico fondendo il dominio del C-linker/CNBD dell'HCN4 umano al dominio del poro del canale procariotico KcsA. Una caratteristica importante di questa proteina chimerica è che ha il vantaggio di poter essere facilmente prodotta e purificata da *E. coli*. Le misure di ITC (Isothermal Titration Calorimetry) e di DSC (Differential Scanning Calorimetry) hanno dimostrato che la chimera purificata è in grado di legare il cAMP. In particolare, l'ITC ha fornito una costante di dissociazione (Kd) di 1.7 μM, che è un valore che concorda con quello precedentemente pubblicato per il frammento isolato del C-linker/CNBD di HCN4. Inoltre, il rescue del fenotipo di un ceppo

di *E. coli* deleto di tre principali sistemi di trasporto del K^+, ha dimostrato che il canale chimerico è in grado di condurre un flusso di ioni K^+ attraverso il poro.

Gli esperimenti di EPR-DEER eseguiti sulla chimera hanno rivelato che il legame di cAMP al dominio CNBD causa evidenti cambiamenti di conformazione nella regione C-terminale, che transita da dimero di dimeri a tetramero. Questi dati confermano le precedenti evidenze emerse da esperimenti di natura biochimica e funzionale svolti sul canale intero e forniscono ulteriori dettagli sulla direzionalità e sull'estensione dello spostamento delle subunità durante la transizione conformazionale.

La transizione del dominio citosolico del canale da dimero di dimero ad una configurazione tetramerica potrebbe costituire un prerequisito per la facilitazione da parte di cAMP dell'apertura del canale e spiegherebbe in parte l'attività stimolatoria esercitata dal cAMP sulla probabilità di apertura e sulla cinetica del canale.

1. Introduction

1.1 The hyperpolarization-activated current

Hyperpolarization-activated cyclic nucleotide-gated (HCN1-4) channels are the molecular correlate of the "hyperpolarization-activated current" (I_h), a mixed cationic inward current (Na^+/K^+). I_h current is activated by hyperpolarization of the membrane potential and is directly regulated by cyclic nucleotides, i.e. cAMP and cGMP (DiFrancesco, 1993; Robinson and Siegelbaum, 2003; Wahl-Schott and Biel 2008). This current was first characterized at the level of the cardiac sinoatrial node (SAN) cells and was identified as "funny current" (I_f) because of its peculiar activation following hyperpolarization of the plasma membrane (Brown et al., 1979). Similarly, the neuronal current that was characterized in various types of neurons, was identified as "queer current" (I_q) (Pape 1996). However, the most general term to identify this current is "hyperpolarization-activated current" (I_h) (Yanagihara et al., 1980).

I_h current plays a key role in the control of neuronal and cardiac rhythmicity. For this reason, I_h is often referred to as "pacemaker current". Indeed, I_h allows the initiation of the action potential both in cardiac cells, such as SAN cells or Purkinje fibers, and in neuronal cells, such as thalamocortical neurons or dendritic arborizations of neocortical and hippocampal neurons (Altomare et al., 2003; Robinson and Siegelbaum, 2003; Wahl-Schott and Biel, 2008).

At the level of the heart, I_h current activates with negative membrane voltages, i.e. from -50 mV to - 60 mV, which are reached during the repolarization phase of the action potential. The generation of this incoming cationic current is considered to play a prominent role as primary initiator of the diastolic depolarization (DD). The presence of a progressive diastolic depolarization in the voltage range between -65 mV to -45 mV is a fundamental phase of the pacemaker action potential. Indeed, DD guides the membrane potential towards the threshold value beyond which a subsequent action potential starts (fig.1A) (Altomare et al., 2003; Robinson and Siegelbaum, 2003; DiFrancesco and Borer, 2007; Wahl-Schott and Biel, 2008). Of extremely important physiological significance is the fine regulation of I_f current by cAMP. This modulation is at the base of the autonomic modulation of the heart rate (see chapter 1.4.1 of this section).

At the neuronal level, the I_h current plays a key role in thalamocortical interneurons pacemaker activity. During an action potential, as the membrane voltage returns to negative values, I_h activates and generates a slow pacemaker depolarization that triggers a rebound Ca^{2+} spike and a burst of action potentials (fig.1B). During the spike I_h is deactivated. Once the I_T current, that generated the Ca^{2+} spike, inactivates, there is a hyperpolarization of the membrane potential that

activates I_h. Once I_h is activated, the cycle repeats determining the rhythmic neuronal burst firing (Robinson and Siegelbaum, 2003; Wahl-Schott and Biel, 2008).

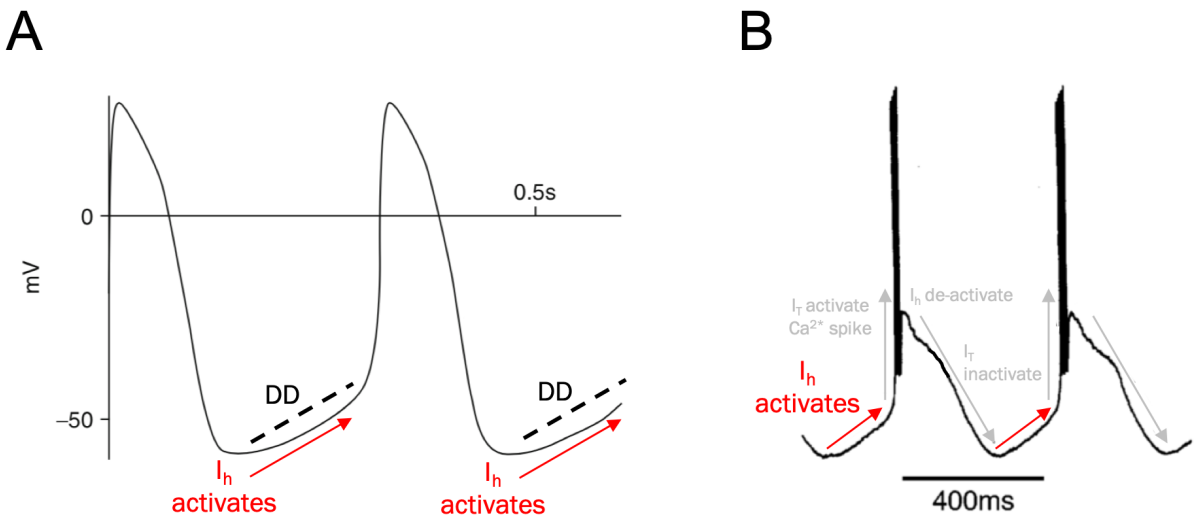

Figure 1: The pacemaker $I_{h/f}$ current. (A) Representation of the action potential in sinus node cells and (B) in cortical thalamus neurons. In both cases, the I_h current is activated by the hyperpolarization of the membrane. At the end of each action potential, I_h produces a phase of slow depolarization that allows the initiation of a new action potential. However, both the depolarization phase and the action potential are generated by the concerted action of several currents among whom I_h plays the pacemaker activity. DD: Diastolic Depolarization. (A) is modified from DiFrancesco and Borer (2007) and (B) from Robinson and Siegelbaum (2003).

This current is also important for the control of the resting membrane potential and the regulation of synaptic transmission and dendritic integration (Altomare, 2003; Robinson and Siegelbaum, 2003; Wahl-Schott and Biel, 2008). Moreover, I_h current is involved in processes concerning the control of long- and short-term memory (Wahl-Schott and Biel, 2008).

Because of its peculiar voltage-dependence, the current regulates the membrane potential. Indeed, I_h tends to stabilize the membrane potential value by actively opposing hyperpolarizing or depolarizing impulses. In neurons, this phenomenon is crucial for the regulation of the intensity of both excitatory post-synaptic potentials (EPSPs) and inhibitory post-synaptic potentials (IPSPs), whose integration at the level of the soma promotes or inhibits the start of an action potential (Robinson and Siegelbaum, 2003; Wahl-schott and Biel, 2008). Notably, as well as at the cardiac level, cAMP modulation of the I_h current is physiologically crucial also in neurons.

1.2 HCN channels

The molecular determinants of the I_h/I_f current are HCN channels. HCN channels belong to the superfamily of voltage-dependent ion channels and, particularly, to the subgroup of cationic channels regulated by cyclic nucleotides (Wahl-Schott and Biel, 2008). The voltage-dependent activation of HCNs occurs at the level of their Voltage Sensor Domain (VSD, see chapter 1.3.1 of this section). Contrary to other voltage-dependent ion channels, their opening is further regulated by the binding of cyclic adenosine monophosphate (cAMP) to the C-terminal cytoplasmic region of the channel, the CNBD (Cyclic Nucleotide Binding Domain) (Ludwig et al., 1998; Santoro et al., 1997; Santoro et al., 1998; Moosmang et al., 2001) (see chapter 1.4 of this section). The opening of HCNs is further regulated by the interaction of the CNBD domain with another cyclic nucleotide, namely cyclic guanosine monophosphate (cGMP). However, HCN channels display a 10-fold lower affinity for cGMP compared to cAMP (Ludwig et al., 1998; Biel et al., 2009).

From a molecular point of view, the CNBD acts as an autoinhibitory system on the opening of the channels by shifting the activation curve towards more negative membrane potentials. The binding of cAMP to this domain removes this self-inhibition action, thus facilitating the opening of the channels at more positive membrane potentials (Zagotta et al., 2003).

The discovery of the four mammal genes that encode for HCN channels in the late 1990s revealed that this family consists of four isoforms (HCN1–4) that share about 60% sequence identity (Ludwig et al., 1998; Santoro et al., 1998). Particularly, the four HCN homologous subunits can assemble forming both homo- and heterotetramers that are characterized by different biophysical properties (Altomare et al., 2003; Biel et al., 2009).

Indeed, all four HCN channel subtypes (HCN1-4) show the main biophysical properties of I_f/I_h current, but differ from each other in voltage-dependence (fig.2A), activation time constant (τ) (fig.2B) and modulation efficiency by cAMP (fig.2C) (Stieber et al., 2005; Wahl-Schott and Biel, 2008). Particularly, the voltage-dependent activation differs quantitatively between the HCN channel subtypes (fig. 2B). Typical values of the half-activation potential ($V_{1/2}$) are: -70 mV for HCN1, -95 mV for HCN2, -77 mV to -95 mV for HCN3 and -100 mV for HCN4 (Altomare et al., 2003; Stieber et al., 2005). Among the four isoforms, HCN1 exhibits the fastest activation kinetics upon hyperpolarization (fig.2B). Both HCN2 and HCN4 are well modulated by cAMP (fig.2C). Indeed, HCN2 and 4 show an evident shift toward more positive membrane potentials of their $V_{1/2}$ (i.e. HCN2 $V_{1/2}$ shifts of 28 mV and HCN4 $V_{1/2}$ of 23 mV). HCN1 is modulated by the cyclic nucleotide to a lesser extent (i.e. the $V_{1/2}$ shifts only by 7 mV), while HCN3 is not affected by cAMP (Stieber et al., 2005).

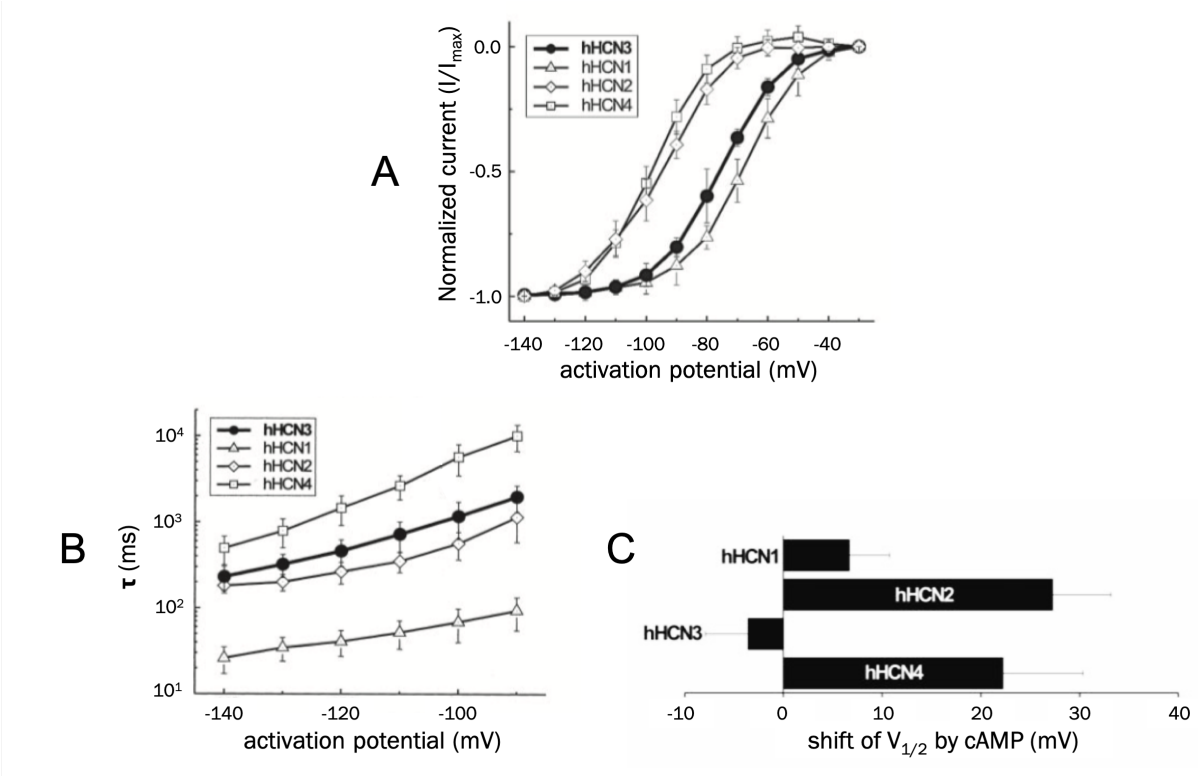

Figure 2: The four isoforms HCN1–4 have different biophysical characteristics. (A) Normalized curves of the voltage-dependent activation of the channels hHCN1-4. (B) Voltage-dependent activation time constants (τ) for hHCN1–4 channels. (B) Shift of the $V_{1/2}$ caused by the addition of 100 µM of the membrane-permeable cAMP analog 8-Br-cAMP. Images are modified from Stieber et al., 2005.

HCN channels are mainly expressed in the nervous system and heart. In these organs, each member of the HCN family (HCN1–4) has a markedly different and characteristic expression profile. In the brain all four isoforms are present. Particularly, HCN2 is the only one to be expressed ubiquitously in almost all regions of the central nervous system, although the highest expression is reported in the thalamus, brain stem nuclei and hippocampus (Biel et al., 2009). The second most common isoform in the brain is HCN1, expressed in the neocortex, hippocampus, cerebellar cortex and brain stem. The expression of HCN4, on the other hand, is generally low and restricted to specific regions of the brain, i.e. in various thalamic nuclei and in the mitral cell layer of the olfactory bulb (Santoro et al., 2000; Moosmang et al., 2001). Finally, HCN3 has the weakest expression (Biel et al., 2009).

All four isoforms of the HCN channels have also been found in the heart, where the expression levels of each of them strongly depend on the heart region and, in addition, appear to vary according to species, age and, perhaps, health status (Wahl-Schott and Biel, 2008; Robinson and Siegelbaum, 2003). However, in human cardiac tissue HCN4 expression is remarkably higher

compared to the other isoforms (Ludwig et al., 1998). Indeed, in the SAN HCN4 constitutes 80 % of the total I_f current. Moreover, HCN4 is the most expressed isoform also in the conduction system (AVN and Purkinje fibers) and in both atria and ventricles. The remaining I_f current fraction is composed mainly of HCN2 and HCN1, whereas HCN3 represents a negligible part in all the cardiac tissues (Sartiani et al., 2017).

In addition, HCN channel expression has been identified in other tissues and cell types (Biel et al., 2009). For example, traces of hHCN4 expression profile were found also in testis. In the latter, the pacemaker activity of the channel is supposed to be involved in the generation of rhythmic activity that controls the waveform of spermatozoa flagellar beating (Seifert et al., 1999).

1.3 Architecture of HCN

HCN channels are tetramers composed of four identical or highly similar α-subunits, which are arranged around a centrally located pore (fig.3) (Wahl-Schott and Biel, 2008). The architecture of the α-subunits is similar to that of many ion channels. Particularly, the architecture of HCN channels reflects the topology of voltage-gated K^+ channels (Kv), even if HCNs display an inverted activation behaviour compared to Kv channels (Decher et al., 2004; James and Zagotta 2018).

Each subunit is formed by highly preserved structural motifs: the N- and C-terminal regions, that are both cytoplasmic, and a transmembrane region (fig.3). The transmembrane region and the C-terminal cytosolic domain co-operate allosterically with each other during channel activation (Robinson and Siegelbaum, 2003; Wahl-Schott and Biel, 2008). Moreover, the recently solved structure of human HCN1 (fig.3) revealed a unique N-terminal domain, i.e. the HCN domain (HCND). A recent study revealed that the HCND is involved in the voltage-dependent opening of the HCN channels. The HCND, by making contacts with both the VSD and the C-linker domain, is an important coupling and transmission element for the cAMP effect on the channel opening. Indeed, it mechanically connects the conformational changes in the C-linker, which are generated by the binding of cAMP to the CNBD, to the VSD. (Porro et al., submitted).

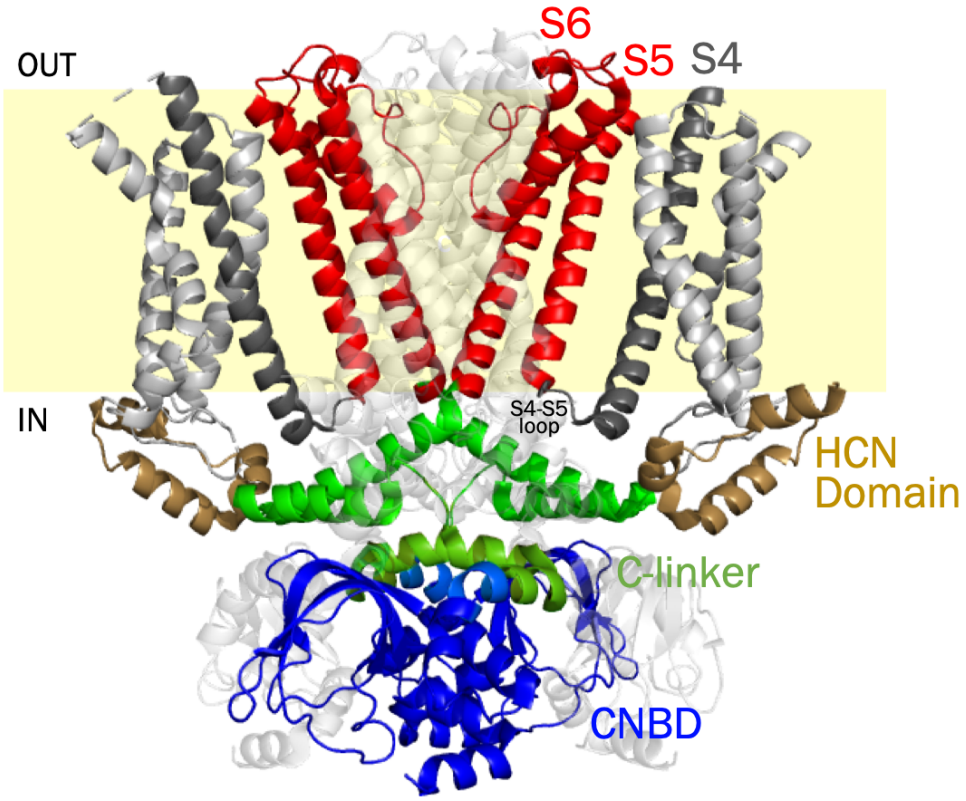

Figure 3: Full-length hHCN1 channel cryo-EM structure (PDB_ID: 5U6O, Lee and MacKinnon, 2017). The secondary structures are represented by ribbons. Two opposite subunits are highlighted. Each domain forming the channel is shown with a color code. In the transmembrane region (S1-S6 α-helices) S1-S3 are in light grey. The voltage sensor domain (S4) and the S4-S5 loop are displayed in dark grey. The pore region (S5 and S6) is represented in red. Of the cytoplasmic regions, the N-terminal HCN domain is shown in sand, whereas the C-terminal C-linker domain is represented in green, followed by the CNBD in blue.

1.3.1 The transmembrane region

The transmembrane core of the HCN channels consists of six α-helices (S1-S6), of which helices S1-S4 form the voltage sensor domain (VSD). The S5 and S6 helices form the pore domain (fig.3). The sensing of the transmembrane potential is due to the presence of positively charged amino acid residues located along the S4 helix (Decher et al., 2004). The detection of changes in the membrane potential by these positively charged residues determine the VSD to be in the hyperpolarized or depolarized state. Particularly, the hyperpolarization of the membrane potential results in a movement of the VSD that directly causes the opening of the activation gate. This phenomenon is based on the presence of a short S4-S5 linker that directly connects the VSD to the pore domain, thus coupling the hyperpolarization of the membrane potential to the pore gating (Lee and MacKinnon, 2017).

1.3.2 The cytoplasmic C-terminal region

The cytoplasmic C-terminal region is well preserved in the four isoforms of the HCN family (Biel et al., 2009). This region is composed by two domains (fig.4A and B). One is the Cyclic Nucleotide Binding Domain (CNBD) that, by binding cAMP, determines the modulation of HCN channels activity. The second is the C-linker domain that, by connecting the CNBD to the pore of the channel, transmits to the pore the opening regulation exerted by the CNBD (Biel et al., 2009).

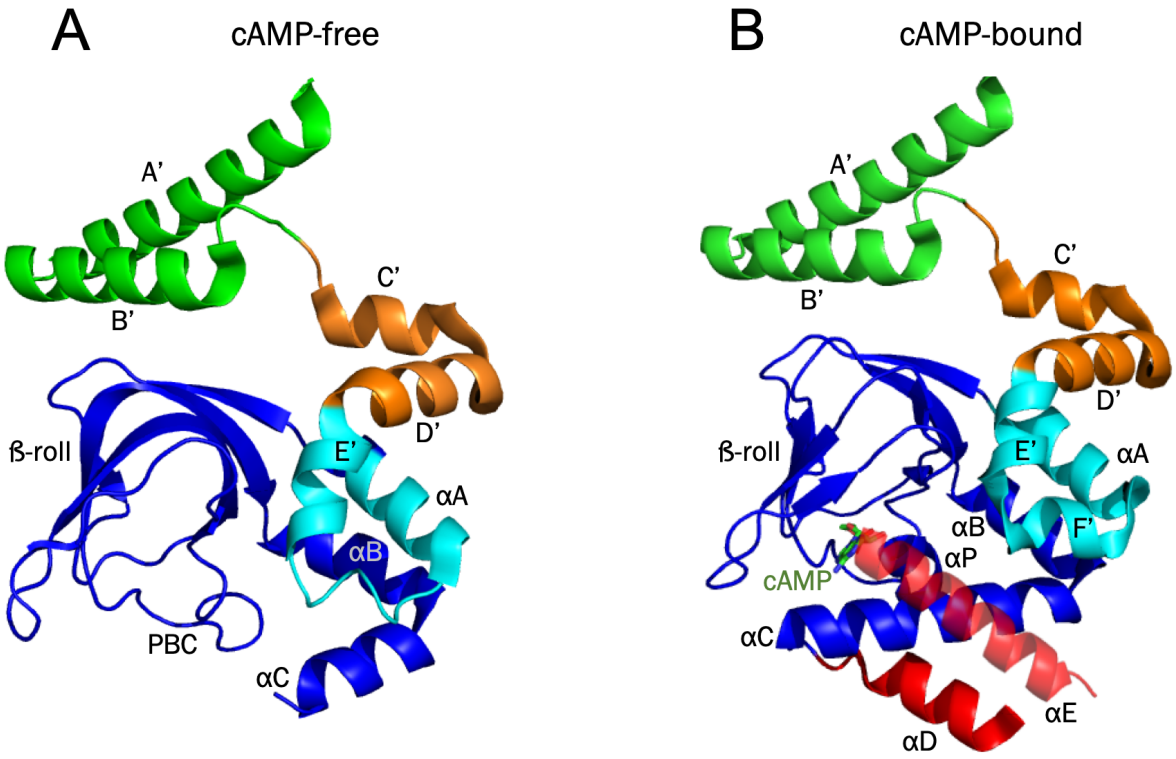

Figure 4: Ribbon representation of the C-linker/CNBD domains of a single subunit of hHCN1 in the apo and holo states. Highlight from the structure solved in the apo ((A), PDB_ID: 5U6O, Lee and MacKinnon, 2017) and in the holo states ((B), PDB_ID: 5U6P, Lee and MacKinnon, 2017). Secondary structure elements are labeled. Each element is shown in a different color. In the C-linker domain of both (A) and (B) A'-B' helices are shown in green and C'-D' helices are shown in orange, whereas E'-helix in (A) and (B) and F'-helix in (B) are in cyan. The two latter helices together with the αA-form the N-terminal helical bundle that is shown in cyan. In the CNBD of both (A) and (B) the ß-roll and αB and αC helices are in blue. (B) Notably, some helices fold up only in the presence of the ligand, i.e. the helices αD and αE that are shown in red, the αP helix in the PBC and the F' helix in the N bundle loop.

1.3.2.1 The CNBD

The CNBD is a structural domain found in several prokaryotic and eukaryotic channels that are part of the Cyclic Nucleotide-Binding Domain (CNBD) channels family, that belongs to the

voltage-gated K^+ channel superfamily. Together with HCN channels, Cyclic Nucleotide-Gated (CNG) channels and the *ether-à-go-go-type* (KCNH) channels are part of the CNBD channels family. Notably, the activity of the latter channels is cyclic nucleotide-independent even if they possess a CNBD domain (James and Zagotta 2018).

The CNBD of HCNs (Fig. 4A apo and B holo) (120 amino acids) consists of an α-helix (αA-helix), followed by a β-antiparallel sheet with β-roll topology formed by eight β-filaments (β1- β8) and two terminal α-helices (αB- and αC-helices). Moreover, the recently solved cryo-EM structures of hHCN1 channel in cAMP-free and -bound states (fig. 4A and B respectively) shown that, upon cAMP binding, the αC-helix is followed by other two helices, i.e. αD and αE helices (fig.4B, in red). Indeed, both αD and αE are not observed in the ligand-free cryo-EM structure as they become ordered only in the cAMP-bound state (Lee and MacKinnon, 2017).

Between the β6 and β7 filaments there is the PBC, the Phosphate Binding Cassette, which forms the binding site for cAMP. The PBC consists of seven amino acid residues present at the interface between the β-sheet and the αC-helix. Particularly, within this site there is an additional helix, i.e. the αP-helix (fig.4B), that is formed as a result of the binding with cAMP.

The N-terminal helical bundle, an evolutionary element preserved in all CNBDs, consists of an antiparallel helix-turn-helix formed by the E'-helix of the C-linker and the αA-helix of the CNBD (fig.4A and B, in cyan) (Saponaro et al., 2014). When the CNBD is in the cAMP bound state, the F'-helix folds up in the N-bundle loop (fig. 4B). Spectroscopic data on the isolated CNBD domain and electrophysiological measurements on the full-length HCN2 channel showed a role of the N-bundle loop in the allosteric modulation of cAMP binding to the CNBD (Saponaro et al., 2018). Moreover, the movements of the N-terminal helical bundle induced by the binding of cAMP to the CNBD, are key steps for the mechanical transduction to the pore via the C-linker of the conformational changes that determine the opening of the channel (Saponaro et al., 2014).

1.3.2.2 The C-linker

The region of the C-linker (80 amino acids) constitutes a crucial domain of HCN channels since it connects the last transmembrane α-helix S6 to the CNBD (fig.3). The C-linker consists of six α-helices (A'-F') (fig.4A and B). Particularly, the first two helices of each subunit (A'- B') form an antiparallel "helix-turn-helix" pattern that interacts with the helices C' and D' of the adjacent subunit (Zagotta et al., 2003).

The C-linker domain is necessary for the cAMP-dependent modulation of the opening of the channels and to promote their functional tetramerization (Zagotta et al., 2003; Lolicato et al., 2011;

Sartiani et al., 2017). Notably, the structures of the intact hHCN1 channel suggest that the C-linkers may also directly influence the state of the VSD, perhaps because of interactions between the C-linker and the S4–S5 loop (Lee and MacKinnon, 2017).

Moreover, this domain is fundamental in the control of many other molecular mechanisms. Indeed, studies on isolated soluble C-terminal regions of HCNs (C-linker and CNBD) have shown that the C-linker domain plays a key role in controlling the different sensitivity to cAMP of HCN isoforms. Indeed, its removal abolishes the differences in affinity of HCN CNBDs to the cyclic nucleotide (Lolicato et al., 2011). Furthermore, specifically concerning the HCN isoform 4, it has been found that the C-linker domain of HCN4 hosts an isoform specific pocket, CLP (C-Linker Pocket), for the binding of cyclic dinucleotides, an emerging class of signaling molecules in humans (Sun et al., 2013), that antagonizes cAMP regulation (Lolicato et al., 2014).

1.4 The physiological importance of cAMP modulation of HCN channels activity

Cyclic adenosine monophosphate (cAMP) is an important molecule that acts as intracellular second messenger. Its production is regulated in many physiological processes. cAMP is produced from the cyclization of ATP by adenylate cyclase, an enzyme associated to the cell membrane and localized on the cytoplasmic side (Rahman et al., 2013). Adenylate cyclase is activated by different signaling molecules such as glucagon (especially at the hepatic level) and adrenaline (in the muscles) through the activation of adenylate cyclase stimulatory G protein-coupled receptors (GPCRs). The degradation of cAMP to AMP is instead catalyzed by the enzyme phosphodiesterase.

One of the targets of cAMP is the PBC in the CNBD domain of HCN channels (see chapter 1.3.2.1 of this section). The binding of cAMP at the level of the PBC promotes the removal of the autoinhibitory action exerted by the CNBD on the channel activity and facilitates the opening of the latter. Indeed, cAMP accelerates the opening and slows down the closing of HCN channels, resulting in a shift in the voltage-dependent activation toward more positive potentials and in an increase in the maximum current at hyperpolarizing voltages (fig.5) (Wahl-Schott and Biel, 2008). However, as previously mentioned, the shift in V1/2 depends on the channel subtype and conditions (see chapter 1.2 of this section) (Wahl-Schott and Biel, 2008; Zagotta et al, 2003).

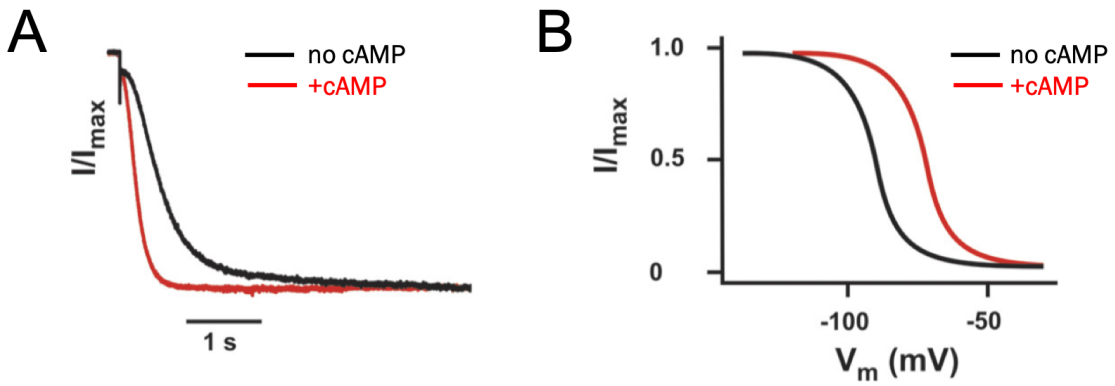

Figure 5: cAMP accelerates the opening of the channel and shifts the channel activation at more positive membrane potentials. (A) $I_{f/h}$ current is activated faster in the presence than in the absence of cAMP at maximum activation voltage (-140 mV). (B) $I_{f/h}$ current activation curve in the presence and absence of cAMP (image modified from Biel et al., 2009).

The regulation of the electrical activity of HCN channels by intracellular levels of cAMP is of crucial importance for the specific role that I_h current fulfills in many physiological functions. Indeed, cAMP endogenous levels, that are directly controlled by the autonomic nervous system, finely modulate the firing frequency of pacemaker cells and, thus, the activity of HCN channels. Moreover, at neuronal level, the modulation of HCN channels activity by intracellular cyclic adenosine monophosphate is involved in the control of working memory networks in prefrontal cortex (Wahl-Schott and Biel 2008) and neuropathic pain perception in both central and peripheral nervous system (Emery et al., 2012). Thus, a detailed description of the molecular mechanism of cAMP regulation of HCN channels activity is crucial for understanding several physiological functions, as well as diseases affecting cardiac and neuronal functions.

1.4.1 cAMP modulation of HCNs activity at cardiac level

The heartbeat originates from specialized myocytes that constitute the conduction tissue at the level of the region of the sinus node (SAN), in the right atrium of the heart. These cells have spontaneous electrical activity thanks to which they are able to generate a particular type of action potential, the pacemaker potential, characterized by the presence of a progressive diastolic depolarization (DD). The activation of the diastolic depolarization is directly related to the I_f current generated by HCN channels, whose activity is modulated by the intracellular levels of cAMP (see chapter 1.1 of this section) (Wahl-Schott and Biel, 2008).

cAMP intracellular levels are involved in the control of the heartbeat in physiologically healthy conditions as well as in diseases. The understanding of pacemaker alterations that leads to cardiac arrhythmias is rapidly growing on genetic basis. Indeed, these pathologies are often due to modifications of HCN channels function such as loss-of-function mutations in HCN4 that results in a slow-down of the pacemaker activity. On the contrary, it has been found a gain-of-function mutation in the A'-helix of the C-linker domain of HCN4 that increases the sensitivity of HCN4 to cAMP. This mutant channel mediates an I_f larger than the normal current during the diastolic depolarization that results in tachycardia (Baruscotti et al., 2017). However, dysfunctional cardiac peacemaking can be caused also by a mis-regulation of the proteins associated with the modulation of the I_f current (Sartiani et al., 2017). For example, cardiac arrest is a syndrome that strictly depends on the intracellular levels of the cyclic nucleotide. Indeed, it is due to the abrupt lack of control of heart rate and a decrease in the force of contraction and relaxation of the heart that normally are under the control of cAMP (Boularan and Gales, 2015). Both cellular apoptosis and loss of blood flow, culminating in cardiac arrest, are caused by high intracellular levels of cAMP due to over-stimulation of β-adrenergic receptors (Lohse et al., 2003; Zhu et al., 2003).

Indeed, at cardiac level, the modulation of the activity of the I_f current occurs thanks to the regulation of the intracellular levels of cAMP by the autonomous nervous system that, with its sympathetic and parasympathetic afferents, directly controls the SAN. Sympathetic afferents of the autonomic nervous system release at the level of the target organ as post-ganglion neurotransmitters mainly noradrenaline (also known as norepinephrine) and adrenaline (also known as epinephrine), while parasympathetic afferents release acetylcholine. The targets of both noradrenaline and adrenaline are β-adrenergic receptors (ß-AR), also known as adrenoceptors. Whereas, acetylcholine binds two different cholinergic receptors, the muscarinic (M-R) and the nicotinic receptors (fig.6A) (Boularan and Gales, 2015).

Both β-adrenergic and muscarinic receptors are G Protein-Coupled Receptors (GPCR). Their activity is essential for the signal transduction that culminates with the control of adenylate cyclase (AC), the enzyme involved in the production of cAMP. Particularly, the β-adrenergic receptors are coupled with stimulatory G proteins (G_S) that activate adenylate cyclase, while muscarinic receptors are associated with inhibitory G proteins (G_I) that inhibit the enzyme activity (fig.6A).

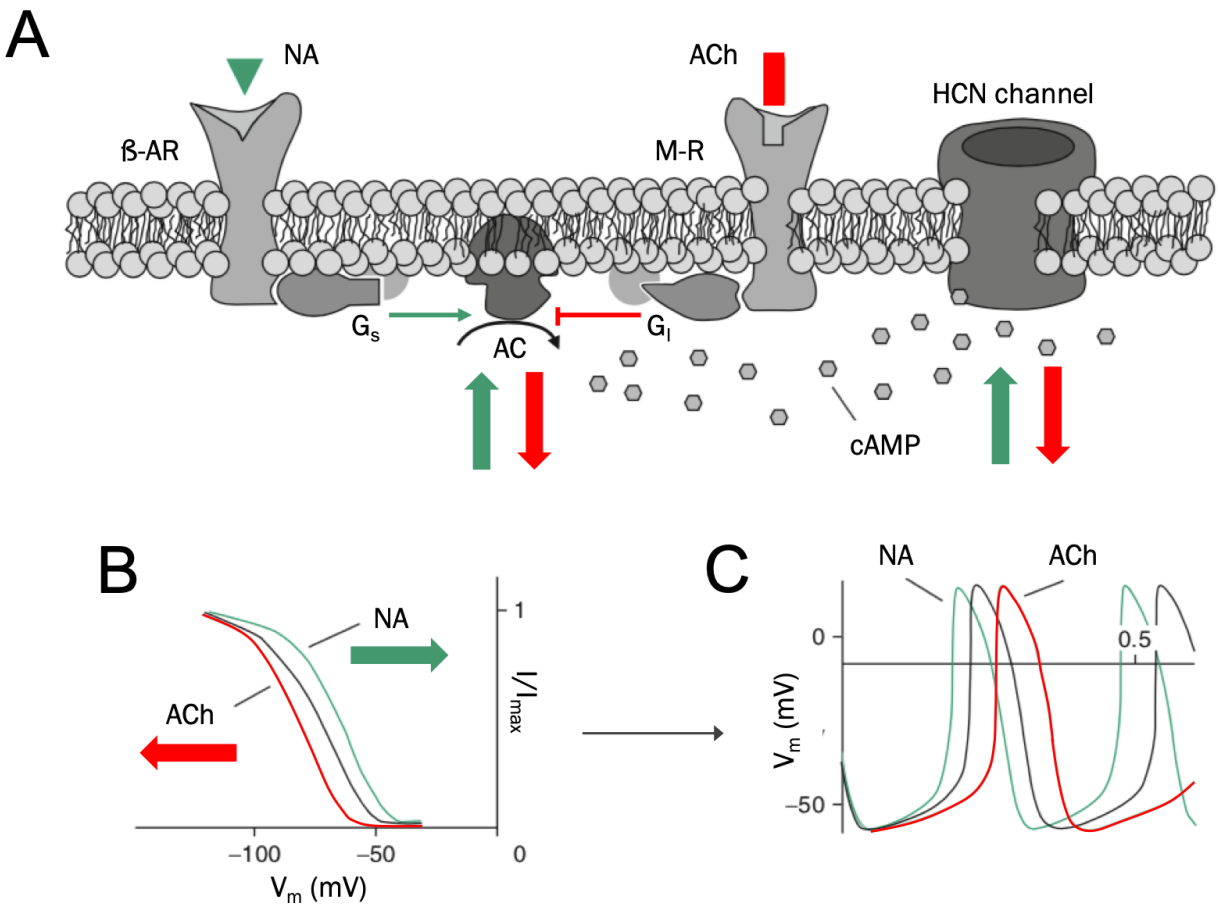

Figure 7: Effects of autonomic neurotransmitters on the rhythmicity of the SAN. (A) Schematic representation of the membrane of sinoatrial myocytes. The modulation of the activity of HCN channels is directly controlled by the up- (green arrow) or down-regulation (red arrow) of the activity of the enzyme Adenylate Cyclase (AC). The resulting intracellular levels of cAMP directly affect the amount of I_f current flowing through HCN channels. The interaction of noradrenaline with ß-AR receptor causes an increase of intracellular levels of cAMP and, thus, an up-regulation of HCN activity. Whereas the interaction of acetylcholine with M-R receptor causes the opposite effect. (B) Activation curves showing the V1/2 of HCN channels under control condition (gray) and in the presence of either NA (green) or ACh (red). NA moves the curve towards more positive voltage values, whereas ACh towards more negative. (C) Action potentials recorded under control conditions (gray) and in the presence of either NA (green) or ACh (red). NA determines an increase in the frequency of pacemaker action potentials, whereas ACh causes a decrease. ACh: acetylcholine; NA: noradrenaline; Gi: inhibitory G protein; Gs: stimulatory G protein; ß-AR: ß-adrenergic receptor; M-R: muscarinic receptor; AC: adenylate cyclase. The image was modified from DiFrancesco and Borer, (2007).

An increase in intracellular levels of cAMP resulting from the binding of noradrenaline (NA) to β-adrenergic receptors, determines a shift in the activation curve of the I_f towards more positive values of the membrane potential (fig.6B, green trace) and reduce the time needed to generate a new action potential (fig.6C, green trace). The final result is an increase in heart rate (Brown et al., 1979; Ludwig et al., 1998; Accili et al., 2002; DiFrancesco and Borer, 2007; Biel et al., 2009).

On the other hand, the binding of acetylcholine (ACh) to the muscarinic receptor causes the inhibition of the activity of the enzyme adenylate cyclase with a consequent decrease in the production of cAMP (fig.6A). The activation of muscarinic receptors results in the shift of the activation curve of the I_f towards more negative values (fig.6B, red trace) and in a decrease of the frequency of generation of action potentials (fig.6C, red trace). The final result is a decrease in heart rate. (Brown et al., 1979; Ludwig et al., 1998; Accili et al., 2002; DiFrancesco and Borer, 2007; Biel et al., 2009).

1.4.2 cAMP modulation of HCNs activity at neuronal level

In the central nervous system, various cognitive processes and emotional aspects are regulated by cAMP endogenous levels (Klamer et al., 2005; Wang et al., 2007; Titus et al., 2013; Sartiani et al., 2017). Many diseases (i.e. epilepsy and neuropathic pain) and neuropsychiatric disorders (i.e. schizophrenia, depression, anxiety and drug abuse) are known to be connected with dysfunctionalities of the activity of HCN channels and, particularly, with unbalanced cAMP–HCN signaling. This results in network disconnection and in either reduction or overstimulation of several neurophysiological tasks (Sartiani et al., 2017).

The cAMP-dependent regulation of HCN is known to be physiologically relevant in the modulation of many neuronal functions (see chapter 1.1 of this section). For instance, the pre-frontal cortex (PFC) controls behavior and thoughts using the working memory. Information can be kept in the working memory by those neurons through excitatory networks that can maintain constant neuronal firing in the absence of external stimuli (Wang et al., 2011). cAMP intracellular levels and, thus, I_h current modulation are directly involved in the control of working memory (Wang et al., 2007). Indeed, elevated intracellular levels of cAMP reduce the persistent firing exerted by PFC neurons by opening HCNs (Arnsten 2007; Wang et al.,2011). In PFC HCN channels are highly concentrated on the spines where neuronal networks are interconnected. In this way, HCNs activity can regulates incoming information (Wang et al., 2007 and 2011).

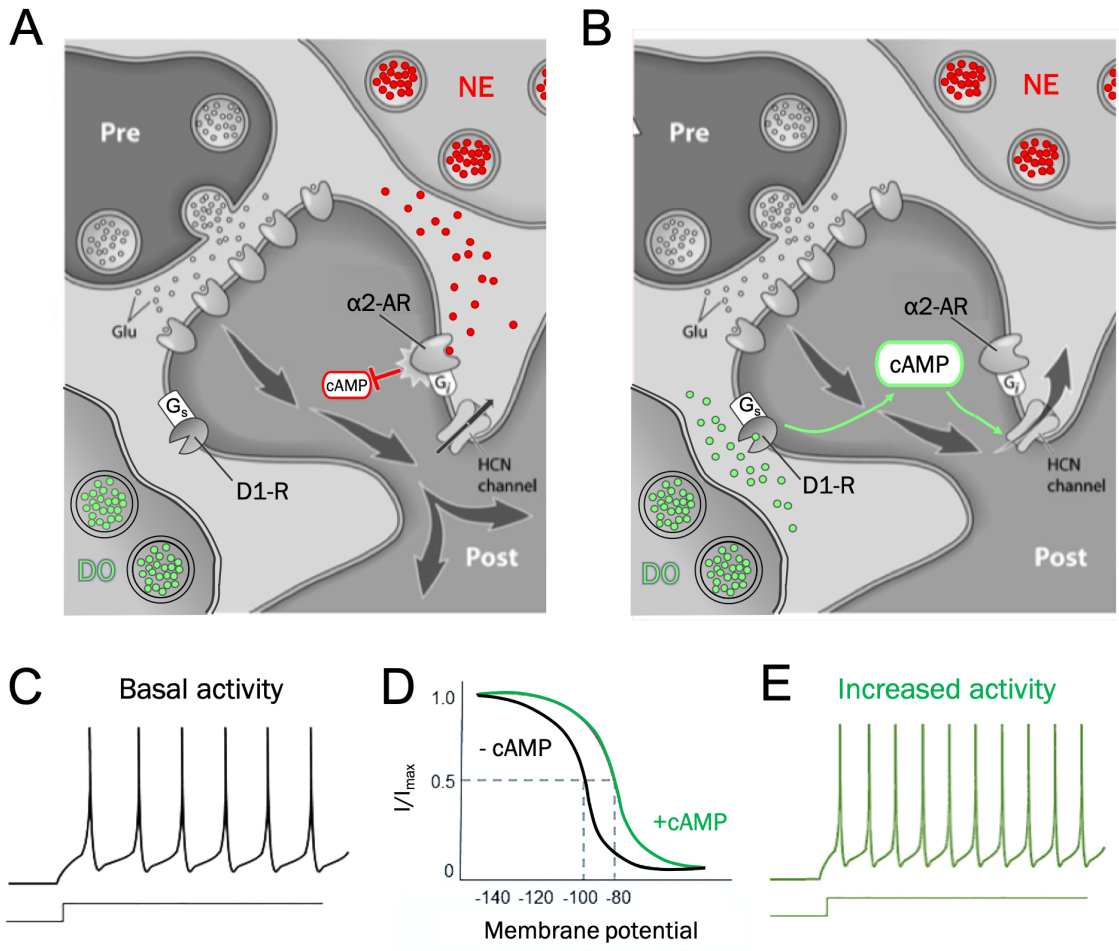

Figure 8: I_h current regulation in the PFC. Schematic representation of (A) α2-AR and (B) D1-R cAMP-HCN regulation in prefrontal cortex microcircuits. (A) α2-adrenergic receptors (α2-AR) stimulation by norepinephrine (NE) activates inhibitory G proteins (Gi) that inhibit the production of cAMP. (D) In the absence of cAMP stimulation, the open probability of HCN decreases and the activation curve is not shifted (black curve). (C) In these physiological conditions, the neuronal firing frequency is basal. (A) As a result, the channels pass little inward current, whereas the efficacy of cortical inputs increases. (B) dopaminergic type 1 receptors (D1-R) stimulation by dopamine (DO) activates stimulatory G proteins (Gs) that promote the production of cAMP. (D) cAMP causes a rightward shift in the voltage-dependence of HCN activation curve (green curve). (E) The increased inward current augments the firing frequency. (B) As a result, the increased opening of HCNs shunts the synaptic inputs onto the dendritic spines and reduces network activity. (A) and (B) are modified from Wang et al., 2007. (C), (D) and (E) are modified from Tsantoulas et al., 2016.

At these levels, HCN channels colocalize and functionally interact with α2-adrenergic receptor (α2-AR) and dopaminergic receptor type 1 (D1-R) via cAMP stimulation (Wang et al., 2007). As in the heart, cAMP-HCN interaction is finely modulated by the opposite action exerted by the two receptors (Sartiani et al., 2017). Indeed, both α2-adrenergic and dopaminergic type 1 receptors

belong to the family of G Protein-Coupled Receptors (GPCR), which generate specific signals that control the production of cyclic nucleotide (Wahl-Schott and Biel, 2008).

Under optimal neurochemical conditions, once α2-adrenoreceptors are activated by norepinephrine (NE), inhibitory G proteins (Gi) promote the inactivation of the enzyme adenylate cyclase, thus blocking the production of cAMP (fig. 8A). This event leads to a reduction of cAMP-HCN interaction and, thus, in the open probability of the channels (fig. 8 A, C and D). The inhibitory action exerted by the activation of α2-adrenoreceptors increase membrane resistance and tightly connects neurons with similar spatial properties. The result is an increase in the efficiency of the summation of synaptic stimuli and neuronal excitability for the preferred direction (fig. 8A) (Arnsten 2007; Wahl- Schott and Biel, 2009). On the contrary, the release of dopamine (DO) enhances I_h current (fig. 8B, D and E). The binding of dopamine at the D1 receptor level activates stimulatory G proteins (Gs) that promote the activation of adenylate cyclase and thus the increase of cAMP synthesis (fig. 8B). The opening facilitation of HCNs causes a reduction in membrane resistance and therefore causes a reduction in synaptic stimuli by weaken the functional connectivity of PFC networks to nonpreferred directions (fig. 8B) (Arnsten 2007; Wahl-Schott and Biel, 2008; Biel et al., 2009; Chu and Zhen 2010).

Another fundamental role played by intracellular cAMP concentration and, thus, by I_h current is the modulation of the perception of inflammatory and neuropathic pain (Emery et al., 2012). Particularly, HCN2, the isoform mainly expressed at the level of nociceptive neurons, is the key element of the molecular mechanism that controls the excitability of nociceptive neurons in response to inflammation and nerve injury. Indeed, in the scenario of neuronal damage or in experimental model of inflammation, has been reported an overexpression of HCN and an increase of I_h current due to elevated intracellular levels of cAMP (Sartiani et al., 2017).

In this pathological condition, high intracellular levels of cAMP facilitate the opening of HCN2 channel at more positive membrane potentials, generating a depolarizing tonic current even when the nociceptor is at rest. This results in an increase of the frequency of action potentials of nociceptive neurons that directly correlates with the intensity of perceived pain. The elevated intracellular levels of cAMP are triggered by inflammatory substances such as prostaglandin E2 (PGE2) and serotonin that promote the activation of adenylate cyclase. The increase in the frequency of PGE2-dependent action potentials is abolished by the pharmacological blocking of HCN channels by ivabradine or ZD-7288, or by the genetic deletion of HCN2 in nociceptive neurons (Emery et al, 2012). On the contrary, the activation of opioid receptors, that are classic pharmacological targets for the treatment of pain, antagonizes the activity of HCN channels by

inhibiting adenylate cyclase and promoting the elimination of intracellular cAMP (Emery et al., 2012; Tsantoulas et al., 2016).

1.5 Molecular mechanism of HCN regulation by cAMP

The pioneering X-ray structure of mouse HCN2 C-linker/CNBD fragment showed at which level cAMP binds to the protein and the residues involved in this interaction (Zagotta et al., 2003). As previously mentioned, cAMP binds the CNBD at the level of the PBC (Phosphate Binding Cassette), a defined region between the ß-roll, the αP-helix and the αC-helix. The phosphate group of the cyclic nucleotide forms hydrogen bonds with a series of residues in the αP-helix and in the adjacent loop, that form the so called PBC. The purine ring of the ligand forms contacts with the β4 and β5 filaments and with the αC-helix. Particularly, seven residues were identified that perform strong interactions with the ligand (fig.9, residues represented as gray sticks).

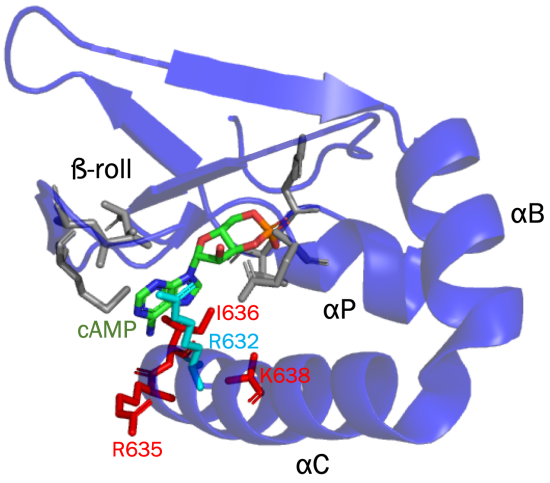

Figure 9: cAMP interaction site on the CNBD domain. Ribbon representation of the CNBD structure bound to cAMP (PDB_ID: 1Q50, Zagotta et al., 2003). The figure shows the main amino acid residues involved in the cyclic nucleotide binding. The numbering refers to the murine HCN2 channel.

Among these, only R632 (mHCN2 numeration, fig.9 in cyan) in the αC-helix of the CNBD is essential for the high efficacy of the ligand. R632 stabilizes the binding of the cyclic nucleotide by coordinating a triad of contacts between the ligand, the αC-helix and the core of the CNBD. This interaction results in the enhancement of the channel opening (Zhou and Siegelbaum, 2007). The residues R635, I636 and K638 (fig. 9, in red) on the αC-helix of the CNBD domain stabilize the binding of cAMP with higher energy instead of cGMP but do not contribute to cAMP efficacy (Zhou and Siegelbaum, 2007). Particularly, I636 is known to form a hydrophobic interaction with the purine ring of the cAMP (Zagotta et al., 2003).

The recent determination of the structures of the full-length hHCN1 channel in the cAMP-free and - bound states (Lee and MacKinnon, 2017) enhanced our understanding of HCNs structure that previously was based primarily on C-terminal fragments (Zagotta et al., 2003; Akimoto et al., 2014; Puljung et al., 2014; Saponaro et al., 2014).

Human HCN1 structures revealed that the complex mechanism that governs the opening of HCN channels is the result of the allosteric interaction between the pore domain, the VDS, the HCND (HCN Domain), the C-linker and the CNBD. Indeed, the inhibitory action exerted by the CNBD on the channel seems to be coupled to the pore through the C-linker domain. The latter may constrain the movement of the S6 helix, thus preventing the opening of the channel. The binding of cAMP would relieve this constrain by causing conformational changes in the CNBD and allowing S6 movement to promote the gating (Lee and MacKinnon, 2017). Moreover, growing evidence suggest the autoinhibitory effect of the CNBD is directly mediated by the HCND. Computational and experimental data suggest that the HCND is involved in the response to cAMP, as it mechanically connects the VSD to the CNBD domain (Porro et al., submitted).

Even if the resolution of the structures of HCN1 represents undeniably a milestone, the comparison between the cAMP-unbound (apo) and cAMP-bound (holo) structures reveals that most of the structural differences are localized only at the level of the CNBDs, whereas both the pore and the C-linker domain result to be stuck in one conformation, even in the presence of cAMP.

In the following chapters will be shown the structural rearrangements of the C-terminal regulatory domains that have been described up to now, that lead to the opening of HCN channels upon the binding of cAMP.

1.5.1 Structural rearrangements of the CNBD

Crystallographic and spectroscopic studies on the isolated HCN2 CNBD fragment in the cAMP-free (Saponaro et al. 2014) and -bound (Zagotta et al. 2003) state allowed to describe in detail the conformational changes that characterize the CNBD domain, thus clarifying the starting point of the molecular mechanism that leads to the cAMP-induced opening of HCN channels. Indeed, the comparison between the structures solved by cryo-EM of the CNBD domain in the cAMP-unbound and -bound states (Lee and MacKinnon, 2017) are nearly identical to the CNBD fragment structures of the apo and holo HCN2 previously published (fig. 10B) (Zagotta et al., 2003; Saponaro et al., 2014).

The main rearrangements caused by the binding of cAMP take part at the level of the α-helix elements, while there are no evident changes in the ß-roll. Indeed, upon cAMP binding the helices

αA, αB and αC move towards the β-roll and, within the PBC, there is the formation of the αP-helix. The rotational movement of αB and αC towards the ß-roll allows the αC-helix to contact the purine ring of cAMP, thus stabilizing the interaction of the cyclic nucleotide. Moreover, the cAMP-bound cryo-EM structure revealed that cAMP induces the formation of the helices αD and αE following the αC-helix (fig. 10A and 4). These two helices interact with both the αC-helix and the β-roll (Lee and MacKinnon, 2017). However, the role of these two helices is still under investigation.

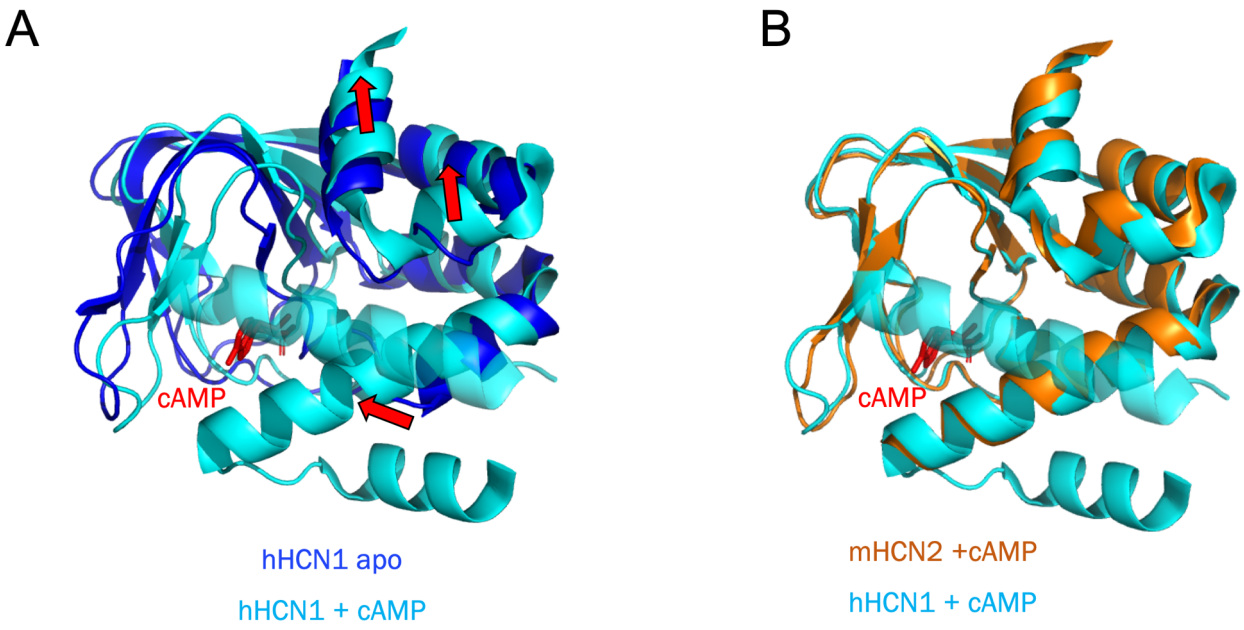

Figure 10: cAMP-induced rearrangements of the CNBD domain. (A) Superimposition of the cryo-EM structures of HCN1 CNBD domain in the cAMP-unbound (apo, in blue) and cAMP-bound state (cyan). (PDB_ID: 5U6O and 5U6P respectively, Lee and MacKinnon, 2017). (B) Superimposition of the holo CNBD structures solved with X-ray diffraction (in orange, PDB_ID:1Q5O, Zagotta et al., 2003) and with cryo-EM (in cyan, PDB_ID: 5U6P, Lee and MacKinnon, 2017).

The rearrangements of the helices αB and αC induce the movement of the αA-helix and thus of the N-terminal helical bundle (fig 10A and 4). Indeed, the αC-helix, by approaching the ß-roll, sterically moves the N-terminal helical bundle that, as a result, undergoes an upward shift coupled with the formation of a new helix, i.e. the F'-helix. The movement of the N-terminal helical bundle is one of the key elements in the transduction of the cAMP signal. Indeed, by directly connecting the CNBD to the C-linker, it propagates the conformational changes induced by the cAMP to the C-linker and, thus, to the pore.

1.5.2 Structural rearrangements of the C-linker domain

The C-linker domain is the crucial element for the transduction of the signal induced by the binding of the cAMP to the pore domain. Indeed, it connects the movement of the CNBD caused by the direct binding of the ligand to that of S6 helix, thus promoting the opening of the channel.

Up to now, the knowledge of the C-linker conformational changes that lead to the opening of the channel is based on crystallographic structures of the cAMP-bound C-terminal C-linker/CNBD fragments of HCN1, 2, and 4 (Zagotta et al., 2003; Xu et al., 2010; Lolicato et al., 2011; Akimoto et al., 2014) and on the cryo-EM cAMP-bound (holo) and unbound (apo) structures of the intact hHCN1 channel (Lee and MacKinnon, 2017).

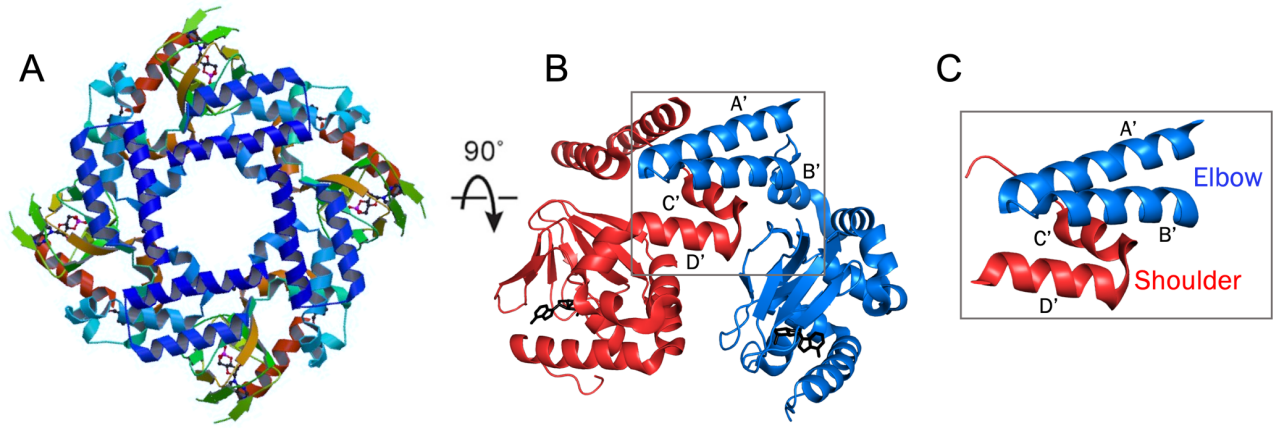

Fig. 11: "Elbow resting on the shoulder of the neighbour subunit". (A) Top view of the ribbon representation of the crystal structure of the cAMP-bound C-linker/CNBD fragment of mHCN2. The four C-linkers are shown in blue. (B) Lateral view showing the contacts between the helices of the C-linkers of two adjacent subunits. (C) Magnification of (B): the helices A' and B' ("elbow") of the blue subunit in lie on the helices C' and D' ("shoulder") of the red subunit. (PDB_ID: 1Q5O; Zagotta et al.; 2003)

The crystal structures of the C-linker/CNBD fragments detached from the pore domain show that, upon the binding of cAMP to the CNBD domain, the fragments adopt a tetrameric conformation, with a four-fold symmetry reminiscent of the intact channel (fig.11 A). Particularly, the crystals revealed that the four monomers interact at the level of the C-linker domain according to a conformation defined as "elbow resting on the shoulder of the neighbour subunit". Indeed, in this conformation the first two helices A' and B' of a subunit, i.e. the so called "elbow", form an antiparallel helix-turn-helix motif that interacts with the helices C' and D', i.e. the so called "shoulder", of the neighbouring subunit, as if they leaned against each other (Zagotta et al., 2003) (fig. 11 B and C).

Subsequent electrophysiological studies on the full-length HCN2 channel demonstrated that the "elbow on the shoulder" conformation adopted by the C-linkers upon cAMP binding, does not correspond to the active conformation of this domain induced by the interaction with the cyclic nucleotide. Indeed, these fine works showed that in the full-length channel the C-linker undergoes great cAMP-induced conformational changes, that do not reflect the arrangement adopted in the crystal. Thus, in the crystallographic structures even if the cAMP-bound CNBD adopts the active conformation, the C-linker is actually in a resting conformation (Craven and Zagotta, 2004; Craven et al., 2008). Furthermore, functional and spectroscopic works performed on HCN C-terminal fragments demonstrated that the C-linker behavior is opposite to that of the CNBD domain, which is functional even if isolated from the channel pore (Lolicato et al., 2011; Saponaro et al., 2014).
Taken together, these data indicate that the C-linker plays undoubtedly a fundamental role in the mechanism of propagation of the cAMP-induced opening signal. Particularly, it is possible to conclude that the C-linker domain must be connected not only to the CNBD but also to the pore domain in order to be in an active state.
However, the comparison between the cAMP-free and -bound cryo-EM structure of hHCN1 failed to reveal any large-scale conformational change in the C-linker domain (fig. 12). Indeed, both apo and holo structure show that the C-linker helices are arranged according to a gating ring reminiscent of the conformation observed in the crystals of the cAMP-bound C-terminal fragments (Zagotta et al., 2003; Xu et al., 2010; Lolicato et al., 2011; Akimoto et al., 2018). Probably, this reduced degree of perturbation by cAMP of HCN1 is caused by the fact that, as shown by previous functional data, in the apo state the C-terminal domain fragment of HCN1 has a significantly greater propensity for tetramerization than the one of either HCN2 and HCN4 (Lolicato et al., 2014). Indeed, the structures reveal only a subtle, counterclockwise rotation of about 1 Å (opposite to the right-handed twist of the S6 helical bundle) of the intracellular domains relative to the transmembrane region (Lee and MacKinnon, 2017). In physiological conditions, this slight rotational movement is thought to go through a further rotation that could dilate the bundle of S6 helices and allow ion permeation (James and Zagotta 2018).

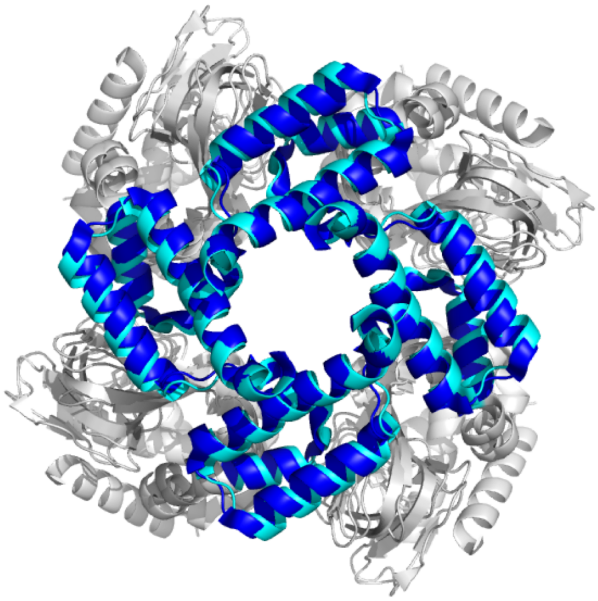

Figure 12: The C-linker movements are inhibited by the VSD in the resting state. Top view of the superimposed cAMP-free (apo, in blue) and cAMP-bound (cyan) cryo-EM structures of hHCN1 (PDB_ID: 5U6O and 5U6P respectively) (Lee and MacKinnon, 2017). In order to facilitate the vision of the four C-linker domains, the transmembrane helices were removed.

Actually, these results are not surprising because the cryo-EM structures of HCN1 were solved at 0 mV. In this condition the VSD is blocked in the resting state. As a result, the VSD inhibits the movements of both the pore and C-linker domains, which are under its allosteric control (Wahl-Schott and Biel, 2008; Lee and MacKinnon, 2017; James and Zagotta 2018).

Thus, these structures show static channel "snapshots", providing limited information about the energetics of the conformational changes that characterize each domain, whose combination results in opening of the channel.

Moreover, previous works showed that cAMP alone is not sufficient to open HCNs. Indeed, in the absence of hyperpolarizing voltages, the channel remains closed even in the presence of high concentrations of cAMP (Gauss et al., 1998; Ludwig et al., 1998; Santoro et al.,1998).

These structural and functional studies suggest that the movement of the C-linker domain must be under the control of the voltage, implying the existence of a direct physical contact between the VSD and the C-linker.

Given these observations, it clearly emerges that up to now there are still no structural data that show the cAMP-induced conformational changes that characterize the active C-linker domain. Thus, further investigations are deserved.

1.6 cAMP modulation of the assembly of HCNs C-terminal domains

As previously mentioned (see chapter 1.1 to 1.3 of this section) HCN channels are tetrameric complexes consisting of either identical (homomeric) or different (heteromeric) types of subunits. Their activity is dually regulated by the hyperpolarization of membrane potential and the binding of cAMP at the level of the CNBD domain. Particularly, the binding of the cyclic nucleotide to the CNBD removes the autoinhibitory action exerted by this domain on the channel activity. Indeed, cAMP induces conformational changes in the CNBD that are propagated through the C-linker domain to the pore. The result is an increase of the open probability of channel (Wahl-Schott and Biel 2008; Zagotta et al., 2003). However, it is still unknown how HCNs are activated by the cooperative action of the subunits.

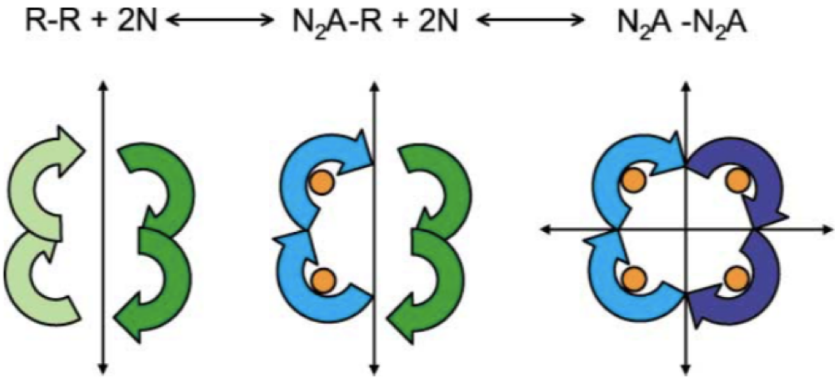

Figure 13: The 4-fold gating ring induced by cAMP arises from a dimer of dimers symmetry. The model was proposed for cAMP- from Ulens and Siegelbaum (2003). The C-terminal regions of the four subunits of HCN channel are suggested to associate as a dimer of dimers in the absence of ligand. The binding of cAMP causes a structural rearrangement that promotes the formation of the gating ring. This event is mediated by the C-linker domain. The letter R refers to a dimer in the resting state; letter A refers to a dimer in the active state; N is the cAMP.

Several works suggest that cAMP action is not limited to the abolishment of the self-inhibitory system controlled by the CNBD. Indeed, there are growing evidences that show a key role of cAMP in inducing the tetramerization of the C-terminal regulatory region of the HCN channels. Indeed, electrophysiological data performed on HCN2 suggest that in the absence of cAMP the tonic inhibition of CNBD on the channel arises from a 2-fold dimer of dimers symmetry of the C-terminal domains. The formation of this symmetry is mediated by neighboring C-linkers. The

opening of the channel is then enhanced by the binding of cAMP that promotes the assembly of a 4-fold symmetrical gating ring (Ulens and Siegelbaum, 2003; Kush et al., 2012).

Furthermore, structural data of the isolated C-linker/CNBD of both HCN2 (Zagotta et al., 2003) and HCN4 (Xu et al., 2010; Akimoto et al.; 2014) channels showed that the presence of cAMP determines the tetramerization of the fragments. Particularly, the four helices of the C-linker composing the C-linker/CNBD tetramerization domain, are stabilized upon tetramer formation by the so called "elbow on the shoulder" arrangement (Zagotta et al., 2003; Akimoto et al., 2014).

Size exclusion chromatography and analytical ultracentrifugation performed on HCNs C-linker/CNBD fragments showed that in the absence of cAMP the protein tend to be in monomeric and dimeric states, whereas the addition of cAMP promotes the tetrameric state (Lolicato et al., 2011). However, the tendency of the C-linker/CNBD fragments to tetramerize upon cAMP binding differs among HCNs since each isoform has a different affinity for cAMP. Indeed, the isolated C-terminal domain of HCN1 has a higher propensity to tetramerize than those of HCN2 and HCN4. This phenomenon is probably due because HCN1 is able to trap endogenous cAMP in the CNBD (Lolicato et al., 2011). Notably, once again was demonstrated that the mediation of the C-linker domain is required in the cAMP-induced tetramerization for forming the 4-fold symmetrical gating ring that promotes the opening of the channel (Lolicato et al. 2011).

The transition from the 2-fold symmetrical dimer of dimers conformation to the 4-fold tetrameric gating ring upon cAMP binding to the CNBD is supported also by MD simulations experiments. Indeed, from MD simulations of apo-HCN4 C-linker/CNBD fragment in a dimeric state, it has been proposed a model for the explanation of the autoinhibitory action exerted by the CNBD on the channel opening. The model hints that the tetrameric gating ring arises from a dimer of dimers conformation of the C-terminal domains. Indeed, in this assembly, the inactive CNBD domain do not sterically clashes with the C-linker domain, a phenomenon that, on the other hand, is observed when the cAMP-unbound C-terminal domain assume a tetrameric assembly. cAMP induces the release of the autoinhibitory effect by causing conformational changes in the CNBD that promote the tetrameric assembly (Akimoto et al., 2018; VanSchouwen and Melacini, 2018).

Moreover, in support of these conformational arrangements that seem to characterize the C-terminal domains of HCN channels there are structural data performed on intact Cyclic Nucleotide-Gated (CNG), that, as HCNs, belong to the family of CNBD channels and the superfamily of voltage-gated K^+ channels. Indeed, electron microscopy and image processing on full-length CNG channel showed that the four CNBD domains present in each tetrameric channel tend to associate as a dimer of dimers in the absence of ligand (Higgins et al. 2002).

Taken together, these data suggest the binding of cAMP enhances the opening of HCN channel by promoting the assembly of a 4-fold symmetric gating ring from a state in which the four subunits interact as a 2-fold symmetric dimer of dimers. However, up to now there were no structural data on a full-length channel in support of this model, leaving open the investigation of HCN dimers and their regulatory role.

2. Aim of the work

The goal of this work is to describe the propagation of the movements caused by the binding of cAMP to the CNBD of HCN channels through the C-linker to the pore domain. Indeed, understanding the molecular mechanism and the structural dynamics determined by cAMP binding to HCN will allow to comprehend many important physiological processes and to develop new therapeutic approaches for HCN-related diseases.

From the works aforementioned it emerged that, in order to characterize the conformational changes and the dynamics of an active C-linker domain, it is necessary to perform structural studies on the full-length protein. Namely, the C-linker domain must be properly connected to the pore at its N-terminus and to the CNBD at its C-terminus, respectively.

Another problem that has to be overcome is the presence of the VSD in the wild type channel. As mentioned above, the resolution of structures using cryo-EM (as well as other techniques aimed to solve protein structures) is performed at 0 mV, which is a condition that locks the VSD in the resting state. In this configuration, the VSD inhibits the movements of both the pore and C-linker domains, which are under its allosteric control (Wahl-Schott and Biel, 2008; Lee and MacKinnon, 2017; James and Zagotta, 2018). Moreover, recent electrophysiological and computational studies based on a close inspection of HCN1 structures suggest that the interactions between the VSD and the C-linker domain are mechanically mediated by the HCND (Porro et.al, submitted).

Thus, in order to overcome these obstacles and to obtain structural information about the dynamics that characterize the C-linker domain, I decided to take advantage of a synthetic biology approach. To this end, I engineered a chimeric protein by fusing the pore domain of the prokaryotic potassium channel KcsA with the regulatory cytoplasmic C-linker/CNBD region of the human HCN4 channel (hereinafter referred to as K-H4).

KcsA is a well-characterized potassium channel with known crystal and NMR structures (Doyle et al., 1998; Chill et al., 2006). Thanks to its versatility and high expression level, KcsA has been used as a reference system for the study of structure-function relations of potassium channels. Indeed, the structure of KcsA has been used as a model template for the study of the pore domain of HCN channels (Cheng et al., 2007; Bucchi et al., 2013).

Like HCN, KcsA (from *Streptomices lividans*) is a tetramer formed by four identical subunits (fig.1A). Each subunit is constituted by two transmembrane alpha-helices called M1 and M2 that are connected by a loop region forming the pore helix and the selectivity filter (fig.1B). The N- and C-terminal regions of the protein are located cytoplasmically. The four subunits assemble to

form a membrane spanning conduction pathway. Particularly, the M2 transmembrane helix of each subunit is lining the central aqueous pore, while the M1 helices are in direct contact with the phospholipid bilayer (Doyle et al., 1998; Williamson et al. 2003).

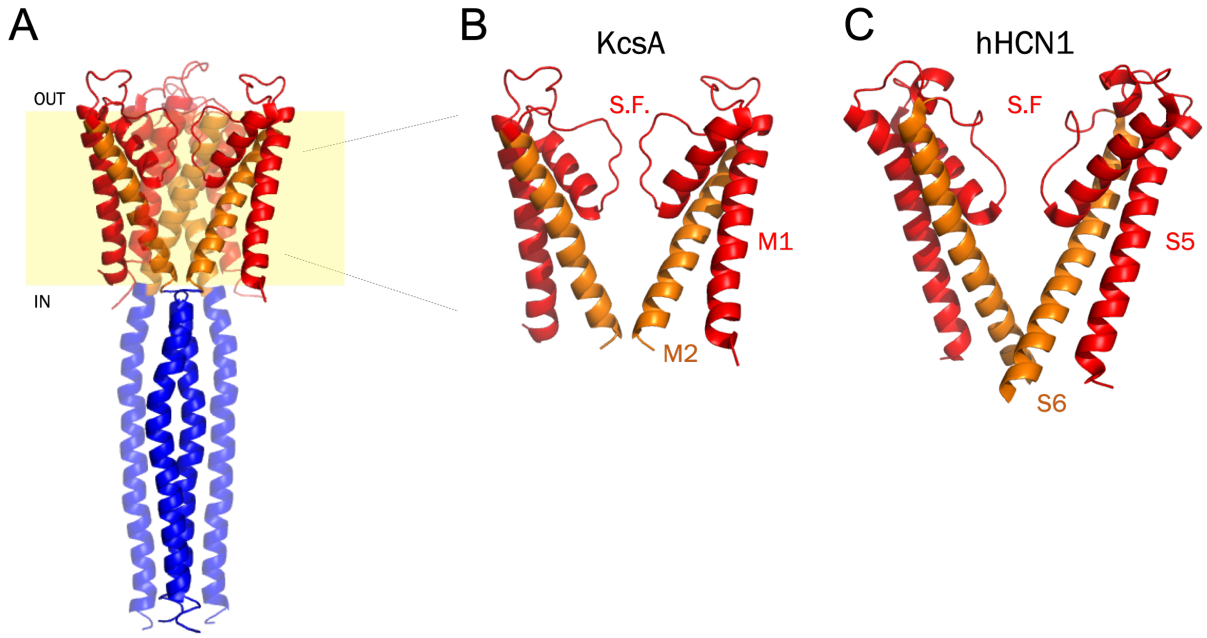

Figure 1: KcsA is a well characterized K^+ channel used as homology model for the pore region of HCN. (A) Cartoon representation of the crystal structure of full-length KcsA (PDB_ID:3EFF, Uysal et al., 2009). The transmembrane domain is colored in red/orange and the C-terminal domain is highlighted in blue. The N-terminal 22 aa are not visualized because of intrinsic disorder. (B) Representation of two of the four subunits forming the pore domain of KcsA. M1 helix is colored in red, M2 is colored in orange and the selectivity filter is indicated with S.F. (C) Representation of two of the four subunits forming the pore domain of HCN1. S5 helix is colored in red, S6 is colored in orange and the selectivity filter is indicated with S.F. (PDB_ID: 5U6O, Lee and MacKinnon, 2017). The comparison between the two structures shows that KcsA and HCN1 share architectural similarities.

Each of the four subunits contributes to the formation of the selectivity filter which contains four K^+ binding sites, a relatively large cavity lined by hydrophobic residues and the activation gate. The selectivity filter is characterized by the signature sequence TVGYG, which is typical for the selectivity filters of all known potassium channels (Doyle et al., 1998; Chill et al., 2006). Furthermore, KcsA does not possess a VSD, as the activity of the wild type channel is not modulated by changes in membrane voltage, but by changes in pH (Thompson et al., 2008).
Moreover, the high versatility of KcsA has been already demonstrated by the successful engineering of chimeric membrane proteins. In these previously published works, the pore domain of KcsA revealed to be a stable and functional building block. Indeed, once it was fused to the

CNBD domain from different prokaryotic cyclic nucleotide-gated channels, the pore domain of KcsA did not lose its conductivity and, indeed, promoted the generation of functional chimeric proteins (Ohndorf and Mackinnon, 2005; McCoy et al., 2014). However, contrary to K-H4, these prokaryotic chimeric channels do not have the C-linker domain.

Hence, given these evidences, it was reasoned that fusing the C-linker/CNBD of hHCN4 to the pore domain of KcsA channel would reflect a condition that resembles as close as possible the physiological one, i.e. of the wild type channel. The use of the pore of KcsA allows the investigation of the dynamics underlying the cAMP-induced interactions between the C-linker/CNBDs of all four subunits in a tetrameric assembly. Thus, this condition should allow the visualization of an active C-linker domain. Particularly, the use of the chimeric channel for studying the structural rearrangements of the C-linker should be advantageous compared to the wild type eukaryotic channel due to the absence of both the VSD and the HCND. This should allow the visualization of the conformational changes and dynamics of the C-linker and, eventually, of the pore domain upon cAMP binding.

In summary, the aim of this work is to engineer a functional chimeric protein consisting of the pore domain of the prokaryotic potassium channel KcsA and the C-linker/CNBD domain of HCN. Once a stable and functional chimera is obtained, the protein will be used to perform structural studies using EPR and DEER, which are spectroscopic techniques that allow to follow the dynamics of an active C-linker domain and, thus, to understand the molecular basis of cAMP modulation of HCN channel activity.

3. Results and discussion

3.1 Construction and expression of the chimera

3.1.1 K-H4ΔN FQ aggregates in the absence of cAMP

The creation of the KcsA - HCN4 C-linker/CNBD chimera (hereafter K-H4ΔN) is the result of the functional fusion between the pore domain of the prokaryotic potassium channel KcsA and the C-linker/CNBD of the human HCN4 channel. Specifically, the N- and C-terminal cytoplasmic regions of KcsA have been removed and the C-terminal domain was substituted with the C-linker/CNBD of HCN4. Indeed, previous studies (Chill et al., 2006) showed that the deletion of the first amino acid residues at the N-terminus of KcsA increases the thermostability of the channel compared to the wild type (WT) (Chill et al., 2006).

Finding the correct junction between different proteins is the major limitation in obtaining a stable and functional chimeric protein. The connection between the pore domain of KcsA and the C-linker/CNBD of HCN4 has required some engineering effort and is based on a previous work from Ohndorf and MacKinnon (Ohndorf and MacKinnon, 2005) that created a functional chimera by fusing the pore domain of KcsA to the CNBD domain of the prokaryotic RP-CNG channel (*Rhodopseudomonas palustris* Cyclic Nucleotide Gated channel). In this relevant work, they identified the correct attachment site between the two prokaryotic domains at the level of F114, which is at the end of the second transmembrane region (M2) of KcsA and S252, the first residue of the C-linker of the RP-CNG channel. Therefore, based on these data, the first junction between the two components that I created was at the level of phenylalanine F114 of KcsA and glutamine Q518 of hHCN4, which is the first residue of the C-linker domain of HCN4. This construct is called K-H4ΔN FQ and is shown in figure 1A. Unfortunately, the expression and the subsequent purification of this chimeric construct showed that K-H4ΔN FQ tended to aggregate in the cAMP-free state. Indeed, as shown by the black chromatogram of figure 1B, the chimera in the apo state eluted mostly in correspondence of the void volume of the chromatographic column. This behavior is typical of aggregated proteins. Surprisingly, this phenomenon was absent upon cAMP application. As shown by the red chromatogram of figure 1B, in the presence of cAMP, the tetrameric channel FQ is soluble. Indeed, the cAMP-bound chimera elutes as a monodisperse peak consistent with the molecular weight of the tetramer (i.e. expected MW: 152 kDa). This data

suggest that the aggregation was caused by the exposure of residues, that are not exposed in the cAMP-bound state.

Moreover, on SDS-polyacrylamide gel, the chimera migrates as a single band corresponding to the tetramer (Fig. 1C, lane 1), thus showing the typical stability of pore-forming potassium channels under denaturing conditions (Pagliuca et al., 2007).

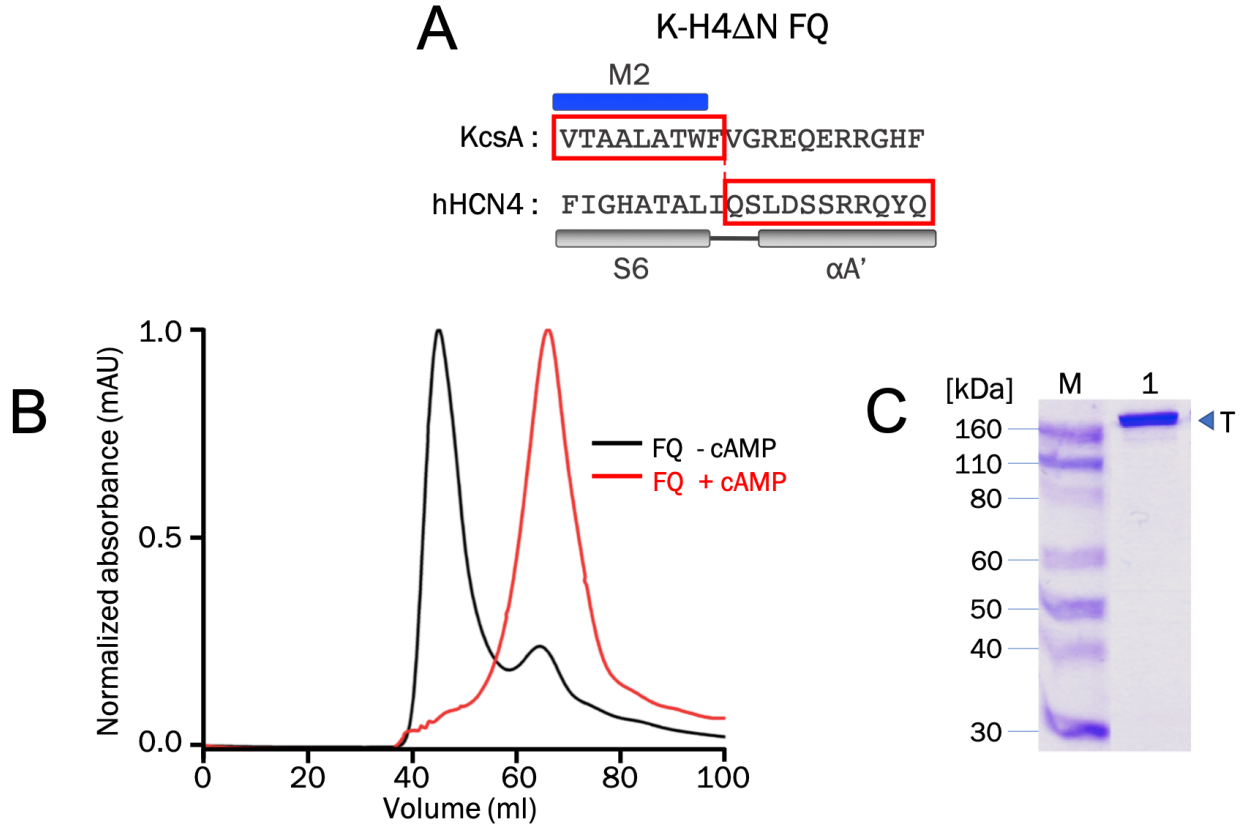

Figure 1: K-H4ΔN FQ is soluble only in the holo state. (A) Construction of K-H4ΔN FQ. Schematic representations of the partial alignment between the amino acid sequences of KcsA and the human HCN4. Red boxes highlight part of the residues of KcsA M2 helix and of hHCN4 C-linker that form the chimera and the amino acids at the level of whom occurs the junction between the two components, i.e. KcsA's F114 and hHCN4's Q518. α-helices are represented with colored planks: KcsA M2 transmembrane helix is blue. hHCN4 S6 transmembrane helix of pore domain, that structurally corresponds to M2 helix, and N-terminal C-linker αA' helix are in grey. (B) Superimposed chromatograms of the gel filtration of K-H4ΔN FQ purified in the absence (black chromatogram) and in the presence of cAMP (red chromatogram). The absorbance values on the ordinate axis were normalized according to the maximum value obtained in the relative experiment. (C) SDS-PAGE analysis of the chimera FQ. The arrowhead marked with letter T indicates the band relative to the tetrameric for of the channel. M: Marker (Novex® Sharp Pre-stained Protein Standards, Invitrogen).

3.2.1 *E.coli* strain C41(DE3) increases the expression level of the chimera

Since the aim of this project was to perform structural studies on the chimeric channel, optimizing the yield of protein production is fundamental because these techniques require large amounts of purified proteins, i.e. in the order of milligrams. Thus, I tested the *Escherichia coli* (*E. coli*) strain called C41(DE3), also known as Walker strain, which is derived from BL21(DE3) (Miroux and Walker, 1996). This strain is more suitable for the overexpression of membrane proteins compared to the so far used BL21(DE3) Codon Plus Rosetta™ (Novagen).

The comparison of the yield obtained with the two *E. coli* strains (Walker and Rosetta™) was performed with the construct K-H4ΔN FQ. The expression of the protein was induced using the same parameters previously set for Rosetta™ (i.e. 100 µM IPTG, overnight at 20°C in an orbital shaker at 75 RPM). Once the induction process was over, two samples from each of the two different cultures were collected and one of the two samples was boiled in order to disrupt the tetrameric form of the channel. Thus, after a previous electrophoretic run on SDS-PAGE, the samples were transferred on a nitrocellulose membrane and analyzed using the Western Blot technique in order to compare the level of expression of the membrane protein in both strains (Fig. 2).

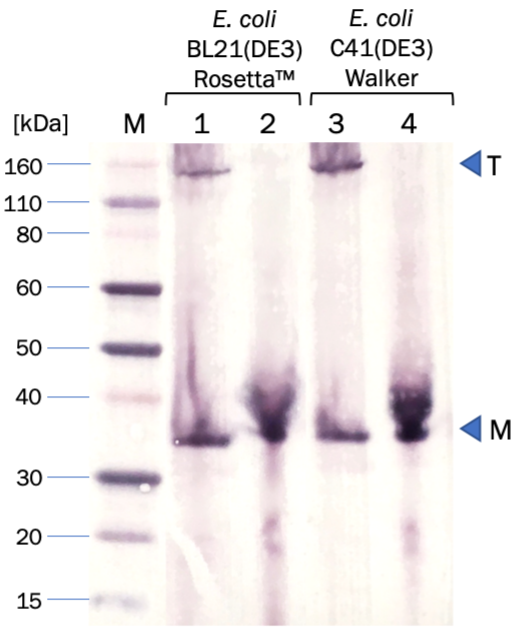

Figure 2: Walker strain expresses higher level of chimeric channel. Western Blot comparing the levels of K-H4ΔN FQ expression between the Rosetta and the Walker strains. The immunodecoration was made using a primary antibody against the His tag. For both the strains were used the same protein

expression parameters. For both the tested strains were loaded two samples of bacterial culture collected at the end of the induction process. M: Marker (Novex® Sharp Pre-stained Protein Standards, Invitrogen). Lanes 1 and 2: samples collected from Rosetta ™ culture. Lanes 3 and 4: samples collected from Walker culture. Samples in lanes 1 and 3 were not boiled. Samples in lanes 2 and 4 were boiled. Arrowhead marked with letter T: bands around 160 kDa that correspond to the tetrameric channel (expected MW: 152 kDa). Arrowhead marked with letter M: bands between 30 kDa and 40 kDa that correspond to the monomer (expected MW: 38 kDa).

The immunodecoration was made using a primary antibody that is able to detect the His-Tag positioned at the N-terminus of the chimeric protein (see chapter 5.3 of the section "Material and Methods"). The performed Western Blot of figure 2 revealed that the protein is produced in both strains and migrates in two bands, at about 160 kDa and above 30 kDa, which are the expected molecular weights of the tetrameric form (152 kDa) and monomeric form (38 kDa) of the channel. Boiling the samples (lanes 2,4) converts the tetramer into monomer, a well-known properties of potassium channels (Pagliuca et al., 2007). The comparison between the intensity of the bands suggested that with the Walker strain it was possible to slightly increase the yield of expressed protein.

Moreover, in order to prove this result, the protein K-H4ΔN FQ expressed from Rosetta^{TM} and from Walker strain was purified in the presence of cAMP following the protocol previously set (see chapter 5.2 of the section "Material and Methods"). In order to obtain comparable results, in both the cases the purification was performed starting from the same volume of bacterial culture. Once the solubilized membrane protein was purified with nickel affinity chromatography, each sample was analyzed with size-exclusion chromatography (SEC), a technique also known as gel-filtration chromatography (see chapter 5.2.3 of the section "Material and Methods"). Figure 3 shows the superimposition of the gel filtration elution profiles obtained for the chimeric protein K-H4ΔN FQ purified respectively from Rosetta^{TM} and from Walker strain. Observing the chromatograms, in both cases at 40 mL there is a first peak that has an elution profile typical of an aggregate since it elutes in correspondence with the void volume of the column. At 60 mL there is a second peak that corresponds to the expected elution profile of the soluble tetrameric form of the chimeric protein.

Notably, the comparison between the height of these last peaks at 60 mL obtained from the two different cultures already suggests that the C41(DE3) Walker strain is able to produce a higher amount of channel protein compared to Rosetta^{TM} (fig. 3). For each different sample the fractions

corresponding to the peak containing the soluble tetrameric protein were collected and pooled together.

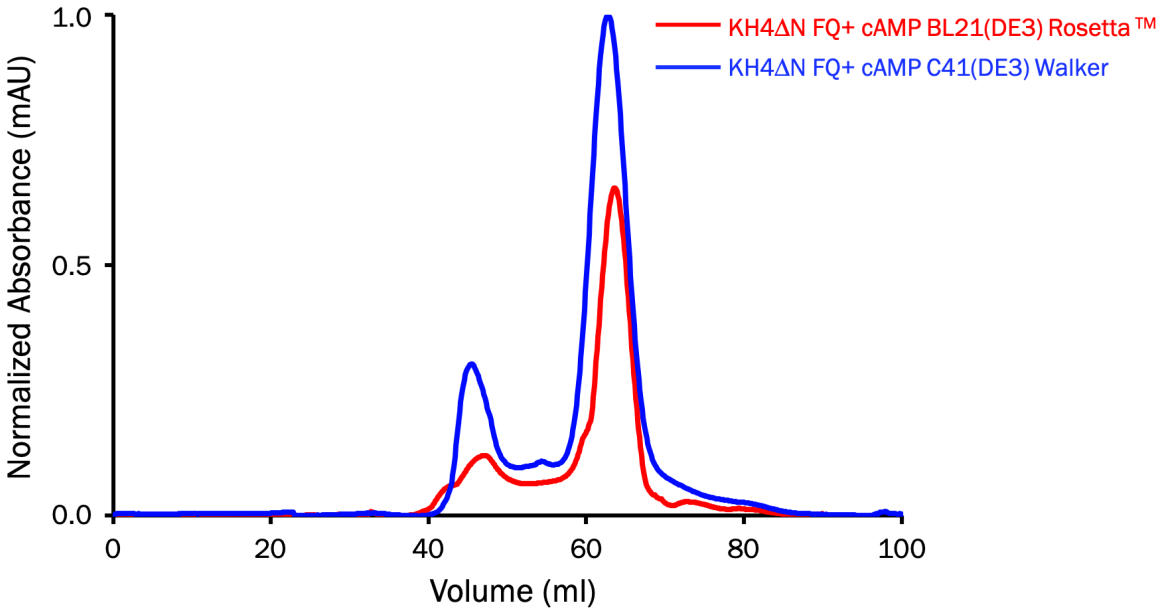

Figure 3: Walker strain increases the yield of chimeric protein. Superimposed chromatograms of the gel filtration of K-H4ΔN FQ purified in the presence of 200 μM cAMP. The elution profiles are relative to the extraction of the chimera from the membranes of the E. coli strains RosettaTM (in red) and Walker (in blue). The absorbance values on the ordinate axis were normalized according to the maximum value obtained in the relative experiment.

The quantification of the amount of purified protein determined that the use of the Walker strain leads almost to a doubling of the yield of purified cAMP-bound chimera. To be more precise, it was obtained 0.5 mg of protein from 1 L of Rosetta^{TM} culture, while 0.8 mg of protein was obtained from the same volume of the Walker culture. Given this result, I decided to use the *E. coli* Walker strain as organism for the heterologous expression of the chimeric channels.

3.2.2 Re-engineering of the junction between the pore and the C- linker/CNBD

The key to success in constructing a functional chimeric protein is the identification of the proper connection between the two elements. The creation of the chimeric protein K-H4ΔN FQ (see chapter 1.1. of this section) demonstrated that the direct fusion between two functional domains may face many different pitfalls such as misfolding events and aggregation of the sample.

The data obtained with the construct FQ suggested that the aggregation in the apo form of the chimera might depend on the junction between the pore and the C-linker domain. Indeed, I

excluded a misfolding of the pore domain since on SDS-PAGE the chimera migrates as a single band corresponding to the tetramer (fig. 1C). This is an indication of the proper four-fold subunit assembly of the channel (Pagliuca et al., 2007). Moreover, the aggregation seems not to be related to a misfolding of the CNBD domain. This is supported by the observation that the aggregation phenomenon is solved upon addition of cAMP, suggesting that the protein can bind and respond to the ligand (see gel filtrations in fig. 1B). Thus, aggregation rather may be caused by the exposure of residues at the junction level between the pore and the C-linker domain, that are not exposed in the cAMP-bound state.

Thus, in order to achieve a stable and functional protein in both cAMP-bound and -free state, I decided to empirically elongate the helix that connects the transmembrane part of the chimera to the C-linker domain. To this end, I decided not to take advantage of a rationally designed linker but rather to use the amino acids that are part of the helix that naturally follows the M2 helix in KcsA. This could determine the proper arrangement of all the elements that compose the chimera. Based on this idea, I gradually added pairs of residues that in the primary sequence of KcsA are downstream to the phenylalanine F114 previously used in the creation of FQ chimera. The glutamine Q518 of hHCN4 was maintained as junction point on the C-linker domain of the eukaryotic channel (fig. 4).

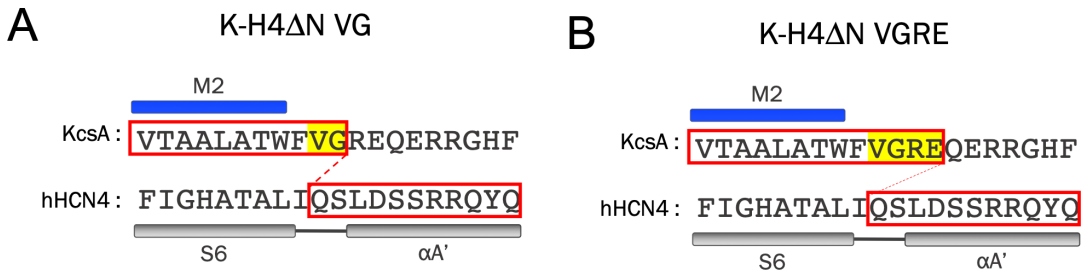

Figure 4: Construction of KcsA-hHCN4 C-linker/CNBD chimera. (A) and (B) are schematic representations of the partial alignment between the amino acid sequences of KcsA and the human HCN4. Red boxes highlight part of the residues of KcsA M2 helix and of hHCN4 C-linker that form the chimera and the amino acids at the level of whom occurs the junction between the two components in each different construct: (A) KcsA G116 and hHCN4 Q518 (hereafter called K-H4ΔN VG) and (B) KcsA E118 and hHCN4 Q518 (hereafter called K-H4ΔN VGRE). α-helices are represented with colored planks: KcsA M2 transmembrane helix is blue. hHCN4 S6 transmembrane helix of pore domain, that structurally corresponds to M2 helix, and N-terminal C-linker αA' helix are in grey.

The first construct was generated by insertion of the apolar amino acids valine V115 and glycine G116 of KcsA (this construct is hereinafter referred to as K-H4ΔN VG, fig. 4A). The second

construct (hereinafter referred to as K-H4ΔN VGRE, fig. 4B) was created by the further incorporation of the amino acids arginine R117 and glutamate E118 of KcsA.

3.2.3 Setting the expression parameters

For testing the new constructs K-H4ΔN VG and K-H4ΔN VGRE, we transformed the *E. coli* Walker strain with the expression vectors carrying the genes of interest. In order to find the best expression conditions for the two new constructs, several expression tests were performed. To this end the main parameters that characterize protein expression were varied: the inducer concentration (i.e. 100 μM or 400 μM), the temperature (i.e. 37°C or 20°C) and the induction phase duration (i.e. 3 hours or overnight) (see chapter 5.2.2 of the section "Material and Methods"). Once the induction process was finished, two samples were collected from each of the two differently treated cultures. One of the two samples was boiled in order to disrupt the tetrameric form of the channel. After separating the samples on SDS-polyacrylamide gel, a Western Blot was performed in order to compare the expression levels of the recombinant membrane proteins under the aforementioned different expression conditions. Once again, the immunodecoration was made using a primary antibody that is able to detect the His-Tag at the N-terminus of the chimera (fig. 5A and B). The performed Western Blots (fig. 5 A and B) revealed that both K-H4 ΔN VG and K-H4 ΔN VGRE have been expressed in all the tested conditions. These chimeric channels migrate mainly in three bands. The first band at 160 kDa correspond to the tetrameric form of the chimera (expected MW: 152 kDa) (fig. 5A and B, bands indicated with letter T). The second band is present above 30 kDa and corresponds to the monomeric form of the chimera (expected MW: 38 kDa) (fig. 4A and B bands indicated with letter M). Both the chimeric constructs K-H4 ΔN VG and VGRE remain a tetramer when assayed by SDS-PAGE in the absence of heating (N.B. lanes, band at 160 kDa). Only after boiling the tetrameric assembly completely disassociates into monomers (B. lanes, band above 30 kDa).

The third band identified by the letter D corresponds, presumably, to degradation products of the chimeric constructs. Indeed, since the overexpression of ion channels is often toxic for the host organism, the target protein can run into proteolytic degradation (Wagner et al., 2008). Notably, when the expression of the proteins was induced at 37°C for 3 hours, with both 100 μM and 400 μM IPTG, the amount of degradation products is higher, as suggested by the intensity of the relative bands and by their increasing number. Given these results, 37°C was rejected as possible optimal temperature for inducing the expression of both the constructs.

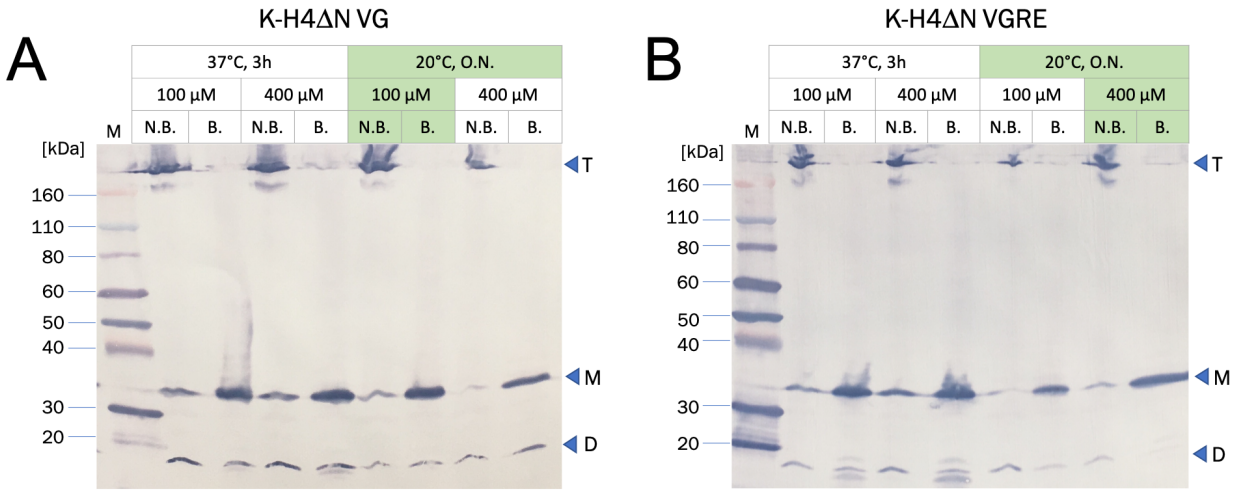

Figure 5: **Setting the expression parameters.** Western Blots revealing the best parameters for the expression of the chimeric proteins (A) K-H4ΔN VG and (B) K-H4ΔN VGRE. The immunodecoration was made using a primary antibody against the His tag. For both (A) and (B) the samples analyzed were collected at the end of the induction phase. For each bacterial culture two samples were loaded. One sample was not boiled (i.e. N.B.), and one was boiled (i.e. B.). The table above each western blot summarizes the parameters that characterized the induction of the expression of VG or VGRE in the underlying sample. In green are highlighted the best parameters identified for the induction of each protein. In both (A) and (B) the expression of the protein was induced at 37 °C for 3 hours or at 20 °C overnight (i.e. O.N.) using 100µM or 400µM IPTG. In both (A) and (B) the arrow head marked with the letter T shows the bands around 160 kDa that correspond to the tetrameric form of the channel (expected MW: 152 kDa). The arrow head marked with the letter M shows the bands above 30 kDa that correspond to the monomer (expected MW: 38 kDa). The arrow head marked with the letter D shows degradation products. M: Marker (Novex® Sharp Pre-stained Protein Standards, Invitrogen.

On the other hand, when the protein expression occurred at 20°C overnight (O.N.), with both 100 µM and 400 µM IPTG, the bands relative to the degradation products are less intense for the construct VG (fig. 5A, lanes 20°C, O.N., arrowhead marked with letter D) and even disappear concerning the construct VGRE (fig. 5B, lanes 20°C, O.N., arrowhead marked with letter D).

By making a comparison between the intensity of the bands relative to the tetrameric form of the channel, it emerged that, concerning K-H4 ΔN VG most of the protein is in the tetrameric state when the expression at 20°C is induced with 100 µM IPTG (fig. 5A, lanes highlighted in green). Whereas, the tetrameric protein K-H4 ΔN VGRE is expressed at its best at 20°C when the concentration of the inducer is 400 µM (fig. 5B, lanes highlighted in green). Therefore, given the high intensity of the bands relative to the tetrameric protein and given the low amount of degradation products, the optimal conditions for the protein expression resulted to be at 20°C,

O.N. with 100 µM IPTG for K-H4 ΔN VG and at 20°C, O.N. with 400 µM IPTG for VGRE construct. These conditions have therefore been adopted for the production of each different chimeric protein in all the experiments shown from now on.

The expression level of the two new constructs was compared with the one of the previously used K-H4ΔN FQ. To this end, samples of *E. coli* C41(DE3) cultures induced to express either K-H4ΔN FQ, VG or VGRE according to the parameters previously described, were run on SDS-polyacrylamide gel and then analyzed with the Western Blot technique (fig. 6). The immunodecoration was made using a primary antibody anti His-Tag. The performed Western Blot revealed that the bands corresponding to the tetrameric form of the chimeric channel are notably more intense in the lanes relative to the two new proteins compared to the one of the old construct (fig.6, lanes FQ, VG and VGRE, arrowhead marked with letter T).

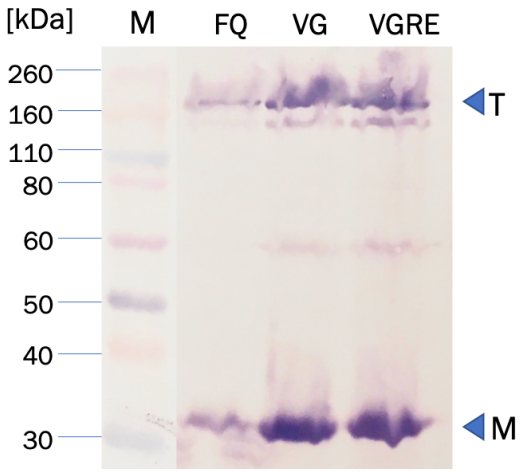

Figure 6: K-H4ΔN VG and VGRE are more expressed than FQ. Western Blot comparing the protein expression levels between the constructs K-H4ΔN FQ (lane FQ), VG (lane VG) and VGRE (lane VGRE). The immunodecoration was made using a primary antibody against the His-tag at the N-terminus of the chimeric channel. For each construct was loaded a sample of bacterial culture collected at the end of the induction process. The arrowhead marked with the letter T shows the bands around 160 kDa that correspond to the tetrameric channel (MW: 152 kDa). The arrowhead marked with the letter M shows the bands above 30 kDa that correspond to the monomer (MW: 38 kDa). M: Marker (Novex® Sharp Pre-stained Protein Standards, Invitrogen).

Thus, these data suggest that, compared to K-H4ΔN FQ, both the constructs VG and VGRE caused an increase in the expression level of the chimeric channel. Indeed, even if the bands relative to the monomeric form of the channel (fig. 6, arrowhead marked with letter M) have also a higher

intensity compared to the one of FQ, both K-H4ΔN VG and VGRE determined a high expression of chimeric potassium channels able to maintain the tetrameric form even in denaturing conditions.

Given these results, in order to test the protein stability and the yield of both K-H4ΔN VG and VGRE, we proceed with the large-scale purification of the two chimeric constructs.

3.2 Purification of the new chimera

3.2.1 K-H4ΔN VG and VGRE are soluble even in the absence of cAMP

Once the best condition for the expression of the two new constructs K-H4ΔN VG and VGRE were set, the proteins were purified in the absence of cAMP. This was done in order to test if the modifications of the junction between the pore and the cytoplasmic domain determined an improvement in the stability of the chimera. Indeed, as previously mentioned, the expression of the so far used construct K-H4ΔN FQ originated a chimera soluble and stable only in the presence of the ligand. For both the constructs, the purification was done starting from 1L of cellular culture.

The extraction process of the proteins from the membranes was performed according to the protocol described in chapter 5.2.3 of the section "Material and Methods". The detergent used to solubilize the membranes was n-Decyl-β-D-Maltopyranoside (DM). The use of a surfactant is necessary to extract the protein of interest from the membranes and to keep it in solution inside micelles. These latter are structures that mimic the hydrophobic environment in which the pore domain is inserted. Subsequently, taking advantage of the six-histidine tag at the N-terminus of the chimeric proteins, the first purification process was carried out using a nickel resin affinity column. Then, the isolated proteins were subjected to a second purification step, the gel filtration, in order to test the oligomeric state of each of the two chimeric constructs.

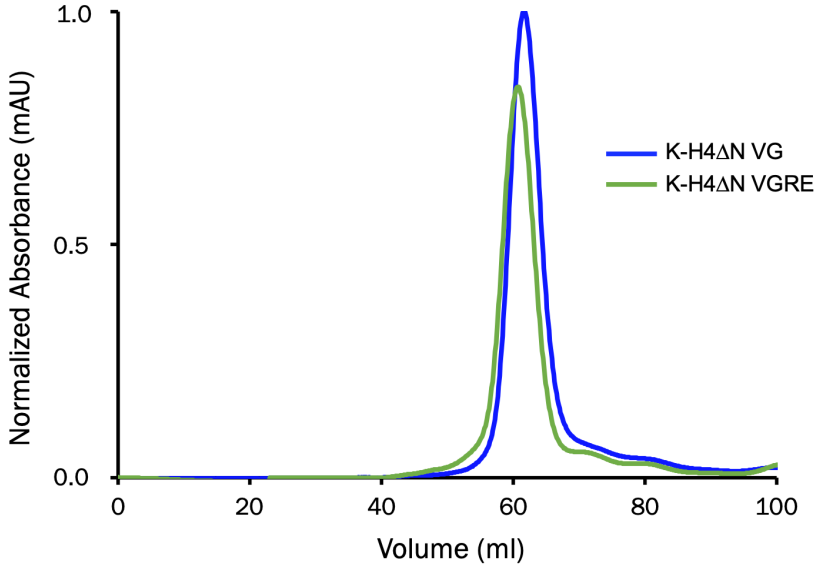

Figure 7: Purification of K-H4ΔN VG and VGRE. Superimposed chromatograms obtained from the gel filtration of the chimeric proteins K-H4ΔN VG (blue) and VGRE (green). The purification was in the absence of cAMP. The absorbance values on the ordinate axis were normalized according to the maximum value obtained in the relative experiment.

In figure 7 are shown the superimposed gel filtration elution profiles obtained for the chimeric protein K-H4ΔN VG and VGRE. Surprisingly, both the constructs VG and VGRE eluted as a monodisperse peak at 60 mL that is consistent with the molecular weight of the soluble tetramer. Thus, I have been finally able to obtain soluble chimeras also in the cAMP-free form. An additional proof of the improvement in the stability of both new chimeric constructs is the fact that the peak at 40 mL, which indicated the presence of aggregated proteins in the chromatogram of the FQ construct, is not present in the elution profiles of the new constructs. However, since K-H4ΔN VGRE tended to precipitate during both the extraction and the purification procedures, we decided to perform all the following experiments using K-H4ΔN VG, that showed a more stable behavior.

3.2.2 cAMP increases the amount of soluble K-H4ΔN VG

The stability and solubility of the chosen protein K-H4ΔN VG in the presence of cAMP was assessed by applying the ligand at saturating concentration during the purification process, as described in chapter 5.2.3 of the section "Material and Methods". Figure 8 A shows the superimposed gel filtration elution profiles of the chimera obtained in the absence and in the presence of the cyclic nucleotide. Observing the chromatograms, it is possible to appreciate that,

even in the presence of the ligand, the protein eluted as a monodisperse peak consistent with the molecular weight of the soluble tetramer. Moreover, it clearly emerged that the addition of cAMP caused an increase in the amount of soluble protein. This evidence suggests that the cyclic nucleotide is binding to the cytosolic C-terminal region of the chimera and is altering the structural and/or dynamic properties of the chimeric channel.

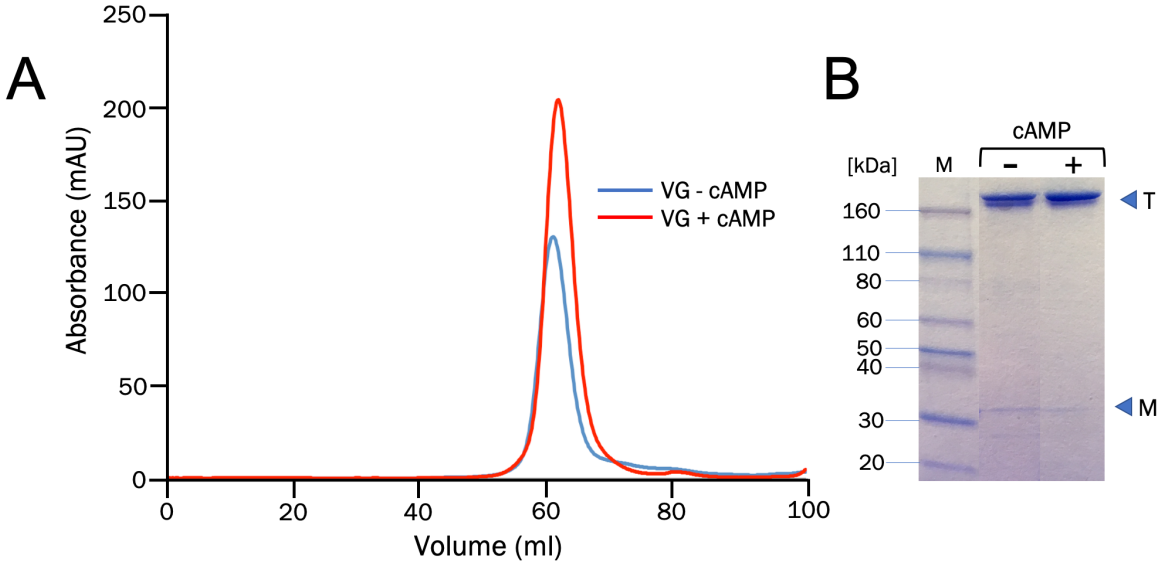

Figure 8: K-H4ΔN VG purification. (A) Superimposed chromatograms obtained from the gel filtration of the chimera purified in the absence (blue) and in the presence of 200 μM cAMP (red). (B) SDS-PAGE analysis of the peaks obtained in (A). Lane -: K-H4ΔN VG purified in the absence of cAMP. Lane +: protein purified in the presence of cAMP. Arrowhead marked with letter T: bands relative to the tetrameric channel (MW:152 kDa). Arrowhead marked with letter M: bands relative to the monomer (MW:38 kDa). M: Marker (Novex® Sharp Pre-stained Protein Standards, Invitrogen).

Moreover, samples of the chimera purified in the apo and holo states were analyzed on SDS-polyacrylamide gel (fig. 8B, respectively lane - and +). In both conditions, the chimera migrated principally as a single band corresponding to the tetramer (expected MW: 152 kDa) (fig. 8B, band indicated with the arrowhead marked with letter T), which is an indication of the proper four-fold subunit assembly of the channel. In both lanes is further visible a very faint band between 30 and 40 kDa that corresponds to the monomeric form of the channel (expected MW: 38 kDa) (fig.8B, band indicated with the arrowhead marked with letter M).

Thus, given these results, it emerged that by adding two residues that are at the boundary between M2 and the cytosolic domain of KcsA, we have been able to purify the soluble chimeric protein

in both its apo and holo states. Moreover, the change in the junction level implicated an improvement in the yield of protein, going beyond to the milligram threshold of purified chimeric protein in the apo state, and reaching the 2 mg threshold of purified channel in the holo state, starting in both the conditions from 1L of cellular culture.

3.2.3 DM is the optimal detergent for the extraction of the chimera

Since the achievement of a good stability of the solubilized protein and, thus, of a high yield strictly depend on the detergent type and concentration, a challenging step of this project was the choice of the proper detergent for the protein extraction. So far, for the purification of the chimeric channel n-Decyl-β-D-Maltopyranoside (DM, CMC: (H_2O) ~ 1.8 mM, Anatrace) has been used. DM is a non-ionic glycosidic detergent that is usually used for KcsA purification (Doyle et al., 1998; Jiang et al., 2002; Chill et al., 2006). The polar head of DM is formed by a carbohydrate, i.e. maltose, while the hydrophobic tail is composed of an alkyl chain. As mentioned above, since this is a trial and error procedure because every membrane protein requires a specific detergent for its extraction, different detergents have been screened in order to find the best candidate for the achievement of a more stable chimeric channel and, especially, for a high yield. Detergents are chemically different concerning both the hydrophilic "head" group (non-ionic, ionic, zwitterionic) and the length of the hydrophobic "tail". Since ionic detergents are extremely effective in the solubilization of membrane proteins, but are frequently denaturing to some extent (Orwick-Rydmark et al., 2016), we screened as non-ionic and zwitterionic detergents respectively n-Dodecyl-β-D-Maltoside (DDM, CMC: (H_2O) ~ 0.17 mM, Anatrace) and Lauryldimethylamine-N-Oxide (LDAO, CMC: (H_2O) ~ 1-2 mM, Anatrace). DDM has a longer apolar chain than DM and has been already used for KcsA purification (Cortes and Perozo, 1997). The lipid-like surfactant LDAO is less denaturing than ionic detergents as it has a net neutral charge and an apolar alkyl chain similar to DM and, moreover, has a high extraction rate (Orwick-Rydmark et al., 2016).

Thus, in order to test the solubilization efficiency and the stability of the solubilized proteins, K-H4ΔN VG was extracted and purified using the two different detergents aforementioned (see chapter 5.2.3 of the section "Material and Methods").

The extraction of the chimera from the native membranes using 5 mM DDM caused the total precipitation of the chimeric protein after the overnight extraction process. Thus, it has not been possible to test the oligomeric state of the extracted chimera upon gel filtration. This data suggests

that DDM tends to bind to the chimeric protein with high affinity, causing significant denaturation events (Arachea et al., 2012).

Afterwards, 25 mM LDAO was tested for the extraction of the chimeric channel from the membranes. The protein extracted with the zwitterionic detergent was analyzed on a gel filtration column. Figure 9 shows the comparison between the elution profiles obtained for the chimera when extracted either with the so far used DM (in blue) or with LDAO (in grey). The performed gel filtration revealed that the chimera extracted with LDAO did not elute as a monodisperse peak consistent with the molecular weight of the soluble tetramer. Indeed, the principal peak was shifted through higher volume values and split in two. In correspondence of the void volume, there was also a peak correspondent to protein in the aggregate state. Moreover, once the fractions relative to the main peak at 60 mL were collected and pooled together, the protein tended to precipitate.

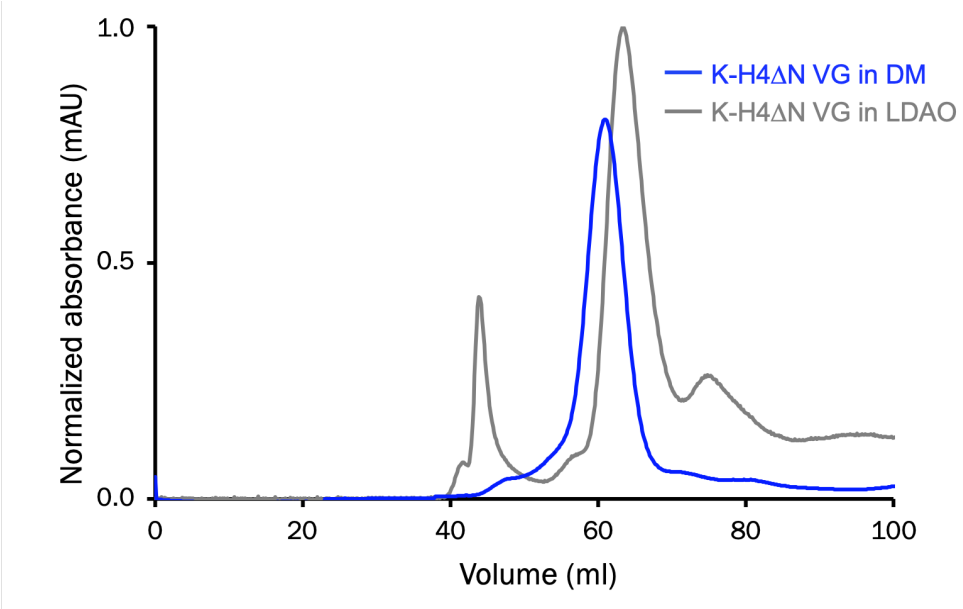

Figure 9: LDAO destabilizes the protein. Superimposed chromatograms obtained from the gel filtration of the chimeric protein K-H4ΔN VG extracted with either DM (blue) or LDAO (grey). The purification was in the absence of cAMP. The absorbance values on the ordinate axis were normalized according to the maximum value obtained in the relative experiment.

This suggested that LDAO, because of its high extraction rate, probably caused a destabilization of the protein structural organization.

Given these results, we decided to keep using DM for the extraction of K-H4ΔN VG. Indeed, this detergent was already employed for the extraction of K-H4ΔN FQ from the native membranes,

keeping the protein in solution and stabilizing the quaternary form of the chimeric channel in the presence of cAMP.

3.3 Functional characterization of K-H4ΔN VG

3.3.1 ITC experiments confirmed the ability of the chimera to bind cAMP

Once it was proven that the protein K-H4ΔN VG is stable in both apo and holo state, the biophysical characterization of the chimera was performed. To investigate the energetics of cAMP binding to the protein I took advantage of Isothermal Titration Calorimetry (ITC), a physical technique used to determine the thermodynamic parameters of interactions in solution. ITC is used in quantitative studies of a wide variety of biomolecular interactions. It works by directly measuring the heat that is either released or absorbed during a biomolecular binding event. Moreover, thanks to this technique, it is possible to measure the affinity of binding partners in their native states.

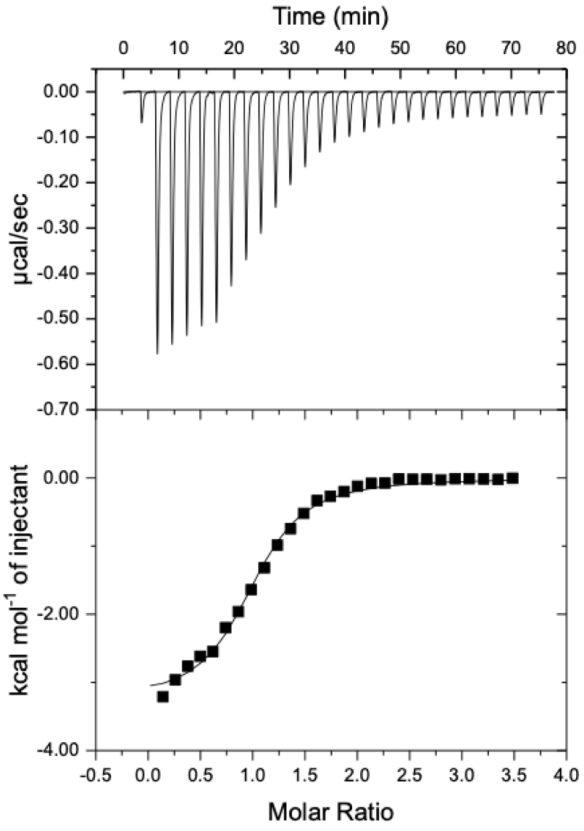

Figure 10: K-H4ΔN VG binds cAMP. ITC measurement showing titration of the chimera K-H4ΔN VG with cAMP. The upper graph shows the raw data. Heat is released upon successive injections of 8 µl of cAMP

(200 µM) to the chimeric protein (20 µM). The peaks were integrated, normalized to the cAMP concentration, and plotted against the molar ratio of cAMP to KcsA-HCN4 to obtain the binding curve (lower graph). The solid line represents a nonlinear least-squares fit to a single-site binding model.

In order to achieve these data, the chimeric channel (20 µM) in detergent (i.e. DM) was titrated with cAMP at saturating concentration of 200 µM (fig. 10). The binding curve shown in the bottom panel of figure 10 was obtained by integration of the exoergic peaks (top part) produced by the titration of the chimeric protein with cAMP. The analysis of the binding curve revealed a dissociation constant, Kd, of 1.7 ± 0.7 µM (n=2). This is a similar value compared to the dissociation constant obtained in a previous work where the isolated C-linker/CNBD fragment of hHCN4 was tested for the cyclic nucleotide binding (Lolicato et al., 2011).
Thus, using ITC we confirmed that the channel is able to bind the cyclic nucleotide cAMP.

3.3.2 The binding of cAMP stabilizes the chimera

Another calorimetric technique adopted for the characterization of the chimeric channel was the differential scanning calorimetry (DSC). This technique allows to acquire the thermodynamic parameters characteristic of a system, such as a protein, that are associated with different processes triggered by changing the temperature. For instance, DSC is a useful tool to characterize the energetics of unfolding of a protein linked to the binding with a specific ligand.

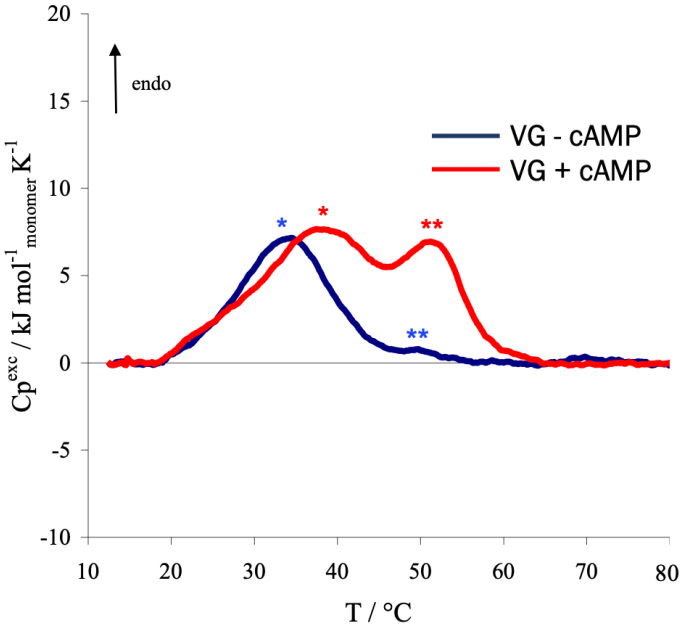

Figure 11: **cAMP slightly stabilizes the chimera**. Superimposed Nano DSC (TA) profiles of K-H4ΔN VG in the absence (blue) and presence of cAMP (red). The scan rate in both the experiments was 0.5 °C·min^{-1}.

DSC experiments were performed in the laboratory of Prof. Dimitrios Fessas (Università degli Studi di Milano, Italy), that provided the nano-DSC instrument (TA instruments) and helped for the further analysis and interpretation of the data. Figure 11 shows a preliminary measurement testing K-H4ΔN VG (80 µM) in the absence (blue signal) and in the presence of cAMP at saturating concentration of 200 µM (red signal). Both the melting curves of K-H4ΔN VG in the cAMP-free and -bound state consist of two transition events. Notably, the experiment performed in the presence of cAMP exhibited a consistent shift of the first transition peak from 33°C (blue star) to 40°C (red star). The second endothermic event (shown by two blue stars in the cAMP-free sample signal) became more evident upon the interaction with the cyclic nucleotide (red stars). This latter is shifted toward higher temperatures compared to that of the cAMP-free sample. These shifts in Tm suggest that the binding of cAMP to the CNBD increases the stability of the chimera. Moreover, the appearance of the second peak in the ligand-bound sample suggests that the binding of cAMP to the chimera is causing structural rearrangement in the protein.

3.3.3 The pore domain of the chimera is able to conduct potassium ions

In order to test the functionality of the chimera and especially its ability to conduct potassium ions, the glutamate at position 88 of the KH4ΔN VG sequence was substituted by an alanine, resulting in the construct KH4ΔN VG E88A (hereinafter called E88A). This mutation is a well-characterized mutation in the pore of KcsA (E71A in KcsA sequence) that is known to abolish the inactivation at the level of the selectivity filter, thus increasing the open probability of the channel at pH 4 (Cordero-Morales et al., 2007). However, the expression of the mutant chimera E88A, caused a drastic decrease of the growth rate of *E. coli* cells (fig. 12A). Moreover, western blot analysis revealed that the mutant protein was not assembled according to the expected tetrameric assembly (Supplementary figure 1). Therefore, it was reasoned that the introduction of this mutation that should promote the opening of the pore domain of the chimeric channel, rendered the chimera toxic for the host organism. Indeed, the increase in the intracellular K^+ level due to the overexpression of an active potassium channel is known to be toxic for *E. coli* as it alters the osmolarity of the bacteria (Radchenko et al., 2006). This toxic effect can result in a slowing down of the bacterial growth (Miroux and Walker, 1996; Dumon-Seignovert et al., 2004; Wagner et al.,

2008). Therefore, a reduction of the channel activity by blockage of the chimera mediated potassium influx should lead to an increase in the growth rate.

To test this hypothesis and thus to confirm that the chimera is a functional potassium channel, the growth was monitored in the absence and presence of $BaCl_2$. Barium is a well-known transient high-affinity blocker of potassium channels, that binds inside the selectivity filter, preventing the flow of K^+ through the channel pore (Armstrong and Taylor, 1980; Miller 1987; Jiang and MacKinnon, 2000). The optical density at a wavelength of 600 nm (OD_{600}) was measured to monitor cell growth after protein induction in the presence or in the absence of 10 mM $BaCl_2$ (fig. 12A). *E. coli* strain C41(DE3) was transformed with the so far used plasmid pET24b containing either the construct KH4ΔN VG, i.e. WT, or the mutant E88A. The overexpression experiments employed the standard conditions used for the heterologous expression of KH4ΔN VG (see chapter 5.2.2 of the section "Material and Methods"). Overexpressing cells were compared with empty-vector control cells (i.e. containing pET24b without an insert).

Figures 12A and B reveal that the addition of 10 mM $BaCl_2$ at the moment of induction causes a detectable improvement of cell growth for all the three different cultures. Surprisingly, the addition of $BaCl_2$ led to an increase in cell density even for the empty-vector control. 16 hours after induction the cell density was increased by 29.7% ± 11.4% (n = 3) in the presence of barium compared to the culture grown in the absence of barium (fig. 12A and B). The underlying mechanism is unknown and will not be further investigated in this work. In the case of bacterial cells expressing the WT chimera, the addition of barium caused an increase in cell density of 46.5 ± 22.9% (n = 3) (fig. 12A and B). Even if this effect is larger than the one of the empty-vector control, this finding cannot be used to conclude that the WT chimera is able to conduct potassium since the difference between both effects is not statistically significant. This was determined by using a two-sided, unpaired t-test that provided a p-value of 0.32. However, an effect that exceeds that of the empty-vector control was not necessarily expected either, since the overexpression of the WT chimera is not toxic for E. coli (fig. 12A, compare WT w/o $BaCl_2$ and empty-vector-control w/o $BaCl_2$).

However, the addition of barium to the medium has a much stronger effect on cells expressing the E88A mutant: 16 hours after induction the cell density was increased by 168% ± 32% (n = 3) in the presence of barium compared to the culture grown in the absence of barium (fig. 12A and B). This effect is statistically very significant compared to the empty-vector control (p = 0.002).

Since $BaCl_2$ increases the growth in a statistically significant manner, it can be reasoned that the aforementioned toxicity is due to a toxic accumulation of potassium inside the cytosol, mediated

by the overexpressed chimera. This experiment clearly supports the assumption that the chimera is a functional potassium channel.

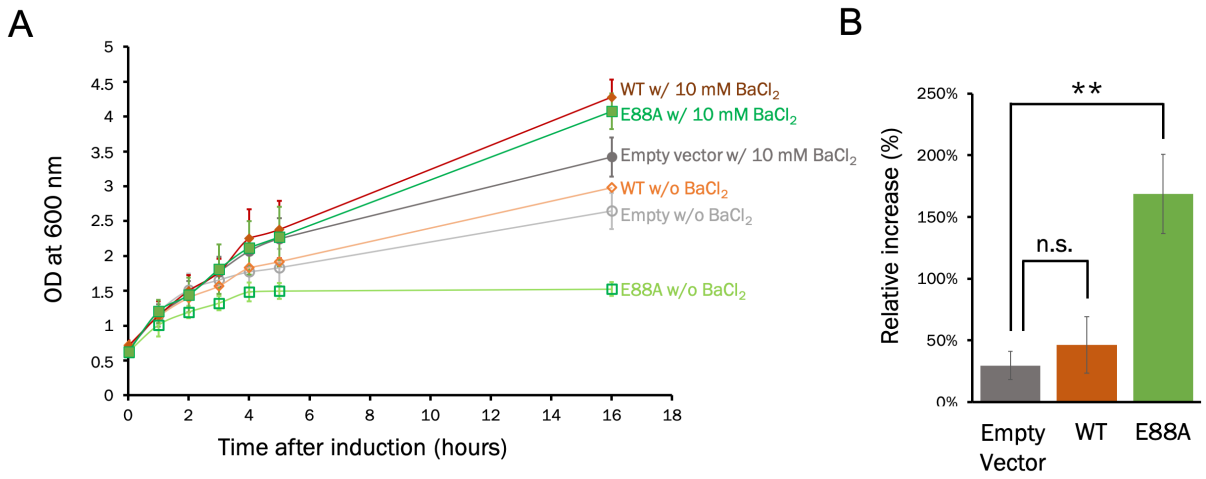

Figure 12: The addition of $BaCl_2$ in the medium promotes cells growth by reducing toxicity. (A) Growth curves of E. coli C41(DE3) cells expressing KH4ΔN VG (WT, green lines) or the open mutant E88A (orange lines). Culture containing the empty pET24b vector has been used as negative control (gray lines). Once the OD_{600} value reached 0.6–0.7, cells were induced with 100 µM IPTG and LB medium was supplemented (w/, solid symbols) or not (w/o, empty symbols) with 10 mM $BaCl_2$. Growth was continued overnight (i.e. 16 hours) at 20°C. (B) Relative increase of cells growth upon $BaCl_2$ addition expressed as percentage. T-test results are indicated above the columns. The relative increase of growth of the WT compared to the control (empty vector) was statistically not significant (n.s.). Whereas the relative increase of growth of E88A compared to the control gave a p-value of 0.002, that is statistically very significant (**). For both (A) and (B) N=3.

In order to further demonstrate that the channel pore of the chimera is able to conduct potassium, a functional complementation assay was conducted using the K^+-uptake deficient *E. coli* strain LB2003. *E. coli* strain LB2003 was kindly provided by Prof. Gerhard Thiel (TU Darmstadt, Germany) and the complementation assay was performed in collaboration with Dr. Oliver Rauh (TU Darmstadt, Germany).

LB2003 lacks the three K^+ uptake systems Trk, Kup and Kdp. For this reason, the strain is known to be incapable of growing in low potassium media unless it is induced to express an active K^+-selective channel (Epstein and Davies, 1970; Buurman et al., 1995; Uozumi et al., 1998; Uozumi 2001). Since the LB2003 strain is not lysogenized by prophage λDE3, it does not have a copy of the gene coding for the T7 RNA polymerase, the enzyme that binds the T7 promotor of pET vectors. Thus, both the chimeric constructs WT and E88A were cloned into the arabinose-

inducible pGM930$_{SD}$ vector, a modified pBAD24 vector (Delvillani et al., 2014), to perform a complementation assay (see chapter 5.7 of the section "Material and Methods"). Cells transformed with the empty-vector were used as control (i.e. containing pET24b without an insert).

The transformed LB2003 cells were used for a serial dilution drop test on LB agar plates that differed in their K^+ concentration (i.e. 0 mM, 10 mM and 100 mM), the presence or absence of the inducer L-arabinose (0.2%) and the presence or absence of the K^+ channel blocker $BaCl_2$ (5 mM) (fig. 13).

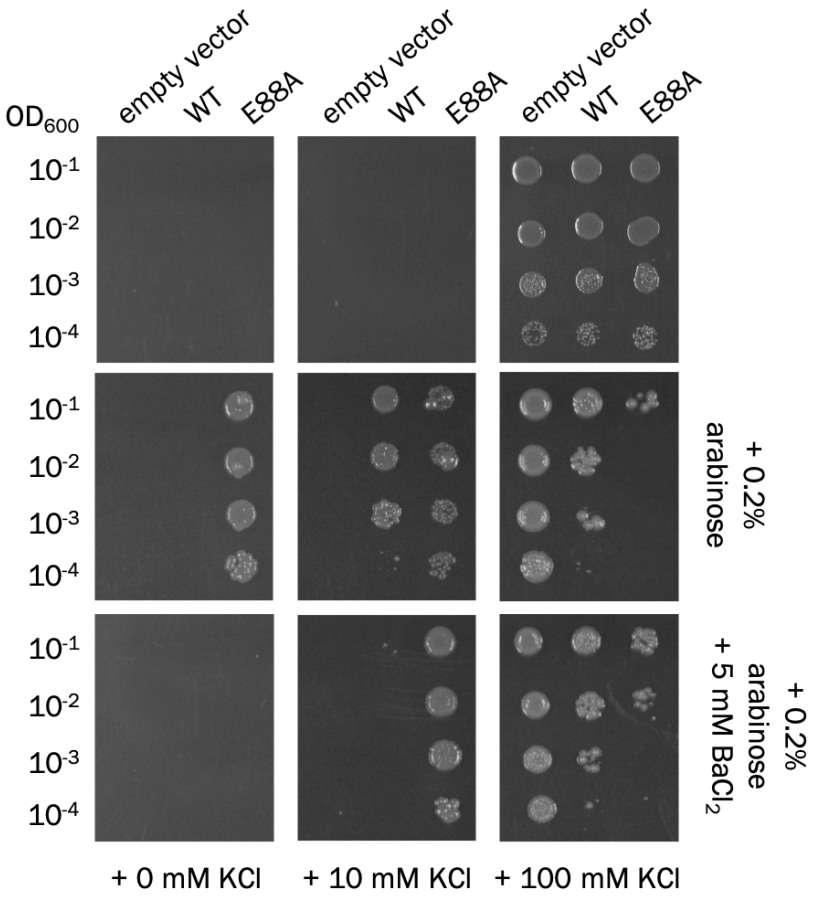

Figure 13: The chimeric channels can mediate potassium transport in the K^+ uptake-deficient strain LB2003. Dilutions of transformant cultures harboring the vector pGM930$_{SD}$ either empty or containing the chimeric constructs WT or E88A, were spotted on Luria-Bertani plates. Each plate contains 100µg/mL ampicillin and different additional concentrations of KCl. Some plates contained the inducer 0.2% L-arabinose and eventual 5mM $BaCl_2$. Plates were incubated overnight at 37°C.

Cells transformed with the empty vector are not able to grow on any media with either 0 mM additional KCl or 10 mM additional KCl, whereas, as expected, they successfully grow on all the

three different media containing 100 mM additional KCl. These data confirm that any effect observed is due to the expression of the chimeric channels. Moreover, in the absence of inducer, even cells transformed with either WT channel or the open mutant grew only on the plate supplemented with 100 mM KCl confirming that LB2003 is not able to grow in the presence of low potassium concentrations.

The expression of the WT channel rescues the K^+-uptake deficient strain in the presence of 10 mM additional KCl. This functional complementation is nicely abolished in the presence of 5 mM $BaCl_2$ confirming that the WT chimera is able to conduct K^+. Moreover, in the presence of 100 mM KCl the growth of the cells expressing the WT chimera was slightly impaired even in the presence of $BaCl_2$.

LB2003 cells induced to express the E88A mutant grow well with both 0 mM and 10 mM additional KCl. In contrast, in the presence of 100 mM additional KCl the expression of the E88A mutant led to a strongly impaired growth, most likely due to a toxic accumulation of K^+ in the cytosol. Impressively, the functional complementation that was observed at 0 mM additional KCl was completely abolished in the presence of $BaCl_2$. Simultaneously, the addition of $BaCl_2$ reduced slightly the toxic effect of the expressed E88A mutant in the presence of 100 mM additional KCl. These results clearly demonstrate that the E88A mutant is a functional K^+ channel. Furthermore, comparison between the WT chimera and the E88A mutant clearly reveals, that the substitution of E88 in the pore domain of the chimeric protein by an alanine leads to an increase in the K^+ channel activity of the chimera. This conclusion is additionally supported by the observed effect of $BaCl_2$ on the growth of LB2003 cells expressing either the WT or mutant chimera at 10 mM additional KCl: while $BaCl_2$ suppresses the growth of cells expressing the WT chimera, it leads to a slight improvement in the growth of cells expressing the E88A mutant. This apparently paradoxical result can only be explained by a substantial difference in the open probability of both constructs. The low open probability of the WT chimera is likely reduced by $BaCl_2$ to a value close to zero, resulting in the loss of the ability to rescue the growth of LB2003. On the other hand, the E88A mutant must possess a drastically higher open probability, that is lowered by the addition of $BaCl_2$ to a value that is still higher than the open probability of the WT chimera in the absence of $BaCl_2$ and that somehow allows the uptake of K^+ in a more cell-compatible way. This substantial difference in the open probability of both constructs also provides an explanation for the observation that the mutant is able to rescue the growth of LB2003 at 0 mM additional KCl, while the wild type is unable to do so.

Taken together, these data indicate that the WT channel KH4ΔN VG and, especially, the open mutant E88A is able to functionally complement the phenotype of the K^+-uptake deficient *E. coli* strain LB2003. These results, together with the observation that the complementation effect at low K^+ concentrations can be eliminated by barium, support the assumption that both chimeras represent functional K^+ channels.

3.4 Cryo-EM studies

The main goal of this project is to study the conformational changes occurring at the C-linker domain of HCN channels. The structure of human HCN1 recently solved by cryo-EM (Lee and Mackinnon, 2017) did not advance our understanding of the C-linker rearrangements during channel gating. Indeed, the structures were solved at 0 mV, a condition that locks the VSD (Voltage Sensor Domain) in the resting state. In this configuration, the VSD inhibits the movements of both pore and C-linker domains, which are under its allosteric control (Wahl-Schott and Biel, 2009; Lee and MacKinnon, 2017). Given these data, the use of the chimeric channel for studying the structural rearrangements of the C-linker using single particle cryo-EM (as well as other dynamical approaches) should be advantageous compared to the wild type eukaryotic channel since the absence of the VSD and of the HCN domain in the chimera should allow to catch the cAMP- induced conformational changes in both the C-linker and possibly in the pore domain.
For the following experiments, the chimera K-H4ΔN VG was first extracted and purified in the absence and presence of cAMP as described in the chapter 5.2.2 and 5.2.3 of the section "Material and Methods". Then, in order to obtain a sample suitable for cryo-EM analysis, the detergent was substituted with A8-35 amphipols (see chapter 5.8.1 section "Material and Methods"). Amphipols are polymers able to bind tightly to the transmembrane domain of membrane proteins and to mimic a membrane lipid environment (Popot et al., 2011). Particularly, A8-35 has been used for the determination of several membrane protein structures by single particle cryo-electron microscopy (Popot et al., 2011; Cheng 2018a; Mio and Sato, 2018; Sgro and Costa, 2018; Thonghin et al.; 2018). This replacement step is highly recommended since the density of detergent micelles can diminish the contrast of membrane proteins in cryo-EM studies, making difficult the achievement of high-resolution structures (Mio and Sato, 2018).
At the end of the detergent replacement process, the excess amphipols were removed by size-exclusion chromatography.

The negative staining, the loading of the grids and the subsequent EM data acquisition and analysis were performed by Dr. Paolo Swuec (Università degli Studi di Milano).

3.4.1 Cryo-EM analisys of cAMP-free K-H4ΔN VG

After detergent exchange, the protein was analyzed on size exclusion chromatography. As shown in figure 14A, the chimera eluted as a monodisperse peak consistent with the molecular weight of the tetramer (MW: 152 kDa).

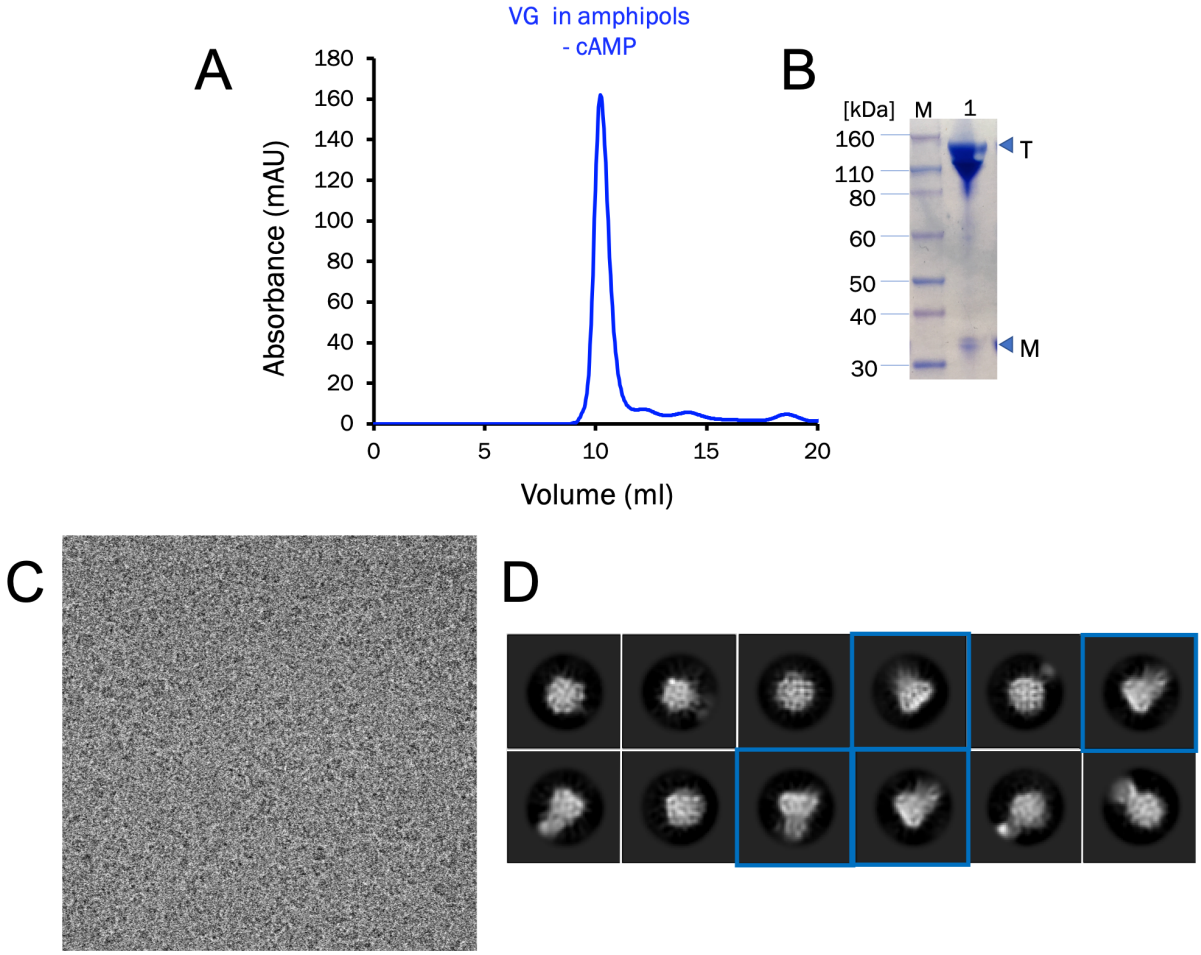

Figure 14: K-H4ΔN VG is stable in amphipols. (A) Gel filtration elution profile of the cAMP-free chimera after exchange in amphipol. (B) SDS-PAGE analysis of the protein in amphipols used for the EM analysis in (C) and (D). Arrowhead marked with letter T: band relative to the tetrameric channel (MW: 152 kDa). Arrowhead marked with letter M: band relative to the monomer (MW: 38 kDa). M: Marker (Novex® Sharp Pre-stained Protein Standards, Invitrogen). (C) Negative staining electron microscopy (sample

concentration= 0.6 mg·mL^{-1}). (D) 2D-class averages. The blue framed images are showing lateral views of the channel.

Moreover, when assayed by SDS-PAGE, most of the protein maintained the tetrameric state (fig. 14B, lane 1, band indicated by the arrowhead marked with letter T). These data suggest that the amphipol exchange did not affect the stability of the chimera.

Subsequently, the quality of the sample was analyzed with negative staining electron microscopy, a fast and inexpensive approach that provides an immediate feedback.

The negative staining of the sample (fig. 14C) showed that the particles are well dispersed and homogeneously distributed, suggesting that the sample is suitable for successive cryo-EM analysis. The sample was then embedded in vitreous ice and imaged at cryogenic temperatures with Talos^{TM} Arctica. After data collection, particles within different micrographs were subjected to selection. The selected particles were used to obtain the 2D protein classification (fig. 14D).

By examining the two-dimensional projections, it was possible to distinguish the morphology of the protein only in a few lateral views (i.e. the transmembrane and the cytosolic domains, the class averages are framed in blue), whereas other class averages did not show clear views of the chimera. Thus, unfortunately, because of the high flexibility of the protein, the sample showed a very high structural heterogeneity that did not allow a 3D reconstruction.

3.4.2 Cryo-EM analisys of cAMP-bound K-H4ΔN VG

Single-particle cryo-EM experiments were performed also with the cAMP-bound chimera. Indeed, from previous functional experiments on K-H4ΔN VG (see chapter 3.3.2 of this section) and on the C-linker/CNBD fragment of HCN4 (Lolicato et al. 2011), cAMP is known to stabilize the protein. In this way, I expected to reduce the high flexibility shown by the chimera in the absence of cAMP.

The performed size-exclusion chromatography of the protein after the exchange in amphipols revealed that, in the cAMP-bound state, K-H4ΔN VG eluted as a monodisperse peak consistent with the molecular weight of the tetramer (MW: 152 kDa) (fig. 13A). The negative staining confirmed the good quality of the sample (fig. 13B). Indeed, the particles are homogeneously distributed and equally dispersed. Once the sample passed the quality control, we prepared grids for image acquisition with the cryo-EM. Two-D class average, once again, confirmed that it was possible to appreciate the morphology of the channel (i.e. the transmembrane and the cytosolic domains, framed in red in fig. 13C). In this case it was possible to align the 2D classes in the 3D space to obtain 3D reconstructions (fig. 13D). The 3D reconstructions nonetheless showed high

conformational variability and, therefore, also in this case it was not possible to obtain any high-resolution structural data.

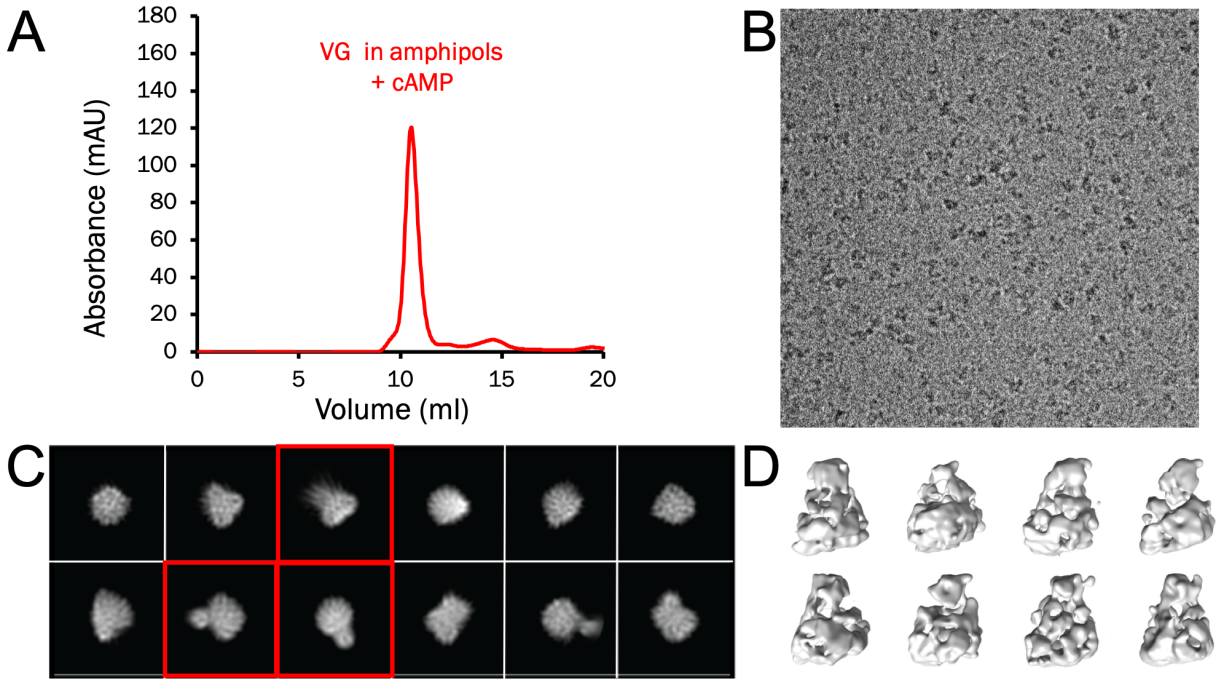

Figure 15: K-H4ΔN VG is very flexible. (A) Gel filtration elution profile of the cAMP-bound chimera after exchange in amphipol. (B) Negative staining electron microscopy (sample concentration= 0.5 mg·mL^{-1}). (C) 2D-class averages. The red framed images are showing lateral views of the channel. (D) 3D reconstruction of the chimera in the holo state.

Taken together, these data suggest that the chimera is undergoing a continuum of different conformational rearrangements that result in high flexibility of the protein, more marked in the absence than in the presence of cAMP. The high flexibility in the particles increased the sample intrinsic heterogeneity. Since the final image achievable with cryo-EM is the sum of all these motions, the quality of the final data was poor and the sample resulted to be not suitable for a structural study using this technique.

3.5 EPR and DEER to study protein dynamics

The cryo-EM analysis of the chimera suggested that the protein possess different conformational states that are more marked in the absence than in the presence of cAMP. Thus, in order to study the structural rearrangements and dynamics that characterize the regulatory region of HCN

channels and, particularly, the active C-linker domain, Site-Directed Spin Labelling Electron Paramagnetic Resonance (SDSL-EPR) and the Double Electron-Electron Resonance (DEER) have been applied. Both EPR and DEER involve the labelling with paramagnetic tag of strategically positioned cysteine residues within the protein of interest. The paramagnetic probes can be monitored by EPR spectroscopy (Jeschke 2012a and 2012b; Klare 2013).

The shape of the recorded continuous wave EPR (CW-EPR) spectrum reflects the mobility of the probe, providing information about the local environment and the dynamic of the protein. On the other hand, using DEER spectroscopy it is possible to measure distances and distance distributions between paramagnetic centers in the range of 15Å to ~80 Å by measuring the dipole interaction as function of time (Jeschke 2012a and 2012b, Klare 2013).

Particularly, DEER could help to understand the quaternary organization of the C-terminal domains of K-H4ΔN VG, by measuring the distance distribution between the paramagnetic probes attached at different regions of the protein. Since the chimeric protein has an homotetrameric structure, distance determinations are the result of the geometric interactions between neighboring and diagonally related subunits. Thus, in this project DEER measurements have been used in order to obtain the distances between each monomer and, then, to study the macromolecular architecture of the system in the absence and in the presence of cAMP.

In order to perform the aforementioned spectroscopic measurements, all native cysteine in the chimera K-H4ΔN VG were removed by substituting them with serine. A preliminary test showed that the cysteine-free mutant protein can be produced and purified with the same protocols of the WT and that its stability was also preserved (data not shown). Afterwards, individual cysteine mutants were prepared. Specific residues were replaced with cysteines using site-directed mutagenesis strategy (see chapter 5.9.1 of the section "Material and Methods") in the C-linker domain either in the "elbow" (E172C, fig. 14A) or in the "shoulder" (E195C, fig. 14D) to allow to study the active movement of the "elbow on the shoulder". For the achievement of an overview on the dynamics that govern the cytosolic C-terminal regulatory region, the natural cysteine residue (C202, fig. 14G) at the level of the N-terminal helical bundle has been selected. This residue is in a strategical border region that connects the CNBD domain to the C-linker. Thus, its spectroscopic study could help to understand how the conformational changes induced by the binding of the cAMP to the CNBD are transmitted to the C-linker domain. Moreover, as control for the reliability of the movements showed by the chimera, a cysteine residue was introduced at the level of the αC-helix of the CNBD domain (R329C, fig. 14J). Indeed, previous spectroscopic

studies on the isolated CNBD of HCN2 channel already shed light on the conformational changes that characterize this domain (Puljung et al., 2014; Saponaro et al., 2014). Subsequently, each of the individual cysteine mutant was expressed and purified following the procedures described in chapters 5.2.2 and 5.2.3 of the section "Material and Methods". The purified proteins were incubated with MTSL tag to perform SDSL reaction (see chapter 5.9.2 of the section "Material and Methods") and consequently to generate a stable spin label side-chain.

EPR and DEER experiments were performed at the Center of Magnetic Resonance (CERM) of the University of Florence. Dr. Alessio Bonucci (CERM, Florence) recorded the spectra and made the further analysis of the data.

3.5.1 CW-EPR

In order to analyze the local dynamics of the protein in the regions where the MTSL spin label were attached, the X-band CW-EPR spectra at room temperature of the four different mutants of K-H4ΔN VG protein were recorded in absence and in presence of cAMP (fig. 16A-L)

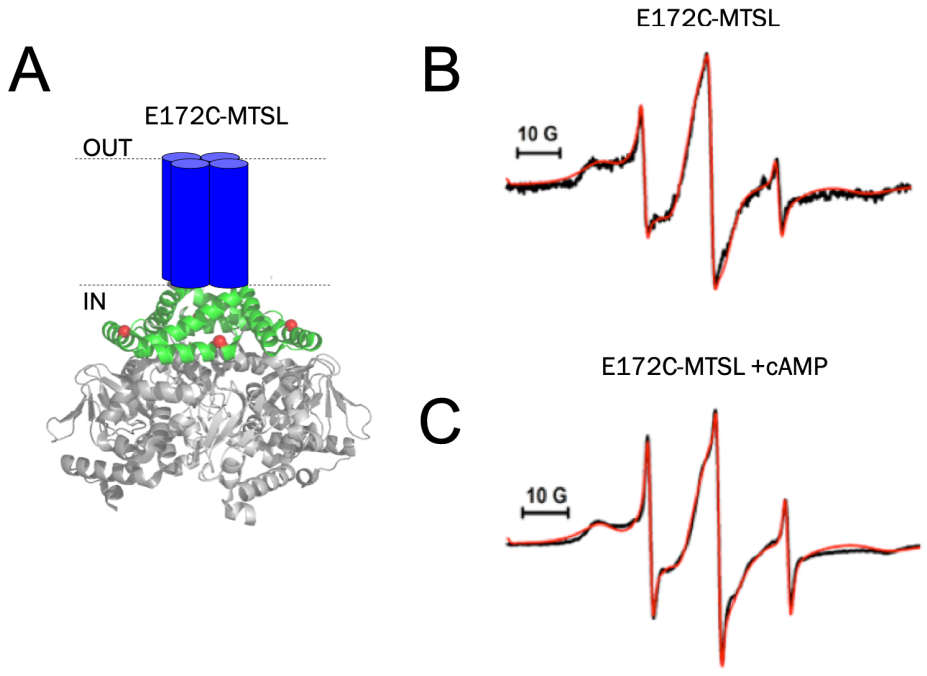

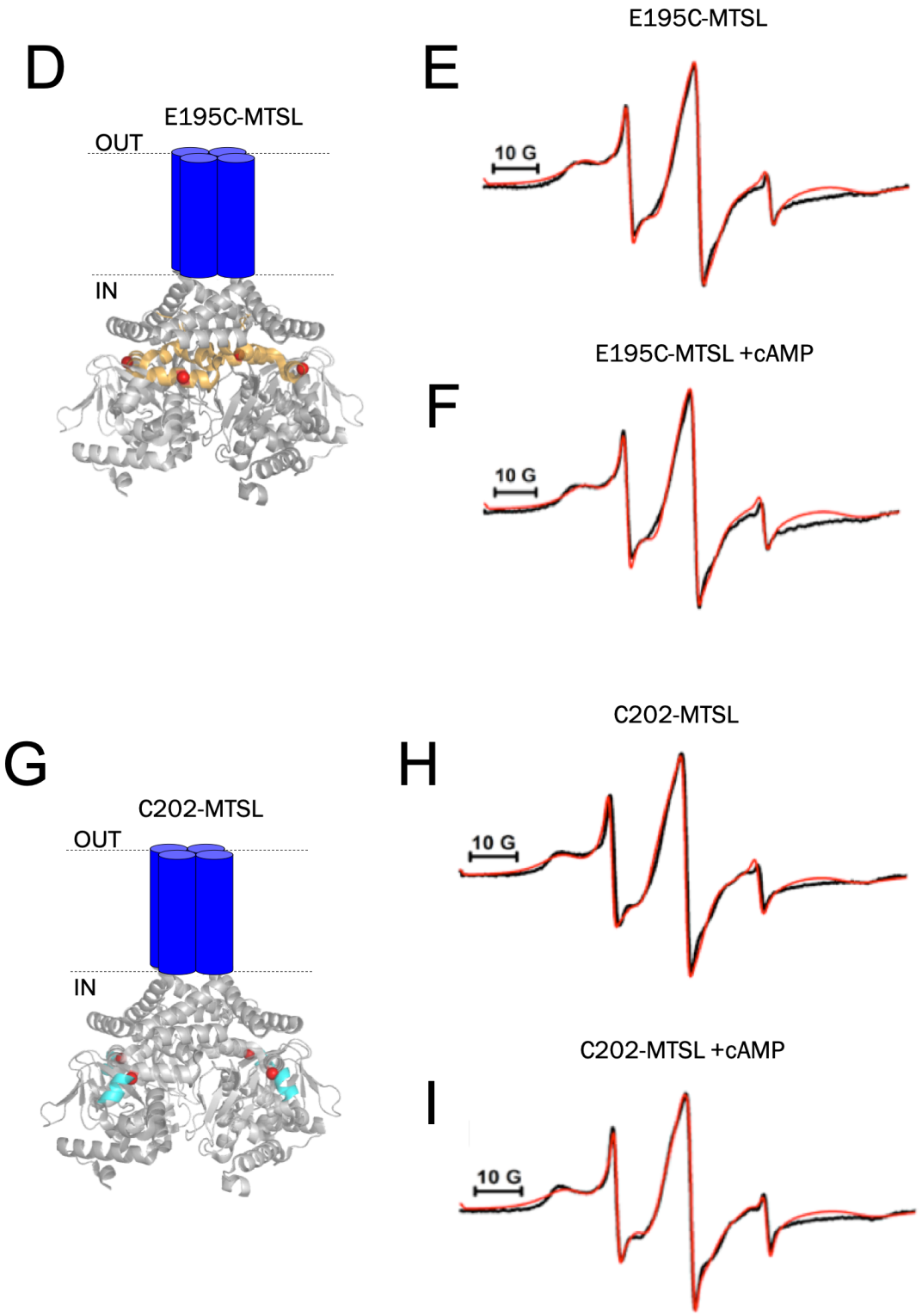
D
E195C-MTSL
OUT
IN
E
E195C-MTSL
10 G
E195C-MTSL +cAMP
F
10 G
G
C202-MTSL
OUT
IN
H
C202-MTSL
10 G
C202-MTSL +cAMP
I
10 G

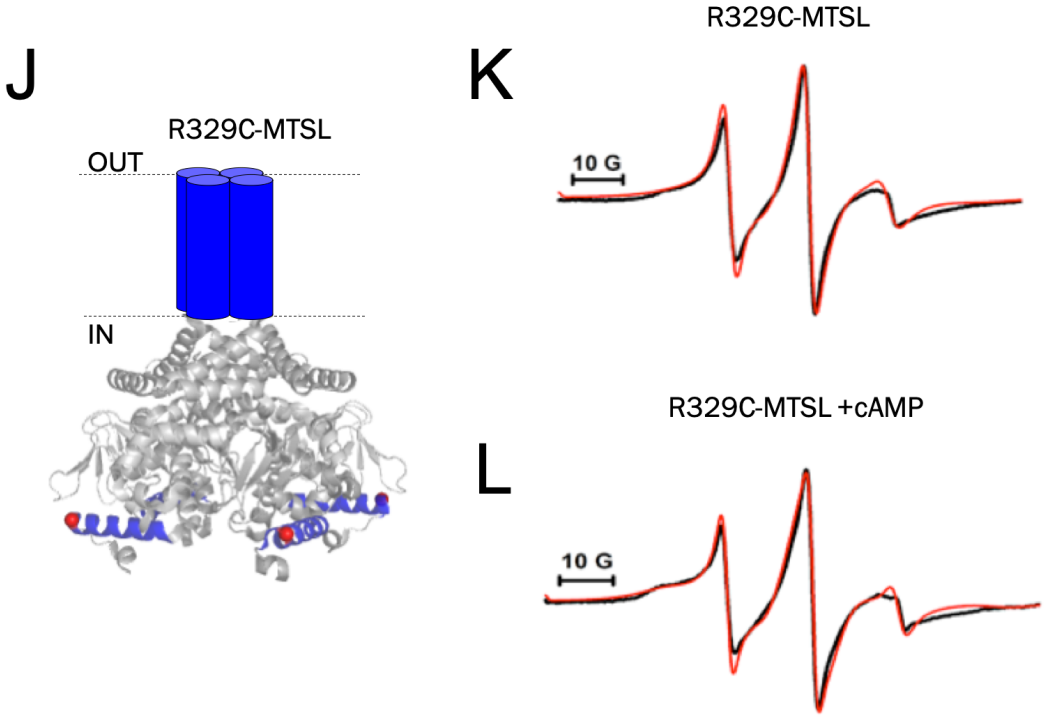

Fig. 16: X-band CW-EPR spectra. (A), (D), (G) and (J) are schematic representations of the cysteine mutants used for DEER experiments. The residues substituted by cysteine and labeled with MTSL are represented as red spheres. The pore domain of the chimeric channel is represented by blue cylinders. The C-linker/CNBD domains are represented by the corresponding parts of the hHCN1 structure (Lee and MacKinnon, 2017, PDB_ID: 5u6o) lacking the pore domain. The "elbow" of the C-linker domain is colored in green (A) and the "shoulder" in yellow (D). The N-terminal helical bundle is highlighted in cyan (G) and the αC-helix of CNBD is highlighted in blue (J). Room temperature X-band CW-EPR spectra (black) and relative simulations (red) for MTSL attached in the positions shown in the left column. The spectra were recorded in the absence (B,E,H,K) and in presence of cAMP (C,F,I,L).

Sample	Comp. 1 (%)	τ_c 1 (ns)	Comp. 2 (%)	τ_c 2 (ns)	Comp. 3 (%)	τ_c 3 (ns)
E172C-MTSL	3.0	0.14	18.0	1.30	79.0	5.40
+ cAMP	4.0	0.15	19.0	1.31	79.0	5.90
E195C-MTSL	3.0	0.18	19.0	1.25	78.0	5.61
+ cAMP	2.0	0.18	17.0	1.25	81.0	5.61
C202-MTSL	4.0	0.18	20.0	1.23	76	5.61
+ cAMP	2.5	0.12	16.5	1.00	81.0	5.56
R329C-MTSL	17.0	0.73	28.0	1.60	55.0	3.67
+ cAMP	10.0	0.51	28.0	1.60	62.0	4.05

Table 1: Component percentage and relative correlational time values (τ_C) calculated through the simulation, using SimLabel software, of the experimental CW-EPR spectra of K-H4ΔN VG MTSL labeled mutants. Error of ± 1.2% and ± 0.07 ns where estimated respectively for component percentage and correlational times.

The CW-EPR experiments provide information on the environments surrounding the residue where the paramagnetic tag is grafted and, thus, also about the secondary structure of the protein. Using SimLabel software (GUI of EasySpin), the experimental data were simulated to obtain the spectral components forming the EPR signal and their relative correlational time values (τ_C). The τ_C value reflects the mobility of the MTSL probe (table 1). Particularly, the movement of the latter is affected by the intrinsic movement of the region of the protein where it is attached: the higher the value of the τ_C (i.e. > 3.5 ns), the higher is the rigidity of the protein in that region and vice versa. This directly correlates with the broadening of the CW spectra. Indeed, high degree of flexibility of the protein region where the paramagnetic tag is attached gives narrow line widths in the spectrum (sharp signal). While a decrease of mobility consists in a widening of the spectrum (broad signal).

The results obtained for all the four mutants revealed that the EPR spectrum is composed by three components with different τ_C indicating that the protein is present in a multi dynamic states, as previously determined by cryo-EM measurements (supplementary fig.2). In particular for E172C-MTSL, E195C-MTSL and C202-MTSL the predominant component (Component 3 ≈76-79% and τ_C = 5.40-5.61 ns, table1) has a broad lineshape and a high τ_C value, indicating that respectively the "elbow" and the "shoulder" of the C- linker domain and the N-terminal helical bundle have a low degree of flexibility and a compact conformation. On the other hand, CW-EPR spectrum of R329C-MTSL mutant is composed by a less pronounced broad component with a faster tumbling motion of MTSL (component 3 ≈ 55% and τ_C = 3.67 ns, table 1). This result clearly indicates that the αC-helix of the CNBD domain is in a more dynamic states and that this region is very flexible compared to the other positions tested.

Successively X-band CW-EPR spectra of MTSL-labeled variants were recorded in presence of cAMP. No evident spectral changes and variation on the relative τ_C were observed for E195C-MTSL and C202-MTSL samples, indicating that the ligand does not affect the structure of the "shoulder" and N-terminal helical bundle regions. However, E17C2-MTSL and R329C-MTSL show an EPR broader spectrum when cAMP is present in solution, as confirmed by the simulations that present a higher τ_C of ≈ 0.5 ns. These results show that the ligand weakly compromise the dynamic of the protein for the "elbow" and the αC-helix of the CNBD. Particularly, the results

obtained for R329C- MTSL are in line with previous EPR data performed on this residue (Puljung et al., 2014; DeBerg et al., 2015).

3.5.2 DEER measurements

The distances and distance distributions between the probes were obtained with Double Electron Electron Resonance (DEER) spectroscopy. In figure 17 are shown the different spin-labelled mutants of the chimeric protein with the relative Q-band background corrected time traces and the resulting distance distributions obtained in the presence and in the absence of cAMP.

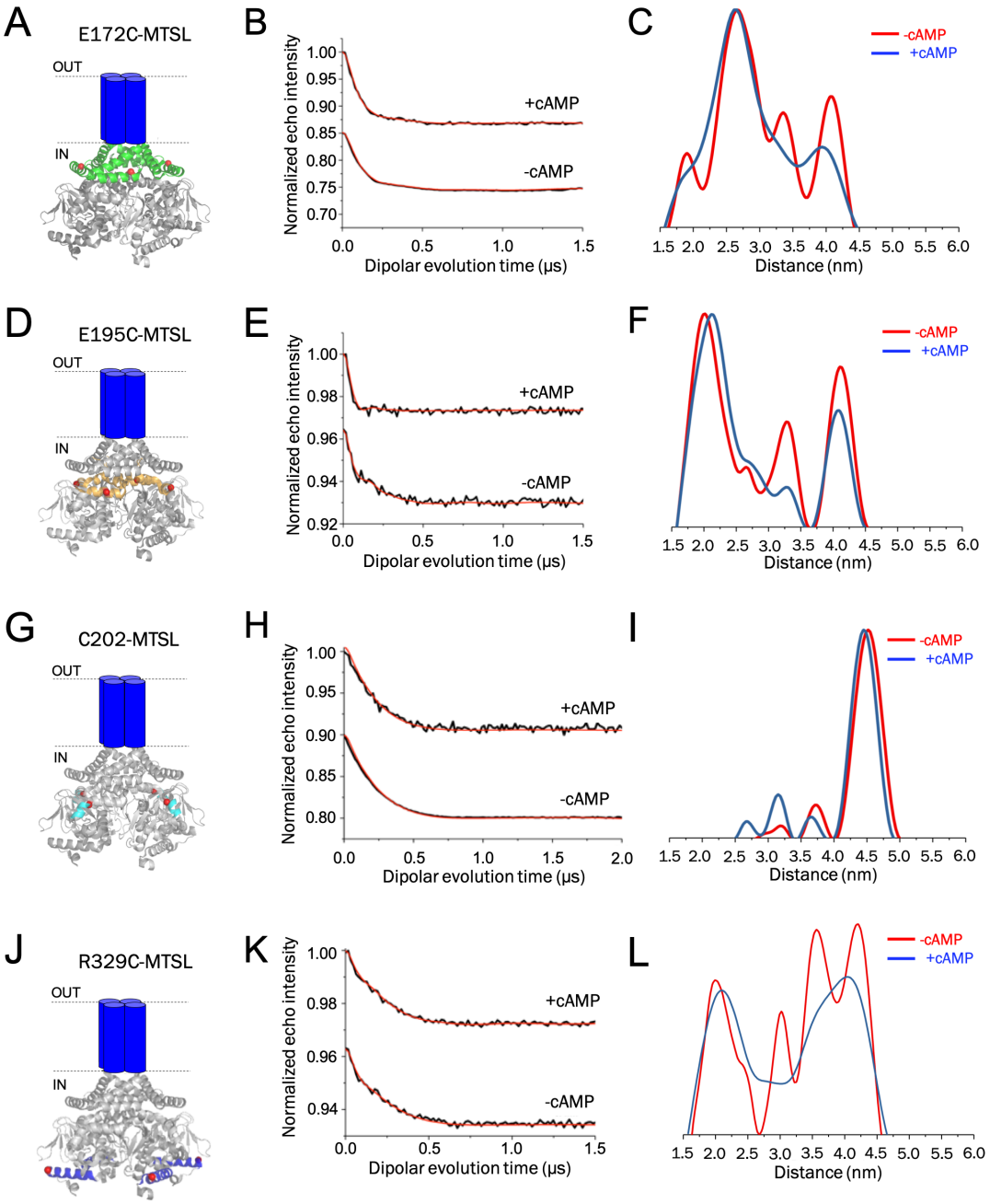

Figure 17: Distance distributions of cAMP-free or -bound MTSL-labelled cysteine mutants using Q-band DEER. Left panel: schematic representations of the cysteine mutants used for DEER experiments. The residues substituted by cysteine and labeled with MTSL are represented as red spheres. The pore domain of the chimeric channel is represented by blue cylinders. The C-linker/CNBD domains are represented by the corresponding parts of the hHCN1 structure (Lee and MacKinnon, 2017, PDB_ID: 5u6o) lacking the pore domain. The "elbow" of the C-linker domain is colored in green (A) and the "shoulder" in yellow (D). The N-terminal helical bundle is highlighted in cyan (G) and the αC-helix of CNBD is highlighted in blue (J). Central panel: background subtracted Q-band DEER-refocused echo intensity (black lines) plotted versus dipolar evolution time for each spin-labeled position. The spectra were recorded in the absence and in the presence of cAMP. The signals were fitted using model-free Tikhonov regularization (red lines). Right panel: inter-spin distance distributions obtained from data in the middle panel. Distances explored by the spin labels in the absence of cAMP are shown in red, whereas blue signals were obtained in the presence of cAMP.

Sample	Modulation depth (%)	r_{MAX} (nm)	<r> (nm)	σ (nm)
E172C-MTSL	10.4	2.65	3.16	0.58
+ cAMP	13.2	2.64	3.08	0.59
E195C-MTSL	4.0	1.99	3.24	0.71
+ cAMP	4.1	2.11	2.95	0.70
C202-MTSL	7.4	4.52	4.74	0.65
+ cAMP	3.8	4.48	4.52	0.72
R329C-MTSL	2.4	4.18	3.90	0.81
+ cAMP	2.1	4.02	3.52	0.82

Table 2: Values of modulation depth, peak maxima (r_{MAX}), average distance (<r>) and relative standard deviation (σ) through DEERAnalysis2016 software using Tikhonov regularization.

3.5.2.1 DEER on residues in the "elbow" and "shoulder"

The Q-band DEER traces for E172C-MTSL (fig. 17B) and E195C-MTSL (fig. 17E) were recorded in the absence and in presence of cAMP. In the central column are shown the background-subtracted dipolar evolution and fitted curves after Tikhonov regularization procedure.

The inter-spin DEER measurements obtained for both E172C-MTSL and E195C-MTSL in the cAMP-free state (Fig. 17C and F respectively, red signal), revealed that in the absence of the cyclic nucleotide the spin labels explore various inter-spin distances. Indeed, the distance distributions show multiple peaks in the range 1.9-4.1 nm. These data indicate that in the absence of cAMP

both the “elbow” and “shoulder” of the C-linker domain are in a multi dynamic state.
For both E172C-MTSL and E195C-MTSL samples in the cAMP-bound state was observed a partial variation on echo oscillations (fig. 17B and E respectively). The relative distance distributions for both the MTSL-labeled mutants result broader and tend to become bimodal, even if the main peaks, i.e. at 2.65 nm for E172C-MTSL and 2.11 nm for E195C-MTSL (table 2), that were present also in absence of the ligand, are still present. These results demonstrate that cAMP influences the conformation of the protein in both the “elbow” and the “shoulder” regions, leading to a stabilization of the chimera at the level of C-linker.

3.5.2.2 DEER on a residue in the N-terminal helical bundle

From the spin-labelled natural cysteine present in the N-terminal helical bundle, i.e. C202-MTSL (fig. 17G), Q-band DEER traces were recorded in the absence and in presence of cAMP (fig. 17H). In both the presence and absence of cAMP, the distance distributions show a maximum peak at similar values. The data indicate an increased structural heterogeneity in this boundary region to which MTSL was attached, suggesting that, even in the absence of cAMP, the protein is able to adopt holo- like conformations.

3.5.2.3 DEER on a residue in the αC-helix of CNBD

The DEER experiments performed on R329C-MTSL and the relative distance distributions (table 2) obtained for the cAMP-free and -bound mutant are shown in figures 17J-L. Similarly to what was observed in the C-linker domain (see chapter 5.2.1 of this section), the distances explored by R329C-MTSL spread out over a wider distance range in the absence than in the presence of cAMP. These results indicate that in the absence of cAMP, the position of the αC- helix is in a multi dynamic state. The conformational space occupied by the αC-helix is then reduced upon cAMP binding as suggested by the bimodal distribution of the distances. These results are in line with previous spectroscopic studies on the isolated CNBD domain that showed the closing movement of the αC-helix towards the ß roll upon cAMP binding (Puljung et al., 2014; Saponaro et al., 2014; DeBerg et al., 2015). Moreover, the presence of multiple distances explored by the spin labelled residue in the absence of cAMP is due to the fact that the C-terminal region of the αC-helix is known to be unstructured and to become ordered upon cAMP binding (Saponaro et al., 2014; Lee and MacKinnon 2017). Taken together these data confirm the reliability of the chimeric channel.

3.6 From the 2-fold symmetrical dimer of dimers to 4-fold symmetrical gating ring

Both CW-EPR and DEER experiments predicted a decrease in the conformational heterogeneity of the C-terminal regulatory domain of HCN4 upon binding to cAMP. This indication emerged especially from the distance distributions obtained from the analysis of the DEER experiments. Particularly, the distributions calculated for both the "elbow" and the "shoulder" of the C-linker and the CNBD domain showed multiple distance peaks in the cAMP-free state. The number of the peaks observed, dropped to two in the presence of the ligand.

Thus, in order to correlate the distance distributions obtained from the multi-spin interactions and the potential inner symmetries assumed by the C-terminal regulatory domain, I decided to use a reduced geometric model.

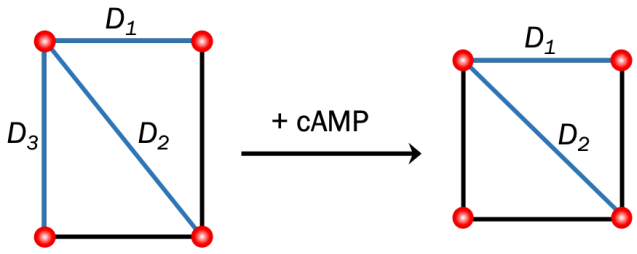

Figure 18: Geometrical shapes for explaining the conformational symmetries taken by the probes within the protein in the cAMP-free and -bound state. D1, D2 and D3 represents the main distances between the spin-labelled residues revealed by DEER experiments.

First of all, we have to consider that the number of expected distances and the mathematical relation between them, depend not only on the number of subunits/monomers of the multimeric assembly of interest but also on the symmetrical conformation adopted from the subunits forming the protein. Considering that the chimera K-H4ΔN VG is a homotetrameric channel, the expected number of distances taken by the MTSL-labelled residues within a tetrameric protein with a 4-fold symmetry is two (fig. 18, D_1 and D_2 in the square). However, this condition, that geometrically corresponds to a square, was observed only for the cAMP-bound protein. In contrast, the number of peaks corresponding to the main distances taken by the probes in the absence of cAMP rises to three. These distances suggest that the spin-labelled residue in the cAMP-free protein are arranged according to a rectangle shape (fig. 18, D_1, D_2 and D_3 in the rectangle).

Thus, the distance distributions obtained from DEER experiments showed that the binding of cAMP to the CNBD domain of the chimera causes relevant conformational changes in the C-terminal regulatory domains of HCN4. Particularly, the geometrical relationship of the distances measured, suggests that both the C-linker and the CNBD domains transit from a 2-fold dimer of dimers conformation to a 4-fold symmetrical gating ring (fig. 19 A, B and C).

This peculiar conformational behavior of the cytosolic regulatory domain of HCN channels was already suggested by previous functional and biochemical data (Ulens and Siegelbaum 2003; Zagotta et al., 2003; Lolicato et al., 2011).

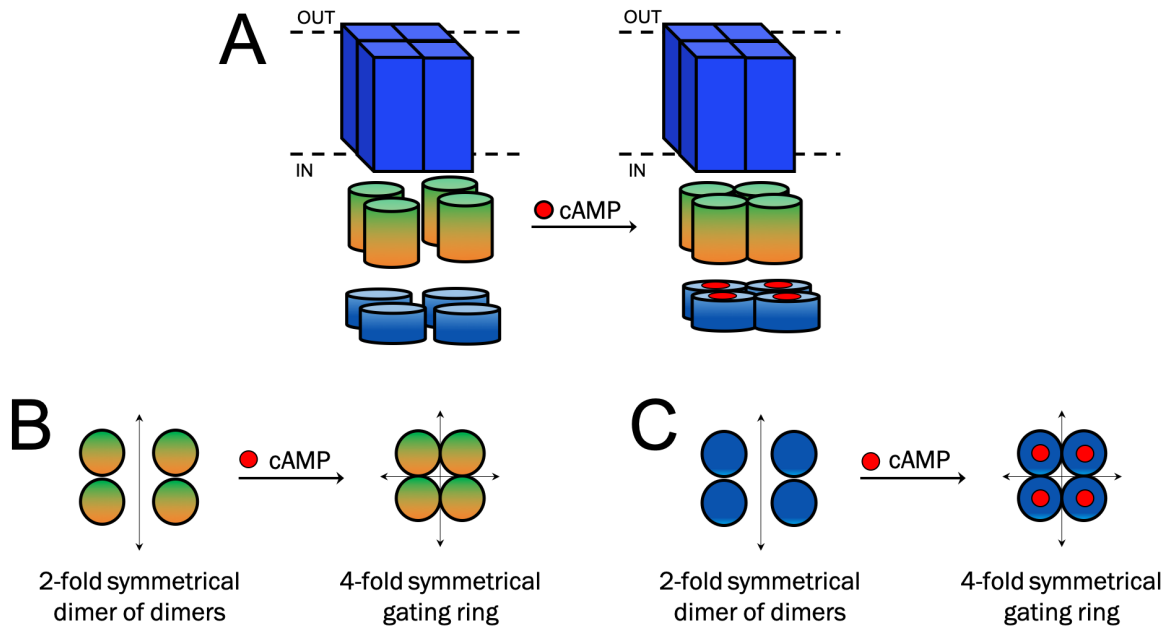

Figure 19: Both the C-linker and the CNBD shift between a 2-fold symmetrical dimer of dimers conformation to a 4-fold symmetrical gating ring upon cAMP binding. (A) Schematic representation of the chimeric channel. The pore domain is shown as blue parallelepipeds. The C-linker is schematized as green/orange cylinders (A) and as green/orange circles (B). These two colors respectively represent the "elbow" and the "shoulder" of the cytoplasmic domain. The CNBD domain is shown as blue cylinders (A) and as blue circles (C). The ligand cAMP is represented as a red circle. (B) and (C) depict the structural rearrangements induced in the cytoplasmic regulatory domains of the HCN channels by the binding of the cAMP to the CNBD.

4. Conclusions and future perspectives

The creation of the chimera K-H4ΔN VG was a challenging and arduous goal, as it is the result of the fusion of two evolutionary distant proteins such as the pore of the prokaryotic KcsA channel and the C-linker/CNBD of eukaryotic HCN4. Indeed, finding the correct junction between the two elements have been the major limitation in obtaining a stable and functional chimera.

The first attempt to engineer a chimeric channel (i.e. K-H4ΔN FQ) resulted in the creation of a chimera that was possible to purify only in the cAMP-bound state. Since the aim of this work was to perform biochemical and structural studies on the cAMP-induced conformational changes that characterize the C-linker domain, it was necessary to design a chimera stable in both the cAMP-free (i.e. apo) and -bound (i.e. holo) state. To this end, I modified the junction between the two elements that compose the chimeric channel by adding two residues, namely V115 and G116, that are naturally present at the boundary between the transmembrane helix M2 and the cytosolic domain of KcsA. The elongation of the junction determined the creation of the chimeric channel K-H4ΔN VG, that is purifiable in both the apo and the holo state. Moreover, the use of the *E. coli* strain C41(DE3) as organism for the heterologous expression of the chimera, allowed to significantly increase the yield of purified protein.

Experiments aimed to characterize the biophysical properties of the chimera showed that K - H4ΔN VG is a functional channel able to bind cAMP. Isothermal Titration Calorimetry (ITC) measurements demonstrated that the purified chimera binds cAMP with a Kd value of 1.7 μM. This value is consistent with the ligand binding affinity for the isolated C-linker/CNBD fragment of hHCN4 previously published (Lolicato et al., 2014). Differential scanning calorimetry (DSC) analysis of the cAMP-bound chimera showed a shift of the thermal denaturation curve toward higher temperatures compared to the curve of the cAMP-free sample. This data suggested that the binding of cAMP to the CNBD increases the stability of the chimera. Moreover, the expression of K- H4ΔN VG in the K^+-uptake deficient *E. coli* strain LB2003 determined the functional complementation of the phenotype under low potassium conditions. Particularly, the complementation effect at low K^+ concentrations was completely abolished in the presence of 5 mM BaCl2, thus confirming that the pore of the chimeric protein is able to conduct K^+ ions.

Structural studies of an active C-linker domain were performed on the purified chimera using two spectroscopic techniques, the Electron Paramagnetic Resonance (EPR) and the Double Electron-Electron Resonance (DEER). The use of these techniques based on the labelling with a paramagnetic tag was possible due to the homotetrameric assembly of the chimeric protein. Thus,

distance determinations between the probes within the protein are the result of the geometric interactions between neighboring and opposing subunits. In order to have a global view of the movements that characterize the C-terminal regulatory domain of HCN channels, paramagnetic probes were placed along the C-linker/CNBD, i.e. at the level of the "elbow" and the "shoulder" in order to study the active movement of the "elbow on the shoulder", in the N-terminal helical bundle (the border region that connects the CNBD domain to the C-linker) and in the CNBD domain. The results of the performed EPR-DEER experiments on the chimeric channel singularly labelled at the different levels aforementioned, interestingly revealed that the binding of cAMP to the CNBD domain induces a conformational switch in the C-terminal region of the protein. Indeed, the range of distance distributions obtained suggest that both the C-linker and CNBD domains transit from a 2-fold symmetrical dimer of dimers conformation in the absence of cAMP to a 4-fold symmetrical gating ring upon the binding of the ligand.

These results are in good agreement with previous functional and biochemical studies that have highlighted a key role of the C-linker domain in mediating the formation of the 4-fold symmetrical gating ring in the presence of cAMP (Zagotta et al., 2003). Particularly, fluorometry and electrophysiological data suggested that, in the absence of cAMP, the four subunits interact as a 2-fold symmetric dimer of dimers (Ulens and Siegelbaum, 2003; Kusch et al., 2012). Notably, the tonic inhibition of the channel in the absence of cAMP is hinted to arise from the 2-fold dimer of dimers symmetry of the C-terminal domains, whose formation is mediated by neighboring C-linkers (Ulens and Siegelbaum, 2003). Moreover, experiments in solution using HCN 2/4 C-linker/CNBD fragments demonstrated that the tetramerization occurs only upon cAMP binding in a C-linker dependent manner (Lolicato et al., 2011).

Interestingly, electron microscopy and image processing experiments performed on intact Cyclic Nucleotide-Gated (CNG) channels showed that the four CNBD domains of the channel associate as a dimer of dimers in the absence of the ligand (Higgins et al. 2002).

My attempt to increase the knowledge about the cAMP-induced conformational changes in HCN channels was successful because the data that I obtained are the first structural evidence that show the transition of the cytosolic domain of HCN channels from a dimer of dimers to a 4-fold symmetrical configuration, thus confirming the previous biochemical and functional data aforementioned.

The transition from a 2-fold symmetrical dimer of dimers conformation to a 4-fold symmetrical gating ring showed by the cytosolic domain of the chimera might reflect a pre-conditioning state

necessary for the action of cAMP on channel gating. Accordingly, these alterations in the structural symmetries of the C-terminal region could promote the autoinhibitory action exerted by the CNBD domain on channel opening. Then, the binding of cAMP could disinhibit the channel opening by promoting the assembly of the tetrameric gating ring. Thus, this symmetry change, that previous functional works showed to be C-linker-dependent (Ulens and Siegelbaum, 2003; Lolicato et al., 2011), could partly explains the agonistic activity exerted by cAMP on channel kinetics and open probability.

In support of the eventual autoinhibitory action of the dimer of dimers assembly on the channel opening there are MD simulations for dimer of dimers based on a cAMP-bound hHCN4 C-linker/CNBD crystal structure (PDB_ID: 3OTF, Xu et al., 2010) (VanSchouwen and Melacini 2018). Indeed, MD simulations demonstrated that the cAMP-free CNBD domain in the tetrameric assembly destabilizes the 4-fold gating ring conformation since it generates steric clashes with the C-linker domain. On the other hand, when the cAMP-free C-terminal region and, thus, the CNBD domain are in a dimer of dimers assembly, the steric clashes are abolished. Moreover, in this pseudo-dimeric state the protein is sensitized to cAMP-modulated allosteric perturbations. The binding of cAMP causes conformational changes in the CNBD domain that avoid steric clashes with the C-linker domain, thus promoting the tetrameric assembly of the C-terminal domains and facilitating the opening of the channel.

Hence, the EPR-DEER structural data obtained in this study suggest that the assembly of the C-terminal region imposed by the CNBD domain represent a possible mechanism for the removal of the autoinhibition that this domain exerts on the opening of the channel.

Particularly, the chimeric channel proved to be a useful tool for enhancing the understanding of the cAMP-dependent regulation of HCN channels. Thereby, the combination of already existing natural systems (i.e. KcsA and HCN4 channels) led to the creation of a synthetic model system that has allowed me to display functions that otherwise would have not been easily accessible to study in the wild type channel. Moreover, the use of the pore of the prokaryotic K^+ channel KcsA proved to be advantageous not only because it promoted the production of the chimera in *E. coli*, but especially because it removed the previously discussed problem of the Voltage Sensor Domain (VSD). This condition allows the visualization of the conformational changes in the active C-linker.

Moreover, KcsA is a well-characterized protein, whose crystal and NMR structures have been solved (Doyle et al., 1998; Chill et al., 2006) and that has been adopted as a model template for

the study of the pore domain of HCN channels (Chen et al., 2007; Bucchi et al, 2013). Thanks to its versatility, the pore of KcsA has been already employed for the engineering of active chimeric channels (Ohndorf and Mackinnon, 2005; McCoy et al., 2014), demonstrating to be a stable and functional building block. Indeed, once attached to another protein domain such as a CNBD, the pore domain of KcsA does not lose its conductivity (Ohndorf and Mackinnon, 2005; McCoy et al., 2014).

Hence, given these evidences, the use of the pore domain of this prokaryotic channel made it possible to investigate the dynamics behind the cAMP-induced interactions between the C-linker/CNBDs of all the four subunits in a tetrameric assembly. This condition should have promoted to reproduce the physiological condition as close as possible to the wild type channel, thus increasing the reliability of the chimera. Indeed, this investigation would not be possible with neither the soluble C-linker/CNBD fragment nor with the wild type channel.

However, I am aware of the limitations of my system since the chimera does not possess two important elements of the wild type channel, i.e. the VSD and the HCN domain (HCND). Indeed, the cryo-EM structure of HCN1 revealed that the VSD makes multiple contacts with the S5 helix of the pore, as well as with the C-linker domain and the HCND. Thus, although the removal of the VSD has abolished the inhibitory effect that this domain exerts on the C-linker domain under experimental conditions that do not impose hyperpolarizing voltages, the existence of a direct physical contact between the VSD and the C-linker domain cannot be ignored (Lee and Mackinnon, 2017). Moreover, a recent study based on the close inspection of the cryo-EM structure of HCN1 revealed that the HCND is involved in the voltage-dependent opening of the HCN channels (Porro et al., submitted). By making contacts with both the VSD and the C-linker domain, the HCND is an important coupling and transmission element, necessary for the cAMP caused effect on the channel activation. Moreover, during the autoinhibitory action exerted by the CNBD domain on the opening of the channel, the HCND could mediate the maintenance of the closed state of the channel by directly promoting a conformation of the VSD that disadvantages the opening of the pore (Porro et al., submitted).

Although the rescue of the phenotype shown by the strain LB2003 demonstrated that the chimera is able to conduct K^+ ions, up to now, it has not been possible to demonstrate if the activity of the channel pore is modulated by cAMP. To this end, firstly it will be necessary to use the open mutant, i.e. the chimera with the glutamate at position 88 of the KH4ΔN VG sequence mutated into an alanine. This mutation is a well-characterized mutation in the pore of KcsA (E71A in KcsA

sequence) that is known to abolish the inactivation at the level of the selectivity filter, thus increasing the open probability of the channel at pH 4 (Cordero-Morales et al., 2007). Then, the electrophysiological characterization of the chimera could be done by inserting the protein in a synthetic lipid bilayer. To this end, in order to increase the thermal stability of the protein, it will be necessary to extract the chimera from the native membranes using a styrene-maleic acid copolymer (SMA) (Dörr et al., 2016). These so called "natural nanodiscs", differently from detergents, do not substitute to the lipid bilayer, but spontaneously self- insert in the membrane and extract intact membrane proteins within a lipid bilayer (Orwick et al., 2012).

Another way to investigate the effect of cAMP on channel gating could be to measure the *in vivo* channel activity in bacteria with the patch-clamp technique. To apply this method, the limit of the diameter of the patch-pipette (i.e. 1μm) has to be overcome and *E. coli* cells have to be treated to become giant spheroplasts in order to allow the recording of current through individual ion channels in the native membrane (Martinac et al., 2013). By using the inside-out patch-clamp configuration it would be possible to investigate the effect of cAMP on channel activity by adding cAMP directly to the bath solution.

The suggested involvement of the dynamical transition of the C-terminal domain from a dimer of dimers into a tetrameric gating ring in the channel's autoinhibitory-system could be used in the future for pharmacological purposes. Indeed, the development of drugs aimed to promote one of the two symmetrical assemblies could allow to create new therapeutic approaches for HCN-related diseases. For instance, HCN2 involvement in neuropathic pain is related to the increased cAMP content of neurons that chronically activates the channel leading to increased firing rates (Emery et al., 2012). In this regard, a drug able to prevent cAMP activation of the channel would be highly desirable.

Potential small molecules whose effect could be tested on the conformational switch from a 2-fold symmetrical dimer of dimers to a 4-fold symmetrical gating ring are cyclic dinucleotides, an emerging class of signaling molecules in humans (Sun et al., 2013). These molecules that antagonize cAMP regulation of HCN (Lolicato et al., 2014) should promote the dimer of dimers state.

Moreover, an eventual natural stabilizer of the dimer of dimers conformation is the HCN auxiliary subunit TRIP8b (Saponaro et al., 2014 and 2018). Indeed, TRIP8b interacts with the CNBD through its core domain and antagonizes the effect of cAMP on channel opening.

Particularly, the peptide drug TRIP8b$_{nano}$, a TRIP8b-derived peptide, that binds to the CNBD and reproduces the effect of the full-length TRIP8b in three HCN isoforms (HCN1, 2 and 4) (Saponaro et al., 2018), could be used for further EPR-DEER experiments on the chimera. Therefore, by directly adding TRIP8b$_{nano}$ to the sample buffer, it should be possible to observe its effect on the dynamical transition from a dimer of dimers to a tetrameric gating ring.

In conclusion, the chimera K - H4ΔN VG enhanced our understanding of cAMP modulation of HCN channels. Indeed, the chimeric protein is the first full-length channel that gave structural information about the dynamical transition of the C-terminal domain of HCN channels from a 2-fold dimer of dimers symmetry to a 4-fold symmetrical gating ring upon cAMP binding. Thus, these structural data rationalize the previously obtained functional and electrophysiological data that had already hinted towards this dynamical behavior of the C-linker/CNBD domain (Ulens and Siegelbaum, 2003; Zagotta et al., 2003; Lolicato et al., 2011; Kusch et al., 2012; VanSchouwen and Melacini 2018). Particularly, the chimera has demonstrated to be a versatile model to study dynamical features otherwise inaccessible with the wild type channel. Such a protein could be used as biological tool for potential future drug screenings in order to find small molecules that antagonize the cAMP-induced transition from a 2-fold symmetrical dimer of dimers conformation to a 4-fold symmetrical gating ring. This will result in a modulation of the channel activity.

5. Material and Methods

5.1 Cloning and mutagenesis of the chimeric constructs used for protein purification

5.1.1 The vector pET-24b(H3C)

For the expression of the proteins destined for purification, the cDNAs encoding the different chimeric constructs were cloned into a modified pET-24b(H3C) vector (kan^r), downstream of a hexa-histidine tag. In this vector the expression of the gene of interest is under control of a *lac*-operator sequence and, upstream to the latter, the T7 promoter. In this way, the system allows the expression of recombinant proteins only under controlled conditions, i.e. by the addition of isopropyl β-D-1-thiogalactopyranoside (IPTG).

The vector was modified in order to allow the cloning of cDNAs into the plasmid using the Ligation-Independent Cloning (LIC) system. A 100 bp long cDNA cassette was inserted between the restriction sites NdeI and XhoI. The cassette is engineered in order to position different elements at the N-terminus of the protein of interest. The elements are in the following order: an N-terminal hexa-histidine tag, used for the purification of the protein on nickel resins; the sequence encoding the target site of the HRV3C protease, for the further removal of the hexa-histidine tag; the LIC sequence with the SmaI restriction site, used to linearize the vector and to generate the overhanging sequences for LIC system; a terminator sequence. The restriction site SmaI within the Kan gene was mutated in order to have only the SmaI site within the LIC sequence of the inserted cassette. The mutation did not alter the plasmid resistance to the antibiotic kanamycin.

5.1.2 The cDNA for KcsA-HCN4 C-linker/CNBD chimera

The first chimeric construct engineered was K-H4ΔN FQ. For the generation of both the chimeric constructs K-H4ΔN VG and VGRE see the chapter 5.1.4 of this section. The cDNA of K-H4ΔN FQ, formed by the truncated transmembrane pore of KcsA (i.e. residues from L16 to F114) and the C-linker/CNBD domain of human HCN4 (i.e. from residue Q518 to H723), was obtained using an overlapping PCR strategy (Horton et al., 1993) (KcsA UniProtKB: P0A334; hHCN4 UniProtKB: Q9Y3Q4). Each fragment was amplified using primers with modified ends. In this way, PCR products were obtained that have common sequences at one end that allow the

overlapping reaction. The ends of the final PCR product were equipped with specific LIC sequences for performing the further cloning of the cDNA into the pET24b(H3C) vector.

The transmembrane pore domain of KcsA was amplified using the following pair of primers (LIC sequences are in **bold**; KcsA sequences are regular; hHCN4 sequences are in *italic*):

Forward: 5'-**CAAGGACCGAGCAGCCCCTCC**CTGCTCGGGCGCC-3'

Reverse: 5'-*CCGGGAGGAGTCCAGGGACTG*GAACCAGGTGGCCAGCGC-3'

The C-linker/CNBD domain of hHCN4 was amplified using the following pair of primers (LIC sequences are in **bold**; KcsA sequences are regular; hHCN4 sequences are in *italic*):

Forward: 5'- GCGCTGGCCACCTGGTTC*CAGTCCCTGGACTCCTCCCGG*-3'

Reverse: 5'- **ACCACGGGGAACCAACCCTTATTA***GTGGAGGAGGATGGAGTTCT*-3'

In order to confirm the overlapping reaction between the two fragments and, thus, the formation of the chimeric cDNA K-H4ΔN FQ, the final DNA fragment was separated electrophoretically in an 1% (w/v) agarose gel. The band corresponding to the DNA fragment of interest (i.e. 1,000 bp) was then purified by gel extraction using the Expin^{TM} Combo GP (GeneAll) following the manufacturer's instructions.

5.1.3 Ligation-Independent Cloning (LIC) system

Once the chimeric cDNA with specific LIC extremities was obtained, the PCR-generated fragment was cloned into the pET24b(H3C) vector using LIC system (Doyle 2005). LIC is a cloning method that is based on the annealing of single-stranded complementary overhangs between the target vector and a PCR-generated cDNA, both equipped with the specific LIC sequences. The specific LIC sequences present in both the vector and the insert were treated with T4 DNA polymerase in the presence of a single dNTP (i.e. dATP for the insert and dTTP for the vector). This reaction mix determined the formation of two complementary single-stranded overhangs, by creating an equilibrium of 3'->5'-exonuclease and 5'->3'-polymerase activity of T4 DNA polymerase at the site of the first occurrence of one of the specific nucleotides. Once the single-stranded overhangs were created, the vector and the cDNA were incubated together at room temperature for 10 minutes to promote the annealing reaction.

After annealing of vector and insert, 5 µl of the mixture were used to transform 50 µl of chemically competent *E. coli* DH5α cells. The transformation procedure consisted of the following steps: after a short incubation on ice, cells were transformed by heat shock at 42°C for 1 minute and 30 seconds and subsequently transferred again on ice. After growing in 500 µl of LB medium (10 g/L tryptone,

5 g/L yeast extract, 5 g/L NaCl (Sigma-Aldrich)) at 37°C for 45 minutes, the transformed cells were then spread on LB agar plates (10 g/L tryptone, 5 g/L yeast extract, 5 g/L NaCl, 20 g/L Agar (Sigma-Aldrich)) containing 50 µg/mL kanamycin and incubated at 37°C overnight. Positive colonies were identified by colony PCR and transferred into LB medium supplemented with 50 µg/mL kanamycin. After incubation at 37°C overnight, the plasmid DNA was purified using the Exprep™ Plasmid SV mini kit (GeneAll). The cloning was verified by DNA sequencing.

5.1.4 Insertion of residues for the creation of K-H4ΔN VG and VGRE

Once the cDNA of the chimeric construct was cloned into the pET24b(H3C) vector, both the chimeric constructs K-H4ΔN VG and VGRE were successively generated by site-directed mutagenesis (QuickChange site-directed mutagenesis kit; Agilent Technologies) following the manufacturer's instructions. For K-H4ΔN VG, residues V and G (i.e. Valine 115 and Glutamine 116 in KcsA sequence) were gradually inserted in K-H4ΔN FQ cDNA after the residue phenylalanine F114. Whereas for K-H4ΔN VGRE, residues R and E (i.e. arginine 117 and glutamate 118 in KcsA sequence) were inserted into K-H4ΔN VG cDNA downstream of the residue G116. Subsequentely, 5 µl of each of the aforementioned reactions were used to transform 50 µl of chemically competent *E. coli* DH5α cells, following the procedure described in chapter 5.1.3 of this section. The mutations were verified by DNA sequencing.

5.2 Heterologous expression and purification of the chimera

5.2.1 *E. coli* C41(DE3) strain

For the heterologous expression of the chimeric proteins the *E. coli* strain C41(DE3) was used. C41(DE3) is a T7 RNA polymerase-based expression host, that was kindly provided by Sir John Walker. C41(DE3) is a derivative of BL21(DE3) and therefore deficient in Lon and OmpT proteases. Particularly, compared to BL21(DE3), C41(DE3) has improved membrane protein overproduction characteristics (Miroux and Walker, 1996; Dumon-Seignovert et al., 2004; Wagner et al., 2008). Indeed, the Walker strain has mutations in the *lac*UV5 promoter, which governs the expression of the T7 RNA Polymerase. These mutations lower the amount of expressed T7 RNA Polymerase, thus preventing the unwanted saturation of the Sec translocon that

normally leads to protein aggregation and cell toxicity when proteins are overexpressed (Wagner et al., 2008). Since the T7 RNA polymerase gene is under control of an IPTG-inducible *lac*UV5 promoter, the expression of the gene of interest can be controlled by the addition of the inducer IPTG.

10 ng of the chimeric constructs described in the previous chapter were used to transform 50 µl of chemically competent C41(DE3) cells. After a short incubation on ice, the mixture of chemically competent bacteria and DNA was heat shocked at 42°C for 1 minute and 30 seconds and then placed back on ice. To the 50 µl of transformed cells 500 µl of LB medium were added and the cells were then grown for 45 minutes at 37°C. Transformed cells were plated on LB agar plates supplemented with 50 µg/mL kanamicin and grown at 37°C overnight.

5.2.2 Heterologous expression of the chimera

Starting from a single clone, overnight cultures of the transformed C41(DE3) cells harboring the pET24b(H3C) plasmid encoding one of the previously described chimeras, were grown at 37°C in LB medium supplemented with 50 µg/mL kanamycin.

The following day, an aliquot of the starting culture was added to a flask containing LB medium supplemented with 50 µg/mL kanamycin. The cells were grown at 37°C in an orbital shaker at 300 rpm (New Brunswick™ Excella® E25). As soon as the optical density at a wavelength of 600 nm (OD_{600}) reached a value of 0.8 the expression of the protein was induced.

Particularly, the expression of the chimeric construct K-H4ΔN VG was induced overnight with 100 µM IPTG at 20°C in an orbital shaker at 75 rpm (New Brunswick™ Excella® E25). The following day, the cells were collected by centrifugation at 3,000 rpm (Sorvall, rotor SLA1500) at 4°C for 30 minutes.

In order to find the best conditions for the expression of the chimeric channels, different induction parameters were tested after an OD_{600} value of 0.8 had been reached: the concentration of the inducer IPTG (i.e. 100 µM or 400 µM), the temperature (i.e. 37°C or 20°C) and the induction phase duration (i.e. 3 hours or overnight).

5.2.3 Purification of the chimeric protein

Although the final chimeric construct used for all the experiments described in this PhD thesis was K-H4ΔN VG, it is necessary to know that the protocols described in this chapter were equally

employed for the expression and purification of the constructs K-H4ΔN FQ and VGRE. For simplicity, from now all descriptions refer only to the construct K-H4ΔN VG.

The cell pellet collected by centrifugation was resuspended in ice-cold lysis buffer for 30 minutes in a ratio original cell culture volume : lysis buffer of 20 : 1 (lysis buffer: 100 mM KCl, 20 mM Tris-HCl (pH 7.6) with the addition of 1 mM β-mercaptoethanol, 10 µg/mL DNase, 0.25 mg/mL lysozyme, 100 µM phenylmethylsulfonyl fluoride, 0.1mg/mL trypsin inhibitor, 1 mM benzamidine, 0.1 mM pefablock (Sigma-Aldrich)). For the purification of the protein in the presence of cAMP, 500 µM of the ligand were added.

After a short incubation on ice, cells were mechanically lysed with a high-pressure cell homogenizer (40 KPSI HEAD) and the lysate was cleared by centrifugation (i.e. 13,000 rpm (Sorvall, rotor SS34) for 10 minutes at 4°C). Cell membranes containing the chimeric protein were isolated by centrifugation of the lysate at 18,000 rpm (Sorvall, rotor SS34) for 2 hours and 30 minutes at 4°C. The pellet containing the membranes was mechanically resuspended with a buffer supplemented with 30 mM n-decyl-β-D-maltopyranoside (DM, CMC: (H_2O) ~ 1.8 mM, Anatrace, Maumee, OH, USA) in a ratio original cell culture volume : resuspension buffer of 20 : 1 (resuspension buffer: 100 mM KCl, 20 mM Tris-HCl (pH 7.6), 1 mM β-mercaptoethanol and 30 mM DM). Chimeric membrane proteins were extracted overnight at 4°C. For the purification of the protein in the presence of cAMP, 500 µM of the ligand were added during the extraction process.

On the following day, solubilized membranes were clarified by centrifugation at 18,000 rpm (Sorvall, rotor SS34) for 30 minutes at 4°C. The obtained supernatant was supplemented with 40 mM imidazole in order to avoid the binding of contaminants to the nickel resin. Subsequently, the histidine-tagged protein was purified using a nickel affinity column (HiTrap IMAC HP (GE Healthcare)). Once the protein had bound to the nickel resin, the column was washed with 10 column volumes of the following buffer: 100 mM KCl, 20 mM Tris-HCl (pH 7.6), 5mM DM and 40 mM imidazole. The chimera was eluted in the latter buffer supplemented with 300 mM imidazole and successively injected to a HiLoad 16/600 Superdex 200 Prep Grade column (GE Healthcare) equilibrated with buffer containing 100 mM KCl, 20 mM Tris-HCl (pH 7.6) and 5 mM DM. The purification process is partly automated and managed by the AKTA purifier system (GE Healthcare). For the purification of the cAMP-bound chimera, each of the aforementioned buffers was supplemented with 200 µM cAMP (Sigma-Aldrich).

The final protein concentration was determined by spectrophotometry using the calculated molecular absorbance coefficient $\varepsilon = 51{,}465\ M^{-1}\ cm^{-1}$.

5.3 SDS-PAGE and Western Blot analysis

Purified protein samples were separated in SDS- polyacrylamide gels (Novex™ 4-20% Tris-Glycine Mini Gels, WedgeWell™, Invitrogen) and successively stained with Coomassie blue (Sigma-Aldrich). Novex Sharp Pre-stained Protein Standards (Invitrogen) were used as size references.

For all the experiments aimed to detect the level of protein expression, once the induction process was finished, samples of 1 mL volume were collected from each different bacterial culture. The cells were centrifuged at 13,000 rpm for 10 minutes and the resulting pellet was resuspended in 50 µl Laemmli (Sigma-Aldrich). If necessary for the purpose of the experiment, the samples were boiled for 3 minutes. An aliquot from each sample was analyzed by SDS- polyacrylamide gel (Novex™ 4-20% Tris-Glycine Mini Gels, WedgeWell™, Invitrogen) and Novex Sharp Pre-stained Protein Standards (Invitrogen) were used as size references. Samples were analyzed with the Western Blot technique. For immunological detection of proteins, the gels were blotted onto a PVDF Transfer Membrane (Invitrogen) and incubated with the primary monoclonal anti-polyHistidine (mouse IgG2a) antibody (Sigma-Aldrich) that is able to detect the histidine-tag positioned at the N-terminus of each chimeric construct. The secondary antibody anti-mouse IgG conjugated to alkaline phosphatase (Sigma-Aldrich) allowed the detection of the bands relative to the histidine-tagged proteins upon addition of the enzyme's substrate (SIGMAFAST™ BCIP®/NBT, Sigma-Aldrich).

5.4 Direct measurement of cAMP binding by Isothermal Titration Calorimetry (ITC)

The Isothermal Titration Calorimetry (ITC) is a quantitative technique that allows the determination of thermodynamic parameters that characterize the interactions between molecules or molecular complexes by measuring the heat released or absorbed at constant pressure during a reaction specifically designed for the experiment. The ITC allows direct measurement of the binding affinity constant (Ka), enthalpy changes (ΔH), entropy changes (ΔS), and the binding stoichiometry (n) of the interacting molecules in solution. From these measurements it is possible to determine the change in Gibbs energy (ΔG) that occur during the reaction using the relationship

$$\Delta G = -R\,T\,ln\,Ka = \Delta H - T\Delta S$$

with R being the gas constant and T the absolute temperature.

The ITC instrument has two identical cells (i.e. the reference and the sample cells) whose temperature differences are monitored by thermoelectric devices. During an experiment, the ligand is added to the cell containing the sample by successive predefined injections. These injections cause an absorption or release of heat (depending on the nature of the reaction) that results in a change in the temperature of the sample cell. In the course of the experiment, the instrument measures the time-dependent energy input that has to be supplied to or subtracted from the sample cell in order to maintain the latter at the same temperature as the reference cell.

Each heat-oscillation peak shown in the raw data corresponds to a single injection of the ligand into the sample cell. The integration of these peaks over time provides the total heat exchanged by each injection. The binding curve of the reaction is obtained by plotting the heat per each injection as a function of the molar ratio of the ligand and the binding partner. The binding curve can be analyzed with the appropriate binding model to determine Ka, n, ΔH and ΔS that characterize the interaction (Wiseman et. al, 1989).

Before the experiment was performed, the protein sample was concentrated with an Amicon Ultra centrifugal filter (MWCO 100 kDa) to 20 μM. For ITC experiments, the chimeric channels and the ligand cAMP were dissolved in elution buffer (100 mM KCl, 20 mM Tris-HCl (pH 7.6) and 5 mM DM). Measurements were carried out at 20°C using MicroCal VP-ITC microcalorimeter (Malvern Panalytical). The volume of the sample cell was 1.4 mL and the reference cell contained water. The chimera K-H4ΔN VG (20 μM) was titrated with cAMP (200 μM) using injection volumes of 8 μL. Calorimetric data were analyzed with MicroCal Origin software (version 7) using equations described for the single-site binding model (Wiseman et. al, 1989).

5.5 Differential Scanning Calorimetry (DSC)

DSC is a technique that measures the amount of heat absorbed or released by a dissolved compound (such as a biomolecule) as it is continuously heated or cooled in time. Indeed, macromolecules such as proteins respond to thermal changes by unfolding at a characteristic temperature. The more intrinsically stable the protein, the higher the melting temperature (Tm) of the unfolding transition. DSC is a valuable tool for studying biomolecular interactions (i.e. protein-ligand, protein-protein and protein-DNA). Particularly, contrary to ITC, DSC allows the

correlation of the thermodynamics that drive the binding with conformational changes in the macromolecule caused by the binding reaction.

The differential scanning calorimeter measures the thermal transition temperature (melting temperature, Tm) and the energy required to disrupt the interactions stabilizing the tertiary structure (enthalpy, ΔH) of proteins.

The thermodynamic study of the interaction between K-H4ΔN VG and cAMP was performed with a nano-DSC (TA instruments). The volume of the capillary sample cell was 0.299 mL. Thanks to the capillary design of the cell, this DSC can be used to analyze structurally unstable samples showing aggregation and precipitation during a scan. Moreover, it provides unparalleled sensitivity, accuracy and precision that make it able to detect processes that exchange microjoule levels of heat. In order to perform the experiment, the protein sample was concentrated with an Amicon Ultra centrifugal filter (MWCO 100 kDa) to 80 μM. The experiments were performed in the absence and in the presence of 200 μm cAMP. Thermal scans were performed between 10°C and 80°C upon a preliminary equilibration of the instrument at 10°C for 10 minutes. The scan rate in both experiments was $0.5°C \cdot min^{-1}$.

5.6 Characterization of cell growth in the presence of barium

For the characterization of cell growth in the presence of barium, a well-known K^+ channel blocker, two variants of the chimeric channel K-H4ΔN VG were used. Indeed, on the construct of the wild type chimera (WT) cloned in pET24b(H3C) vector, the glutamate 88 (in KH4ΔN VG sequence) was mutated into an alanine by site-directed mutagenesis (QuickChange site-directed mutagenesis kit; Agilent Technologies) following the manufacturer's instructions. The reaction mix was used to transform DH5α as described in chapter 5.1.3 of this section. The mutation (hereinafter referred to as E88A) was verified by DNA sequencing.

C41(DE3) cells were transformed with pET24b(H3C) plasmid containing the gene codifying either for the WT or the open mutant E88A or with the empty vector as control, following the procedure described in chapter 5.2.1 of this section.

Transformed cells were then grown in flasks as described in chapter 5.2.2 of this section. Once the optical density at a wavelength of 600 nm (OD_{600}) of the cells was around 0.6-0.7, the protein expression was induced with 100 μM IPTG and the medium was supplemented either with 10 mM $BaCl_2$ or with the same volume of sterilized ddH_2O. The protein expression followed the optimal parameters identified for K-H4ΔN VG. After the induction in the presence or in the absence of

10 mM $BaCl_2$, OD_{600} of the cells was used to monitor the growth. Measurements were conducted on culture aliquots diluted 1:10 with LB medium.

5.7 Complementation assay

5.7.1 Cloning and mutagenesis of the chimeric construct

For the complementation assay, the cDNA of K-H4ΔN VG (i.e. WT, wild type) was cloned into the pGM930 vector (amp^r) using Gibson cloning (Gibson et al., 2009), an isothermal single-reaction method that allows the assembly of multiple overlapping DNA molecules by the concerted action of a 5' exonuclease, a DNA polymerase and a DNA ligase. For this experiment pGM930 vector, a modified pBAD24 plasmid, was kindly provided by Prof. Federica Briani (Università degli Studi di Milano) (Delvillani et al., 2014).

Firstly, the DNA fragment encoding K-H4ΔN VG was amplified with the following pair of primers in order to add at each end overlapping sequences that are complementary to the NcoI/KpnI linearized pGM930 vector (vector sequences are in **bold**; K-H4ΔN VG sequences are grey):

Forward: 5'- **ACTCTCTACTGTTTCTC**ATGCACCATCATCATCACCATCATCATGGC-3'

Reverse: 5'-**CGACTCTAGAGGATCCCCGG**TTATTAGTGGAGGAGGATGGAGTT-3'

1 µg of pGM930 vector was linearized in a double digest reaction with NcoI and KpnI (NEB, Ipswich, MA, USA) and subsequently blunted with a T4 DNA polymerase (NEB, Ipswich, MA, USA).

The NcoI/KpnI digested pGM930 vector and the K-H4ΔN VG fragment were loaded on a 1% (w/v) agarose gel. The bands corresponding to the DNA fragments of interest (i.e. 4,600 bp for pGM930 and 1,000 bp for the insert) were extracted from the gel and purified using the Expin™ Combo GP kit (GeneAll).

The double-stranded DNA fragment was then inserted into the linearized vector using Gibson Assembly Cloning Kit (NEB, Ipswich, MA, USA), following the manufacturer's instructions.

50 µl of chemically competent *E. coli* DH5α cells were transformed with 5 µl of the reaction mix as described in chapter 5.1.3 of this section. The transformed cells were grown on LB agar plates containing 100 µg/mL ampicillin and incubated at 37°C overnight. The plasmid DNA from positive colonies was purified using the Exprep™ Plasmid SV mini kit (GeneAll). The cloning was verified by DNA sequencing.

5.7.2 The vector pGM930$_{SD}$

The pGM930 vector was modified by inserting a ribosomal binding site (Shine-Dalgarno (SD) sequence) in order to allow the protein synthesis. The vector containing the cDNA of the chimera was firstly linearized by PCR reaction using the following pair of primers:

Forward: 5'-ATGCACCATCATCATCACCATC-3'

Reverse: 5'-GAGAAACAGTAGAGAGTTGCG-3'

The double-stranded DNA fragment carrying the SD was generated by PCR amplification, using the following pair of primers that simultaneously served also as templates. Indeed, they were designed in order to anneal only partially.

Forward: 5'-CGCAACTCTCTACTGTTTCTCGAATTCTTTGTTTAACTTTAAGAAGGAGA TATACAT-3'

Reverse: 5'-GATGGTGATGATGATGGTGCATATGTATATCTCCTTCTTAAAGTTAAACA AA-3'

The resulting double-stranded DNA fragment is the following:

5'-

CGCAACTCTCTACTGTTTCTC*GAATTC*TTTGTTTAACTTTAAGAAGGAGATATA*CAT ATG*CACCATCATCATCACCATC-3'

The SD sequence is shown in red, whereas the vector sequence is in **bold** and K-H4ΔN VG sequence is grey. The fragment was equipped with overlapping ends for subsequent cloning in the linearized pGM930 vector upstream to the coding sequence of the chimeric channel. Moreover, restriction sites for both EcoRI (i.e. *GAATTC)* and NdeI (i.e. *CATATG*) were inserted for an eventual future use of the RBS sequence in other vectors.

The double-stranded SD fragment was inserted into the linearized vector using the Gibson Assembly Cloning Kit (NEB, Ipswich, MA, USA), following the manufacturer's instructions. Once *E. coli* DH5α were transformed, the plasmids containing the correct insert were selected and purified as described in the previous chapter. The cloning of the SD sequence was verified by DNA sequencing. The mutated vector containing the Shine-Dalgarno sequence was called pGM930$_{SD}$.

Subsequently, the mutation E88A was introduced in this construct by site-directed mutagenesis (QuickChange site-directed mutagenesis kit; Agilent Technologies) following the manufacturer's instructions. The mutation was verified by DNA sequencing.

5.7.3 Complementation of LB2003 *E. coli* strain

The complementation assay was performed using *E. coli* strain LB2003, one of the K-dependent mutants of the *E. coli* strain K-12 that were selected for their slower growth in media containing low concentrations of potassium (Epstein and Davies, 1970). Indeed, LB2003 is a strain that lacks the three major K^+ uptake systems, Trk (TrkG and TrkH), Kup (TrkD) and Kdp. Because of this lack, LB2003 requires for half-maximal cell growth a medium supplemented with 25 mM K^+. Since the endogenous K^+ influx activity in this strain is very low, an increase in K^+ uptake permeability resulting from an exogenous gene product can be easily measured (Epstein and Davies, 1970; Buurman et al., 1995; Uozumi et al., 1998).

50 µl of LB2003 cells were transformed with 10 ng of the empty $pGM930_{SD}$ plasmid or the plasmid encoding either the WT chimera or the mutant E88A. After a short incubation on ice, the mixture of chemically competent bacteria and DNA was heat shocked at 42°C for 40 seconds and then placed back on ice. Subsequently, 200 µl of LB medium supplemented with 100 mM KCl were added and the cells were then grown for 45 minutes at 37°C. Transformed cells were plated on LB agar plates (10 g/L tryptone, 5 g/L yeast extract, 10 g/L NaCl, 20 g/L agar, pH 6.8) supplemented with 100 mM KCl and 100 µg/mL ampicillin and afterwards grown at 37°C overnight.

Starting from a single clone, overnight cultures of the transformed cells were grown at 37°C in LB medium (10 g/L tryptone, 5 g/L yeast extract, 10 g/L NaCl, pH 6.8) supplemented with 100 mM KCl and 100 µg/mL ampicillin. On the following day, transformed LB2003 cells were diluted with LB medium, not supplemented with KCl but containing 100 µg/mL ampicillin, in order to reach an optical density value (OD_{600}) of 0.1. Starting from the latter, serial dilutions were prepared in the aforementioned K^+-free LB medium (i.e. from 10^{-1} to 10^{-4}). The different serial dilutions were used to perform a drop test on LB agar plates (10 g/L tryptone, 5 g/L yeast extract, 10 g/L NaCl, 20 g/L agar, pH 6.5 adjusted with 10% (v/v) HCl) containing different additional KCl concentrations (i.e. 0 mM, 10 mM and 100 mM), in the presence or absence of 0.2% (w/v) of the inducer L-arabinose and in the presence or absence of 5 mM $BaCl_2$. Plates were incubated overnight at 37°C.

5.8 Cryo-EM

5.8.1 Amphipol-detergent exchange

For cryo-EM experiments, K-H4ΔN VG chimeric protein was expressed and purified in the absence or in the presence of cAMP as described in chapters 5.2.2 and 5.2.3 of this section.
The purified protein was concentrated by Amicon Ultra centrifugal filter (MWCO 100 kDa) to a final volume of 1.5 mL. For the detergent exchange, amphipols A8-35 (Anatrace, Maumee, OH, USA) were dissolved in 100 µl of buffer not supplemented with detergent (amphipol buffer: 100 mM KCl and 20 mM Tris-HCl (pH7.6)). For a successful exchange the weight ratio of amphipols : protein was 10 : 1. Dissolved amphipols were added to the protein sample and the mixture was gently blended on an end-over-end shaker for 4 hours at 4°C. Bio-Beads SM-2 (Biorad, Hercules, CA, USA) were activated and equilibrated in amphipol buffer (100 mg of beads for each mL of protein/amphipol mixture). At the end of the 4 hours incubation, the detergent was removed from the protein/amphipol mixture by adding activated Bio-Beads and gently mixing on the end-over-end shaker overnight at 4°C. After the overnight incubation, the sample was separated from the beads and centrifuged at 13,000 rpm for 10 minutes at 4°C to remove eventual aggregates. Successively, the sample was concentrated by Amicon Ultra centrifugal filter (MWCO 100 kDa) up to 0.5 mL and injected to a Superose 6 increase 10/300 column (GE Helthcare) equilibrated with amphipol buffer for size exclusion chromatography. The peak fractions were pooled together and concentrated to 0.5 mg/mL.
The final protein concentration was determined by using the calculated molecular absorbance coefficient $\varepsilon = 51{,}465\ M^{-1}\ cm^{-1}$.

5.8.2 Grids preparation

For the negative staining of both the cAMP-free and cAMP-bound proteins, 4 µl of each sample at 0.5 mg/mL were applied onto 400-mesh copper carbon-coated grids (Agar Scientific), glow discharged for 30 seconds at 30 mA using a GloQube system (Quorum Technologies). After the sample was adsorbed, the grids were stained with 2% (w/v) uranyl acetate and blotted dry. After 1 minute incubation at room temperature, the grids were imaged on a LEO 912Ab transmission electron microscope (Zeiss) operating at 100 keV.

For cryo-EM grids preparation, 3 µl of each sample at 0.5 mg/mL were applied onto a glow discharged 300-mesh holey carbon grids (Quantifoil R1.2/1.3). After a short incubation for 30 seconds, the grids were plunged into liquid ethane using a Vitrobot Mk IV (Thermo Fischer Scientific) operating at 4 °C and 100% humidity.

5.8.3 Cryo-EM data collection and image processing

The grids were loaded onto a Talos Arctica transmission electron microscope (Thermo Fisher Scientific) operated at 200 kV. For each vitrified sample were collected a total of 2000 images. Each image was acquired with an exposure time of 1 second and a total accumulated dose of 50 electrons per A2 equally distributed over 39 movie frames. Images were acquired at a nominal magnification of ×120,000, corresponding to a pixel size of 0.889 Å/pixel at the specimen level, with applied defocus values between −0.5 and −2.5 µm.
Prior to image processing, anisotropic magnification distortion was automatically estimated using mag_distortion_estimate (Grant and Grigorieff, 2015). Images were corrected for anisotropic magnification distortion (resulting in a corrected pixel size of 0.887 Å), motion-corrected and dose-weighted using MOTIONCOR2 (Zheng et al., 2017). Contrast transfer function (CTF) estimation was performed on aligned, unweighted sum images using CTFFIND4 (Rohou and Grigorieff, 2015). The average maximal signal from the entire micrograph dataset was around 2.8 Å. A total of about 500K single particles were selected for each dataset and imported in RELION 2.1 (Scheres 2012) for further 2-D and 3-D analysis. For both datasets was possible only to perform the 2-D classification with regularization value of T = 2 to remove contaminants. Subsequent rounds of reference-free 2-D classification were performed with regularization value of T = 4.
For the cAMP-bound chimera 3-D classifications were performed in order to attempt to isolate a particle population that could have contributed to an isotropic structure.

5.9 EPR and DEER experiments

Electron Paramagnetic Resonance (EPR) is a magnetic resonance technique aimed to detect the transitions of unpaired electrons in an applied magnetic field. This technique is also known as Site- Directed Spin Labelling Electron Paramagnetic Resonance (SDSL-EPR) since pairs of cysteine residues strategically positioned in sites of interest on a cysteine-free protein can be specifically spin- labelled with a paramagnetic tag. Paramagnetic tags, such as a nitroxide radical,

can be further monitored by EPR spectroscopy (Jeschke 2012). The shape of the relative continuous wave EPR (CW-EPR) spectrum recorded reflects the mobility of the probe. This provides information concerning the local environment and the dynamic of the protein. Particularly, high degree of flexibility of the protein region where the paramagnetic tag is placed gives narrow line widths in the spectrum (sharp signal), while a decrease of mobility consists in a widening of the spectrum (broad signal). For this reasons, SDSL-EPR spectroscopy is widely use to study conformational transition in protein and others bio-macromolecules (Jeschke 2012; Giannoulis et al., 2013; Klare 2013; Sahu and Lorigan, 2018). In Double Electron-Electron Resonance (DEER) experiments, as in EPR, two or more paramagnetic probes are inserted at strategical positions within the protein at the level of cysteine residues previously introduced by mutagenesis or naturally occurring in the sample. By measuring the dipole interaction between the paramagnetic probes as function of time, it is possible to calculate the distance between these spin centers in the 15-80 Å range, using a specific sequence of microwave pulses (Jeschke 2012; Klare 2013; Basak et al., 2016). DEER permits to obtain advanced information about the structural organization of various biological systems. For this reason, it has been largely applied in various studies on membrane proteins aimed to define their mechanism of action (Endeward et al. 2009; Mchaourab et al., 2011; Orwick-Rydmark et al., 2012; Dellisanti et al., 2013; Velisetty et al., 2017).

5.9.1 Generation of the cysteine free chimera and mutants for EPR experiments

The cysteine-free chimeric channel used for EPR experiments was generated starting from the construct K-H4ΔN VG cloned in pET24b(H3C) vector. The cysteine-free channel was obtained upon substitution of the cysteine residues of the chimera (i.e. C202, C278 and C295 in KH4ΔN VG sequence) into serine residues by site-directed mutagenesis (QuickChange site-directed mutagenesis kit; Agilent Technologies) following the manufacturer's instructions. In order to perform EPR studies, on the background of the cysteine free chimera, the residues indicated in chapter 3.5 of the section "Results and discussion", were singularly mutated into a cysteine by site-directed mutagenesis (QuickChange site-directed mutagenesis kit; Agilent Technologies) following the manufacturer's instructions.

Successively, 5 µl of each of the aforementioned reactions was used to transform 50µl of chemically competent *E. coli* DH5α as described in chapters 5.1.3 of this section. The transformed cells were grown on agar plates containing 50 µg/mL kanamycin and incubated at 37°C overnight.

The plasmid DNA was purified from a selected colony using the kit Exprep™ Plasmid SV mini (GeneAll). The mutations were verified by DNA sequencing.

5.9.2 Spin Labeling

Each single mutant (i.e. E172C, E195C, C202 and R329C) was purified as described in chapter 5.2.3 of this section. Successively, each different cysteine mutant was concentrated by Amicon Ultra centrifugal filter (MWCO 100 kDa) to approximately 100 µM. The protein solution was incubated with a 10-fold molar excess of DTT at 4°C in order to reduce the cysteine thiol group. After 30 minutes, the reaction mixture was eluted into a PD-10 desalting column to remove the reducing agent using the buffer containing 100 mM KCl, 20 mM Tris-HCl (pH 7.6) and 5mM DM as mobile phase. Successively S- (1-oxyl-2,2,5,5-tetrmethyl-2,5-dihydro-1H-pyrrol-3yl) methylmethanesulfonothioate (MTSL) was added to the solution with 1:10 protein : label molar ratio. The reaction was kept at 4°C under gentle stirring and in absence of light for at least 16 hours. The unreacted spin label was removed using a PD-10 desalting column and the same buffer applied previously. The fractions containing MTSL-labeled chimeric mutants were checked by recording the relative X-band EPR spectrum and, successively, they were pooled together and concentered using by Amicon Ultra centrifugal filter (MWCO 100 kDa). Half of each sample was supplemented with 200 µM cAMP in order to perform the spectroscopic studies in the presence of the ligand.

The final protein concentration was determined by using the calculated molecular absorbance coefficient ($\varepsilon = 51{,}340\ M^{-1}\ cm^{-1}$) and the labelling yield was estimated.

5.9.3 CW-EPR spectroscopy

All CW-EPR spectra were recorded with an ELEXYS E580 spectrometer equipped with a Super High Q resonator operating at X-band (9.9 GHz). The following spectroscopic parameters were used to record every spectrum: microwave power= 10 mW; magnetic field amplitude= 1G; field sweep= 150 G; receiver gain= 60 dB.

The labelling yield of each sample was calculated from the double integral of CW-EPR spectrum and comparing it with a calibration curve obtained for free MTSL in water solution at different molar concentrations.

All EPR spectra were simulated with SimLabel software (a GUI of Easyspin software) in order to obtain each spectral component and the relative parameters, such as the g-tensor, the hyperfine constants (A) and the correlational times τc.

5.9.4 DEER spectroscopy

All DEER experiments on K-H4ΔN VG spin labeled mutants were performed on Elexys E580 spectrometer coupled with the standard resonator EN5107D2 operating at Q-band (34 GHz). The spectrometer was equipped with an Oxford helium temperature regulation unit and the relative experiments were carried out at cryogenic temperatures (i.e. -200°C). Each spin labeled sample was prepared as described above with a final concentration of ~100 μM, in the absence or in the presence of 200 μM cAMP. Finally, glycerol (10% v/v) was added as cryoprotectant.

DEER experiments were performed using the four-pulse dead-time free DEER sequence with an inversion pulse length of 40 ns. The interpulse t1 was set to 200 ns and the t2 was adjusted basing on the phase memory constant time recorded for each sample. The pump ELDOR pulse (40 ns) was positioned at the center of the MTSL absorption spectrum and the frequency difference between the pump and the observer pulses was 56 MHz. The DEER traces were accumulated at least 14 hours in order to minimize the signal to noise ratio.

DeerAnalysis 2016 software was used to realize the correction of background echo decay and consequently to obtain the inter-spin distances involving the Tikhonov regularization. The regularization factor (α) was used with a value equal to 100, according to L-curve criteria.

Supplementary figures

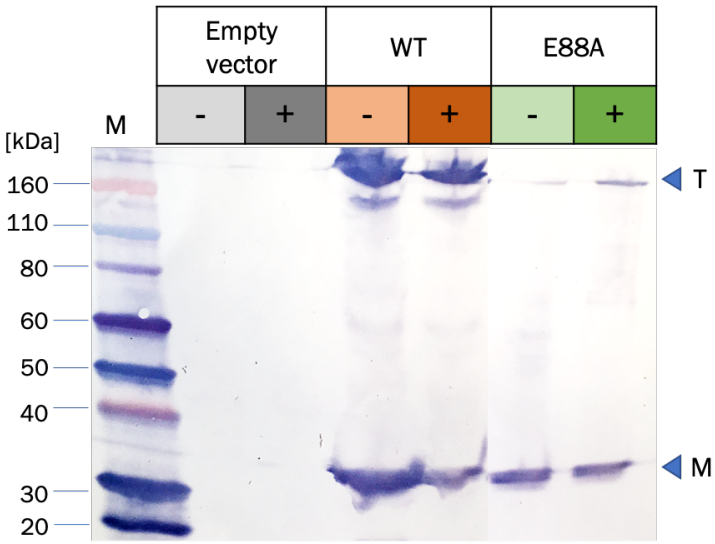

Supplementary figure 1: $BaCl_2$ promotes the expression of the open mutant E88A. Western Blot comparing the protein expression levels in *E. coli* C41(DE3) transformed with the empty vector (as control) and either with K-H4ΔN VG wild type (lanes WT) or the open mutant (lanes E88A). Protein expression was induced in the absence (-) or in the presence (+) of 10 mM $BaCl_2$. The samples were collected at the end of the induction process. The immunodecoration was made using a primary antibody against the His-tag at the N-terminus of the chimeric channels. The arrowhead marked with the letter T shows the bands around 160 kDa that correspond to the tetrameric channel (MW: 152 kDa). The arrowhead marked with the letter M shows the bands above 30 kDa that correspond to the monomer (MW: 38 kDa). M: Marker (Novex® Sharp Pre-stained Protein Standards, Invitrogen). As expected, the lanes corresponding to the cells transformed with the empty vector do not show any band. The cells expressing the WT chimeric channel do not show a significant increase in growth upon addition of $BaCl_2$ compared to the control cells (see chapter 3.3.3 of the section "Results and discussion"), however the western blot suggests that the stability of the tetrameric channel is improved. Indeed, the intensity of the bands corresponding to the monomer is decreased in the treated sample (+) compared to the untreated one (-), while the intensity of the bands that correspond to the tetramer is comparable for untreated (-) and treated (+) cells. The addition of barium to the medium has a much stronger effect on cells expressing the E88A mutant. Indeed, in the untreated cells (-), the channel is almost completely in the monomeric state, while the treated cells (+) show a pronounced band corresponding to the functional tetrameric state. These data suggest that K-H4ΔN VG E88A does not assemble as functional tetramer in the absence of the blocker barium, probably as a reaction to the toxic effect of the channel on the bacterial ion homeostasis. This phenomenon is reflected in the low growth rate of cells (see chapter 3.3.3 of the section "Results and discussion"). Whereas, the addition of $BaCl_2$ drastically promotes the growth of the cells and the expression of the tetrameric channel by blocking the K^+ flow through the channel pore. This experiment supports the assumption that the chimera is a functional potassium channel.

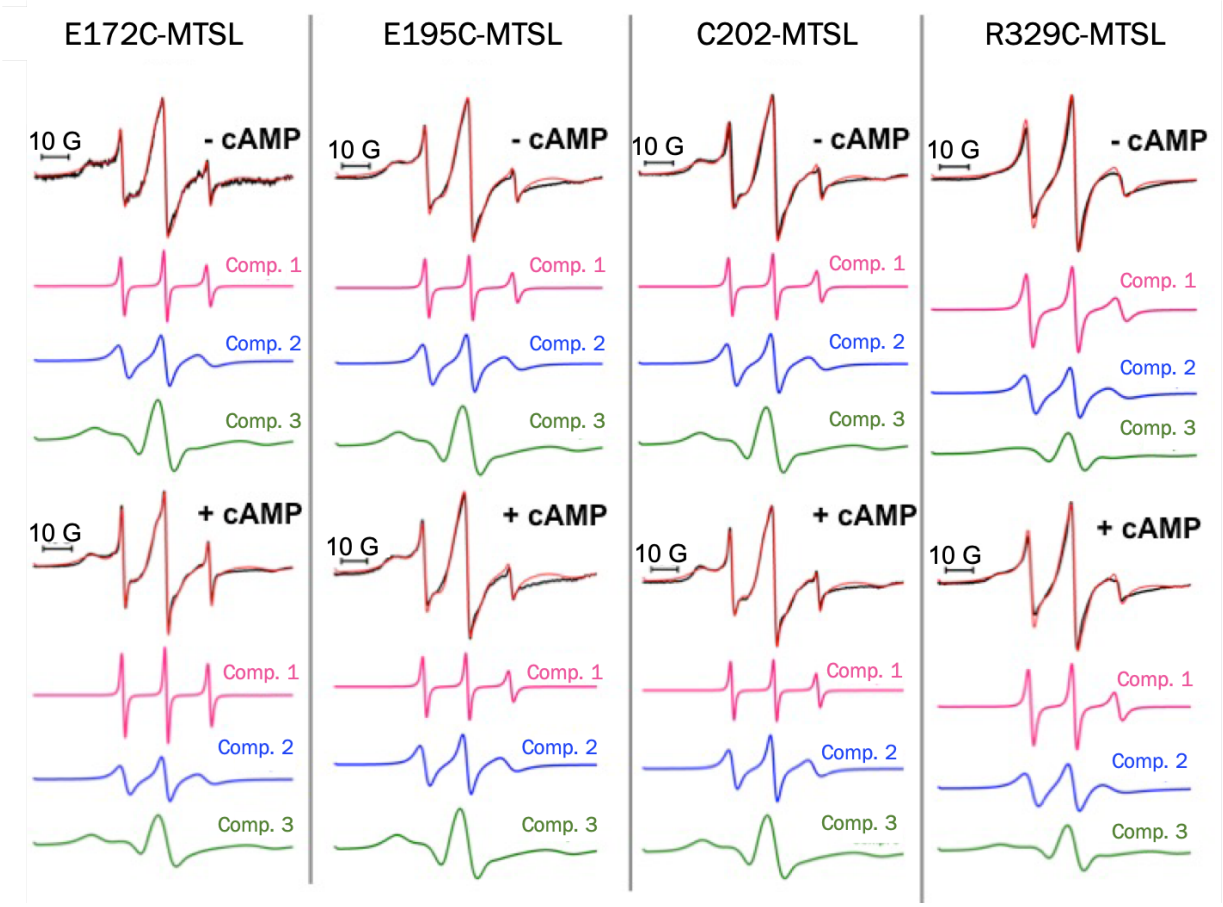

Supplementary figure 2: X-band CW-EPR spectra (black) and relative simulations (red) for E172C-MTSL, E195C-MTSL, C202-MTSL and R329C-MTSL in absence (top panel) and in presence (bottom panel) of cAMP. For each spectra the relative components constituting the EPR signal are listed below. The simulations were performed after baseline correction usinf SimLabel software (GUI of EasySpin).

Refrences

Accili, E.A., Proenza, C., Baruscotti, M., DiFrancesco, D., 2002. From Funny Current to HCN Channels: 20 Years of Excitation. Physiology 17, 32–37. https://doi.org/10.1152/physiologyonline.2002.17.1.32

Akimoto, M., VanSchouwen, B., Melacini, G., 2018. The structure of the apo cAMP-binding domain of HCN4 – a stepping stone toward understanding the cAMP-dependent modulation of the hyperpolarization-activated cyclic-nucleotide-gated ion channels. The FEBS Journal 285, 2182–2192. https://doi.org/10.1111/febs.14408

Akimoto, M., Zhang, Z., Boulton, S., Selvaratnam, R., VanSchouwen, B., Gloyd, M., Accili, E.A., Lange, O.F., Melacini, G., 2014. A Mechanism for the Auto-inhibition of Hyperpolarization-activated Cyclic Nucleotide-gated (HCN) Channel Opening and Its Relief by cAMP. Journal of Biological Chemistry 289, 22205–22220. https://doi.org/10.1074/jbc.M114.572164

Altomare, C., Terragni, B., Brioschi, C., Milanesi, R., Pagliuca, C., Viscomi, C., Moroni, A., Baruscotti, M., DiFrancesco, D., 2003. Heteromeric HCN1-HCN4 channels: a comparison with native pacemaker channels from the rabbit sinoatrial node. J Physiol 549, 347–359. https://doi.org/10.1113/jphysiol.2002.027698

Arachea, B.T., Sun, Z., Potente, N., Malik, R., Isailovic, D., Viola, R.E., 2012. Detergent selection for enhanced extraction of membrane proteins. Protein Expression and Purification 86, 12–20. https://doi.org/10.1016/j.pep.2012.08.016

Armstrong, C.M., Taylor, S.R., 1980. Interaction of barium ions with potassium channels in squid giant axons. Biophysical Journal 30, 473–488. https://doi.org/10.1016/S0006-3495(80)85108-3

Arnsten, A.F.T., 2007. Catecholamine and Second Messenger Influences on Prefrontal Cortical Networks of "Representational Knowledge": A Rational Bridge between Genetics and the Symptoms of Mental Illness. Cerebral Cortex 17, i6–i15. https://doi.org/10.1093/cercor/bhm033

Baruscotti, M., Bucchi, A., Milanesi, R., Paina, M., Barbuti, A., Gnecchi-Ruscone, T., Bianco, E., Vitali-Serdoz, L., Cappato, R., DiFrancesco, D., 2017. A gain-of-function mutation in the cardiac pacemaker HCN4 channel increasing cAMP sensitivity is associated with familial Inappropriate Sinus Tachycardia. European Heart Journal 38, 280–288. https://doi.org/10.1093/eurheartj/ehv582

Basak, S., Chatterjee, S., Chakrapani, S., 2016. Site Directed Spin Labeling and EPR Spectroscopic Studies of Pentameric Ligand-Gated Ion Channels. JoVE e54127. https://doi.org/10.3791/54127

Biel, M., Wahl-Schott, C., Michalakis, S., Zong, X., 2009. Hyperpolarization-Activated Cation Channels: From Genes to Function. Physiological Reviews 89, 847–885. https://doi.org/10.1152/physrev.00029.2008

Boularan, C., Gales, C., 2015. Cardiac cAMP: production, hydrolysis, modulation and detection. Frontiers in Pharmacology 6, 203. https://doi.org/10.3389/fphar.2015.00203

Brown, H.F., DiFrancesco, D., Noble, S.J., 1979. How does adrenaline accelerate the heart? Nature 280, 235–236. https://doi.org/10.1038/280235a0

Bruylants, G., Wouters, J., Micheaux, C., n.d. Differential Scanning Calorimetry in Life Science: Thermodynamics, Stability, Molecular Recognition and Application in Drug Design. Current Medicinal Chemistry Volume 12, 2011–2020. https://doi.org/10.2174/0929867054546564

Bucchi, A., Baruscotti, M., Nardini, M., Barbuti, A., Micheloni, S., Bolognesi, M., DiFrancesco, D., 2013. Identification of the molecular site of ivabradine binding to HCN4 channels. PLoS One 8, e53132–e53132. https://doi.org/10.1371/journal.pone.0053132

Buurman, E.T., Kim, K.-T., Epstein, W., 1995. Genetic Evidence for Two Sequentially Occupied K+ Binding Sites in the Kdp Transport ATPase. Journal of Biological Chemistry 270, 6678–6685. https://doi.org/10.1074/jbc.270.12.6678

Chen, S., C Liang, M., N Chia, J., K Ngsee, J., Ting, A., 2001. Rab8b and Its Interacting Partner TRIP8b Are Involved in Regulated Secretion in AtT20 Cells. The Journal of biological chemistry 276, 13209–16. https://doi.org/10.1074/jbc.M010798200

Chen, X., Zaro, J.L., Shen, W.-C., 2013. Fusion protein linkers: property, design and functionality. Adv Drug Deliv Rev 65, 1357–1369. https://doi.org/10.1016/j.addr.2012.09.039

Cheng, L., Kinard, K., Rajamani, R., Sanguinetti, M.C., 2007. Molecular Mapping of the Binding Site for a Blocker of Hyperpolarization-Activated, Cyclic Nucleotide-Modulated Pacemaker Channels. J Pharmacol Exp Ther 322, 931. https://doi.org/10.1124/jpet.107.121467

Cheng, Y., 2018a. Single-particle cryo-EM—How did it get here and where will it go. Science 361, 876. https://doi.org/10.1126/science.aat4346

Cheng, Y., 2018b. Membrane protein structural biology in the era of single particle cryo-EM. Current Opinion in Structural Biology 52, 58–63. https://doi.org/10.1016/j.sbi.2018.08.008

Chill, J.H., Louis, J.M., Miller, C., Bax, A., 2006. NMR study of the tetrameric KcsA potassium channel in detergent micelles. Protein Sci 15, 684–698. https://doi.org/10.1110/ps.051954706

Chu, H., Zhen, X., 2010. Hyperpolarization-activated, cyclic nucleotide-gated (HCN) channels in the regulation of midbrain dopamine systems. Acta Pharmacol Sin 31, 1036–1043. https://doi.org/10.1038/aps.2010.105

Cordero-Morales, J.F., Jogini, V., Lewis, A., Vásquez, V., Cortes, D.M., Roux, B., Perozo, E., 2007. Molecular driving forces determining potassium channel slow inactivation. Nature Structural & Molecular Biology 14, 1062–1069. https://doi.org/10.1038/nsmb1309

Cortes, D.M., Cuello, L.G., Perozo, E., 2001. Molecular Architecture of Full-Length KcsA. J Gen Physiol 117, 165. https://doi.org/10.1085/jgp.117.2.165

Cortes, D.M., Perozo, E., 1997. Structural Dynamics of the Streptomyces lividans K+ Channel (SKC1): Oligomeric Stoichiometry and Stability,. Biochemistry 36, 10343–10352. https://doi.org/10.1021/bi971018y

Craven, K.B., Olivier, N.B., Zagotta, W.N., 2008. C-terminal Movement during Gating in Cyclic Nucleotide-modulated Channels. Journal of Biological Chemistry 283, 14728–14738. https://doi.org/10.1074/jbc.M710463200

Craven, K.B., Zagotta, W.N., 2004. Salt Bridges and Gating in the COOH-terminal Region of HCN2 and CNGA1 Channels. J Gen Physiol 124, 663. https://doi.org/10.1085/jgp.200409178

DeBerg, H.A., Bankston, J.R., Rosenbaum, J.C., Brzovic, P.S., Zagotta, W.N., Stoll, S., 2015. Structural mechanism for the regulation of HCN ion channels by the accessory protein TRIP8b. Structure 23, 734–744. https://doi.org/10.1016/j.str.2015.02.007

DeBerg, H.A., Brzovic, P.S., Flynn, G.E., Zagotta, W.N., Stoll, S., 2016. Structure and Energetics of Allosteric Regulation of HCN2 Ion Channels by Cyclic Nucleotides. J Biol Chem 291, 371–381. https://doi.org/10.1074/jbc.M115.696450

Decher, N., Chen, J., Sanguinetti, M.C., 2004. Voltage-dependent Gating of Hyperpolarization-activated, Cyclic Nucleotide-gated Pacemaker Channels: molecular coupling between the s4–s5 and c-linkers. Journal of Biological Chemistry 279, 13859–13865. https://doi.org/10.1074/jbc.M313704200

Delvillani, F., Sciandrone, B., Peano, C., Petiti, L., Berens, C., Georgi, C., Ferrara, S., Bertoni, G., Pasini, M.E., Dehò, G., Briani, F., 2014. Tet-Trap, a genetic approach to the identification of bacterial RNA thermometers: application to Pseudomonas aeruginosa. RNA 20, 1963–1976. https://doi.org/10.1261/rna.044354.114

DiFrancesco, D., 1993. Pacemaker Mechanisms in Cardiac Tissue. Annu. Rev. Physiol. 55, 455–472. https://doi.org/10.1146/annurev.ph.55.030193.002323

DiFrancesco, D., Borer, J.S., 2007. The Funny Current. Drugs 67, 15–24. https://doi.org/10.2165/00003495-200767002-00003

Donnelly, M.I., Stevens, P.W., Stols, L., Su, S.X., Tollaksen, S., Giometti, C., Joachimiak, A., 2001. Expression of a highly toxic protein, Bax, in Escherichia coli by attachment of a leader peptide derived from the GroES cochaperone. Protein Expr Purif 22, 422–429. https://doi.org/10.1006/prep.2001.1442

Doyle, D.A., Cabral, J.M., Pfuetzner, R.A., Kuo, A., Gulbis, J.M., Cohen, S.L., Chait, B.T., MacKinnon, R., 1998. The Structure of the Potassium Channel: Molecular Basis of K^+ Conduction and Selectivity. Science 280, 69. https://doi.org/10.1126/science.280.5360.69

Doyle, S.A., 2005. High-Throughput Cloning for Proteomics Research. Zanders E.D. (eds) Chemical Genomics. Methods in Molecular Biology™, vol 310, Humana Press.

Dörr, J. M., Scheidelaar, S., Koorengevel, M. C., Dominguez, J. J., Schäfer, M., van Walree, C. A., & Killian, J. A. 2016. The styrene-maleic acid copolymer: a versatile tool in membrane research. European biophysics journal : EBJ, 45(1), 3–21. doi:10.1007/s00249-015-1093-y https://dx.doi.org/10.1007/s00249-015-1093-y

Dumon-Seignovert, L., Cariot, G., Vuillard, L., 2004. The toxicity of recombinant proteins in Escherichia coli: a comparison of overexpression in BL21(DE3), C41(DE3), and C43(DE3). Protein Expression and Purification 37, 203–206. https://doi.org/10.1016/j.pep.2004.04.025

Emery, E.C., Young, G.T., McNaughton, P.A., 2012. HCN2 ion channels: an emerging role as the pacemakers of pain. Trends in Pharmacological Sciences 33, 456–463. https://doi.org/10.1016/j.tips.2012.04.004

Epstein, W., Davies, M., 1970. Potassium-Dependant Mutants of Escherichia coli K-12. J. Bacteriol. 101, 836.

Gauss, R., Seifert, R., Kaupp, U.B., 1998. Molecular identification of a hyperpolarization-activated channel in sea urchin sperm. Nature 393, 583–587. https://doi.org/10.1038/31248

Gewering, T., Januliene, D., Ries, A.B., Moeller, A., 2018. Know your detergents: A case study on detergent background in negative stain electron microscopy. Journal of Structural Biology 203, 242–246. https://doi.org/10.1016/j.jsb.2018.05.008

Giannoulis, A., Ward, R., Branigan, E., Naismith, J.H., Bode, B.E., 2013. PELDOR in rotationally symmetric homo-oligomers. Molecular Physics 111, 2845–2854. https://doi.org/10.1080/00268976.2013.798697

Gibson, D.G., Young, L., Chuang, R.-Y., Venter, J.C., Hutchison, C.A., Smith, H.O., 2009. Enzymatic assembly of DNA molecules up to several hundred kilobases. Nature Methods 6, 343–345. https://doi.org/10.1038/nmeth.1318

Grant, T., Grigorieff, N., 2015. Automatic estimation and correction of anisotropic magnification distortion in electron microscopes. Journal of Structural Biology 192, 204–208. https://doi.org/10.1016/j.jsb.2015.08.006

Gubellini, F., Verdon, G., Karpowich, N.K., Luff, J.D., Boël, G., Gauthier, N., Handelman, S.K., Ades, S.E., Hunt, J.F., 2011. Physiological response to membrane protein overexpression in E. coli. Mol Cell Proteomics 10, M111.007930-M111.007930. https://doi.org/10.1074/mcp.M111.007930

Guzman, L.M., Belin, D., Carson, M.J., Beckwith, J., 1995. Tight regulation, modulation, and high-level expression by vectors containing the arabinose PBAD promoter. J. Bacteriol. 177, 4121. https://doi.org/10.1128/jb.177.14.4121-4130.1995

He, S., Scheres, S.H.W., 2017. Helical reconstruction in RELION. Journal of Structural Biology 198, 163–176. https://doi.org/10.1016/j.jsb.2017.02.003

Higgins, M.K., Weitz, D., Warne, T., Schertler, G.F.X., Kaupp, U.B., 2002. Molecular architecture of a retinal cGMP-gated channel: the arrangement of the cytoplasmic domains. EMBO J 21, 2087–2094. https://doi.org/10.1093/emboj/21.9.2087

Horton, R.M., Ho, S.N., Pullen, J.K., Hunt, H.D., Cai, Z., Pease, L.R., 1993. [17]Gene splicing by overlap extension, in: Methods in Enzymology. Academic Press, pp. 270–279. https://doi.org/10.1016/0076-6879(93)17067-F

Huynh, K.W., Cohen, M.R., Moiseenkova-Bell, V.Y., 2014. Application of amphipols for structure-functional analysis of TRP channels. J Membr Biol 247, 843–851. https://doi.org/10.1007/s00232-014-9684-6

James, Z.M., Zagotta, W.N., 2018. Structural insights into the mechanisms of CNBD channel function. J Gen Physiol 150, 225. https://doi.org/10.1085/jgp.201711898

Jeschke, G., 2012a. Characterization of Protein Conformational Changes with Sparse Spin-Label Distance Constraints. J. Chem. Theory Comput. 8, 3854–3863. https://doi.org/10.1021/ct300113z

Jeschke, G., 2012b. DEER Distance Measurements on Proteins. Annu. Rev. Phys. Chem. 63, 419–446. https://doi.org/10.1146/annurev-physchem-032511-143716
Jiang, Y., Lee, A., Chen, J., Cadene, M., Chait, B.T., MacKinnon, R., 2002. The open pore conformation of potassium channels. Nature 417, 523.
Jiang, Y., MacKinnon, R., 2000. The Barium Site in a Potassium Channel by X-Ray Crystallography. J Gen Physiol 115, 269. https://doi.org/10.1085/jgp.115.3.269
Klamer, D., Pålsson, E., Fejgin, K., Zhang, J., Engel, J.A., Svensson, L., 2005. Activation of a nitric-oxide-sensitive cAMP pathway with phencyclidine: elevated hippocampal cAMP levels are temporally associated with deficits in prepulse inhibition. Psychopharmacology 179, 479–488. https://doi.org/10.1007/s00213-004-2051-z
Klare, J.P., 2013. Site-directed spin labeling EPR spectroscopy in protein research. bchm 394, 1281. https://doi.org/10.1515/hsz-2013-0155
Kusch, J., Thon, S., Schulz, E., Biskup, C., Nache, V., Zimmer, T., Seifert, R., Schwede, F., Benndorf, K., 2012. How subunits cooperate in cAMP-induced activation of homotetrameric HCN2 channels. Nature Chemical Biology 8, 162.
Lee, C.-H., MacKinnon, R., 2017. Structures of the Human HCN1 Hyperpolarization-Activated Channel. Cell 168, 111-120.e11. https://doi.org/10.1016/j.cell.2016.12.023
LeMasurier, M., Heginbotham, L., Miller, C., 2001. Kcsa. J Gen Physiol 118, 303. https://doi.org/10.1085/jgp.118.3.303
Lohse, M.J., Engelhardt, S., Eschenhagen, T., 2003. What Is the Role of β-Adrenergic Signaling in Heart Failure? Circulation Research 93, 896–906. https://doi.org/10.1161/01.RES.0000102042.83024.CA
Lolicato, M., Bucchi, A., Arrigoni, C., Zucca, S., Nardini, M., Schroeder, I., Simmons, K., Aquila, M., DiFrancesco, D., Bolognesi, M., Schwede, F., Kashin, D., Fishwick, C.W.G., Johnson, A.P., Thiel, G., Moroni, A., 2014. Cyclic dinucleotides bind the C-linker of HCN4 to control channel cAMP responsiveness. Nature Chemical Biology 10, 457.
Lolicato, M., Nardini, M., Gazzarrini, S., Möller, S., Bertinetti, D., Herberg, F.W., Bolognesi, M., Martin, H., Fasolini, M., Bertrand, J.A., Arrigoni, C., Thiel, G., Moroni, A., 2011. Tetramerization Dynamics of C-terminal Domain Underlies Isoform-specific cAMP Gating in Hyperpolarization-activated Cyclic Nucleotide-gated Channels. Journal of Biological Chemistry 286, 44811–44820. https://doi.org/10.1074/jbc.M111.297606
Ludwig, A., Zong, X., Jeglitsch, M., Hofmann, F., Biel, M., 1998. A family of hyperpolarization-activated mammalian cation channels. Nature 393, 587–591. https://doi.org/10.1038/31255
Martinac B., Rohde P.R., Cranfield C.G., Nomura T., 2013 Patch Clamp Electrophysiology for the Study of Bacterial Ion Channels in Giant Spheroplasts of E. coli. In: Delcour A. (eds) Bacterial Cell Surfaces. Methods in Molecular Biology (Methods and Protocols), vol 966. Humana Press, Totowa, NJ https://doi.org/10.1007/978-1-62703-245-2_23
McCoy, J.G., Rusinova, R., Kim, D.M., Kowal, J., Banerjee, S., Jaramillo Cartagena, A., Thompson, A.N., Kolmakova-Partensky, L., Stahlberg, H., Andersen, O.S., Nimigean, C.M., 2014. A KcsA/MloK1 chimeric ion channel has lipid-dependent ligand-binding energetics. J Biol Chem 289, 9535–9546. https://doi.org/10.1074/jbc.M113.543389

Miller, C., 1987. Trapping single ions inside single ion channels. Biophys J 52, 123–126. https://doi.org/10.1016/S0006-3495(87)83196-X

Mio, K., Sato, C., 2018. Lipid environment of membrane proteins in cryo-EM based structural analysis. Biophys Rev 10, 307–316. https://doi.org/10.1007/s12551-017-0371-6

Miroux, B., Walker, J.E., 1996. Over-production of Proteins inEscherichia coli: Mutant Hosts that Allow Synthesis of some Membrane Proteins and Globular Proteins at High Levels. Journal of Molecular Biology 260, 289–298. https://doi.org/10.1006/jmbi.1996.0399

Missale, C., Nash, S.R., Robinson, S.W., Jaber, M., Caron, M.G., 1998. Dopamine Receptors: From Structure to Function. Physiological Reviews 78, 189–225. https://doi.org/10.1152/physrev.1998.78.1.189

Moosmang, S., Stieber, J., Zong, X., Biel, M., Hofmann, F., Ludwig, A., 2001. Cellular expression and functional characterization of four hyperpolarization-activated pacemaker channels in cardiac and neuronal tissues. European Journal of Biochemistry 268, 1646–1652. https://doi.org/10.1046/j.1432-1327.2001.02036.x

Ohndorf, U.-M., MacKinnon, R., 2005. Construction of a Cyclic Nucleotide-gated KcsA K+ Channel. Journal of Molecular Biology 350, 857–865. https://doi.org/10.1016/j.jmb.2005.05.050

Orwick, M.C., Judge, P.J., Procek, J., Lindholm, L., Graziadei, A., Engel, A., Grobner, G., and Watts, A. 2012. Detergent-free forma- tion and physicochemical characterization of nanosized lipid-polymer complexes: Lipodisq. Angew. Chem. Int. Ed. Engl. 51:4653-4657. https://doi.org/10.1002/anie.201201355

Orwick-Rydmark, M., Arnold, T., Linke, D., 2016. The Use of Detergents to Purify Membrane Proteins. Current Protocols in Protein Science 84, 4.8.1-4.8.35. https://doi.org/10.1002/0471140864.ps0408s84

Pagliuca, C., Goetze, T.A., Wagner, R., Thiel, G., Moroni, A., Parcej, D., 2007. Molecular properties of Kcv, a virus encoded K+ channel. Biochemistry 46, 1079–1090. https://doi.org/10.1021/bi061530w

Pape, H.-C., 1996. Queer Current and Pacemaker: The Hyperpolarization-Activated Cation Current in Neurons. Annu. Rev. Physiol. 58, 299–327. https://doi.org/10.1146/annurev.ph.58.030196.001503

Popot, J.-L., Althoff, T., Bagnard, D., Banères, J.-L., Bazzacco, P., Billon-Denis, E., Catoire, L.J., Champeil, P., Charvolin, D., Cocco, M.J., Crémel, G., Dahmane, T., de la Maza, L.M., Ebel, C., Gabel, F., Giusti, F., Gohon, Y., Goormaghtigh, E., Guittet, E., Kleinschmidt, J.H., Kühlbrandt, W., Le Bon, C., Martinez, K.L., Picard, M., Pucci, B., Sachs, J.N., Tribet, C., van Heijenoort, C., Wien, F., Zito, F., Zoonens, M., 2011. Amphipols From A to Z. Annu. Rev. Biophys. 40, 379–408. https://doi.org/10.1146/annurev-biophys-042910-155219

Porro, A., Saponaro, A., Gasparri, F., Bauer, D., Gross, C., Pisoni, M., Abbandonato, G., Hamacher, K., Santoro, B., Thiel, G., Moroni, A., Submitted to eLIFE. The HCN domain couples voltage gating and cAMP response in Hyperpolarization-activated Cyclic Nucleotide-gated channels.

Puljung, M.C., DeBerg, H.A., Zagotta, W.N., Stoll, S., 2014. Double electron–electron resonance reveals cAMP-induced conformational change in HCN channels. Proc Natl Acad Sci USA 111, 9816. https://doi.org/10.1073/pnas.1405371111

Puljung, M.C., Zagotta, W.N., 2013. A Secondary Structural Transition in the C-helix Promotes Gating of Cyclic Nucleotide-regulated Ion Channels. Journal of Biological Chemistry 288, 12944–12956. https://doi.org/10.1074/jbc.M113.464123

Radchenko, M.V., Tanaka, K., Waditee, R., Oshimi, S., Matsuzaki, Y., Fukuhara, M., Kobayashi, H., Takabe, T., Nakamura, T., 2006. Potassium/Proton Antiport System of Escherichia coli. Journal of Biological Chemistry 281, 19822–19829. https://doi.org/10.1074/jbc.M600333200

Rahman, N., Buck, J., Levin, L., 2013. pH sensing via bicarbonate-regulated "soluble" adenylyl cyclase (sAC). Frontiers in Physiology 4, 343. https://doi.org/10.3389/fphys.2013.00343

Ramírez, D., Zúñiga, R., Concha, G., Zúñiga, L., 2018. HCN Channels: New Therapeutic Targets for Pain Treatment. Molecules 23. https://doi.org/10.3390/molecules23092094

Robinson, R.B., Siegelbaum, S.A., 2003. Hyperpolarization-Activated Cation Currents: From Molecules to Physiological Function. Annu. Rev. Physiol. 65, 453–480. https://doi.org/10.1146/annurev.physiol.65.092101.142734

Rohou, A., Grigorieff, N., 2015. CTFFIND4: Fast and accurate defocus estimation from electron micrographs. Journal of Structural Biology 192, 216–221. https://doi.org/10.1016/j.jsb.2015.08.008

Rosano, G.L., Ceccarelli, E.A., 2014. Recombinant protein expression in Escherichia coli: advances and challenges. Front Microbiol 5, 172–172. https://doi.org/10.3389/fmicb.2014.00172

Santoro, B., Chen, S., Lüthi, A., Pavlidis, P., Shumyatsky, G.P., Tibbs, G.R., Siegelbaum, S.A., 2000. Molecular and Functional Heterogeneity of Hyperpolarization-Activated Pacemaker Channels in the Mouse CNS. J. Neurosci. 20, 5264. https://doi.org/10.1523/JNEUROSCI.20-14-05264.2000

Santoro, B., Grant, S.G., Bartsch, D., Kandel, E.R., 1997. Interactive cloning with the SH3 domain of N-src identifies a new brain specific ion channel protein, with homology to eag and cyclic nucleotide-gated channels. Proc Natl Acad Sci U S A 94, 14815–14820. https://doi.org/10.1073/pnas.94.26.14815

Santoro, B., Liu, D.T., Yao, H., Bartsch, D., Kandel, E.R., Siegelbaum, S.A., Tibbs, G.R., 1998. Identification of a Gene Encoding a Hyperpolarization-Activated Pacemaker Channel of Brain. Cell 93, 717–729. https://doi.org/10.1016/S0092-8674(00)81434-8

Saponaro, A., Cantini, F., Porro, A., Bucchi, A., DiFrancesco, D., Maione, V., Donadoni, C., Introini, B., Mesirca, P., Mangoni, M.E., Thiel, G., Banci, L., Santoro, B., Moroni, A., 2018. A synthetic peptide that prevents cAMP regulation in mammalian hyperpolarization-activated cyclic nucleotide-gated (HCN) channels. Elife 7, e35753. https://doi.org/10.7554/eLife.35753

Saponaro, A., Pauleta, S.R., Cantini, F., Matzapetakis, M., Hammann, C., Donadoni, C., Hu, L., Thiel, G., Banci, L., Santoro, B., Moroni, A., 2014. Structural basis for the mutual antagonism of cAMP and TRIP8b in regulating HCN channel function. Proc Natl Acad Sci U S A 111, 14577–14582. https://doi.org/10.1073/pnas.1410389111

Sartiani, L., Mannaioni, G., Masi, A., Novella Romanelli, M., Cerbai, E., 2017. The Hyperpolarization-Activated Cyclic Nucleotide–Gated Channels: from Biophysics to Pharmacology of a Unique Family of Ion Channels. Pharmacol Rev 69, 354. https://doi.org/10.1124/pr.117.014035

Scheres, S.H.W., 2012. RELION: implementation of a Bayesian approach to cryo-EM structure determination. J Struct Biol 180, 519–530. https://doi.org/10.1016/j.jsb.2012.09.006

Seifert, R., Scholten, A., Gauss, R., Mincheva, A., Lichter, P., Kaupp, U.B., 1999. Molecular characterization of a slowly gating human hyperpolarization-activated channel predominantly expressed in thalamus, heart, and testis. Proc Natl Acad Sci USA 96, 9391. https://doi.org/10.1073/pnas.96.16.9391

Serna, M., 2019. Hands on Methods for High Resolution Cryo-Electron Microscopy Structures of Heterogeneous Macromolecular Complexes. Frontiers in Molecular Biosciences 6, 33. https://doi.org/10.3389/fmolb.2019.00033

Sgro, G.G., Costa, T.R.D., 2018. Cryo-EM Grid Preparation of Membrane Protein Samples for Single Particle Analysis. Frontiers in Molecular Biosciences 5, 74. https://doi.org/10.3389/fmolb.2018.00074

Stieber, J., Stöckl, G., Herrmann, S., Hassfurth, B., Hofmann, F., 2005. Functional Expression of the Human HCN3 Channel. Journal of Biological Chemistry 280, 34635–34643. https://doi.org/10.1074/jbc.M502508200

Sun, L., Wu, J., Du, F., Chen, X., Chen, Z.J., 2013. Cyclic GMP-AMP synthase is a cytosolic DNA sensor that activates the type I interferon pathway. Science 339, 786–791. https://doi.org/10.1126/science.1232458

Thompson, A.N., Posson, D.J., Parsa, P.V., Nimigean, C.M., 2008. Molecular mechanism of pH sensing in KcsA potassium channels. Proc Natl Acad Sci U S A 105, 6900–6905. https://doi.org/10.1073/pnas.0800873105

Thonghin, N., Kargas, V., Clews, J., Ford, R.C., 2018. Cryo-electron microscopy of membrane proteins. Methods 147, 176–186. https://doi.org/10.1016/j.ymeth.2018.04.018

Titus, D.J., Furones, C., Kang, Y., Atkins, C.M., 2013. Age-dependent alterations in cAMP signaling contribute to synaptic plasticity deficits following traumatic brain injury. Neuroscience 231, 182–194. https://doi.org/10.1016/j.neuroscience.2012.12.002

Tribet, C., Audebert, R., Popot, J.L., 1996. Amphipols: polymers that keep membrane proteins soluble in aqueous solutions. Proc Natl Acad Sci U S A 93, 15047–15050. https://doi.org/10.1073/pnas.93.26.15047

Tsantoulas, C., Mooney, E.R., McNaughton, P.A., 2016. HCN2 ion channels: basic science opens up possibilities for therapeutic intervention in neuropathic pain. Biochem J 473, 2717. https://doi.org/10.1042/BCJ20160287

Uysal, S., Vásquez, V., Tereshko, V., Esaki, K., Fellouse, F. A., Sidhu, S. S., … Kossiakoff, A. 2009. Crystal structure of full-length KcsA in its closed conformation. Proceedings of the National Academy of Sciences of the United States of America, 106(16), 6644–6649. https://doi.org/10.1073/pnas.0810663106

Ulens, C., Siegelbaum, S.A., 2003. Regulation of Hyperpolarization-Activated HCN Channels by cAMP through a Gating Switch in Binding Domain Symmetry. Neuron 40, 959–970. https://doi.org/10.1016/S0896-6273(03)00753-0

Uozumi, N., 2001. Escherichia coli as an expression system for K+ transport systems from plants. American Journal of Physiology-Cell Physiology 281, C733–C739. https://doi.org/10.1152/ajpcell.2001.281.3.C733

Uozumi, N., Nakamura, T., Schroeder, J.I., Muto, S., 1998. Determination of transmembrane topology of an inward-rectifying potassium channel from Arabidopsis thaliana based on functional expression in Escherichia coli. Proc Natl Acad Sci U S A 95, 9773–9778. https://doi.org/10.1073/pnas.95.17.9773

VanSchouwen, B., Melacini, G., 2016. Structural Basis of Tonic Inhibition by Dimers of Dimers in Hyperpolarization-Activated Cyclic-Nucleotide-Modulated (HCN) Ion Channels. J. Phys. Chem. B 120, 10936–10950. https://doi.org/10.1021/acs.jpcb.6b07735

VanSchouwen, B., Melacini, G., 2018. Role of Dimers in the cAMP-Dependent Activation of Hyperpolarization-Activated Cyclic-Nucleotide-Modulated (HCN) Ion Channels. The Journal of Physical Chemistry B 122, 2177–2190. https://doi.org/DOI: 10.1021/acs.jpcb.7b10125

Wagner, S., Klepsch, M.M., Schlegel, S., Appel, A., Draheim, R., Tarry, M., Högbom, M., van Wijk, K.J., Slotboom, D.J., Persson, J.O., de Gier, J.-W., 2008. Tuning Escherichia coli for membrane protein overexpression. Proc Natl Acad Sci U S A 105, 14371–14376. https://doi.org/10.1073/pnas.0804090105

Wahl-Schott, C., Biel, M., 2008. HCN channels: Structure, cellular regulation and physiological function. Cellular and Molecular Life Sciences 66, 470. https://doi.org/10.1007/s00018-008-8525-0

Wang, M., Gamo, N.J., Yang, Y., Jin, L.E., Wang, X.-J., Laubach, M., Mazer, J.A., Lee, D., Arnsten, A.F.T., 2011. Neuronal basis of age-related working memory decline. Nature 476, 210–213. https://doi.org/10.1038/nature10243

Wang, M., Ramos, B.P., Paspalas, C.D., Shu, Y., Simen, A., Duque, A., Vijayraghavan, S., Brennan, A., Dudley, A., Nou, E., Mazer, J.A., McCormick, D.A., Arnsten, A.F.T., 2007. α2A-Adrenoceptors Strengthen Working Memory Networks by Inhibiting cAMP-HCN Channel Signaling in Prefrontal Cortex. Cell 129, 397–410. https://doi.org/10.1016/j.cell.2007.03.015

Williamson, I.M., Alvis, S.J., East, J.M., Lee, A.G., 2003. The potassium channel KcsA and its interaction with the lipid bilayer. Cellular and Molecular Life Sciences CMLS 60, 1581–1590. https://doi.org/10.1007/s00018-003-3172-y

Wiseman, T., Williston, S., Brandts, J.F., Lin, L.-N., 1989. Rapid measurement of binding constants and heats of binding using a new titration calorimeter. Analytical Biochemistry 179, 131–137. https://doi.org/10.1016/0003-2697(89)90213-3

Xu, X., Vysotskaya, Z.V., Liu, Q., Zhou, L., 2010. Structural Basis for the cAMP-dependent Gating in the Human HCN4 Channel. Journal of Biological Chemistry 285, 37082–37091. https://doi.org/10.1074/jbc.M110.152033

Yanagihara, K., Noma, A., Irisawa, H., 1980. Reconstruction of sino-atrial node pacemaker potential based on the voltage clamp experiments. Jpn J Physiol 30, 841–857. https://doi.org/10.2170/jjphysiol.30.841

Zagotta, W.N., Olivier, N.B., Black, K.D., Young, E.C., Olson, R., Gouaux, E., 2003. Structural basis for modulation and agonist specificity of HCN pacemaker channels. Nature 425, 200–205. https://doi.org/10.1038/nature01922

Zheng, S.Q., Palovcak, E., Armache, J.-P., Verba, K.A., Cheng, Y., Agard, D.A., 2017. MotionCor2: anisotropic correction of beam-induced motion for improved cryo-electron microscopy. Nature Methods 14, 331.

Zhou, L., Siegelbaum, S.A., 2007. Gating of HCN channels by cyclic nucleotides: residue contacts that underlie ligand binding, selectivity, and efficacy. Structure 15, 655–670. https://doi.org/10.1016/j.str.2007.04.012

Zhu, W.-Z., Wang, S.-Q., Chakir, K., Yang, D., Zhang, T., Brown, J.H., Devic, E., Kobilka, B.K., Cheng, H., Xiao, R.-P., 2003. Linkage of β1-adrenergic stimulation to apoptotic heart cell death through protein kinase A–independent activation of Ca2+/calmodulin kinase II. J Clin Invest 111, 617–625. https://doi.org/10.1172/JCI16326

Own Work

All the experimental work discussed in this thesis was carried out by Bianca Introini, with exception of:

- For Differential Scanning Calorimetry (DSC) experiments Prof. Dimitrios Fessas (Università degli Studi di Milano, Italy) provided the nano-DSC instrument (TA instruments) and helped for the further analysis and interpretation of the data.

- *E. coli* strain LB2003 was kindly provided by Prof. Gerhard Thiel (TU Darmstadt, Germany) and the complementation assay was performed in collaboration with Dr. Oliver Rauh (TU Darmstadt, Germany).

- The negative staining, the loading of the grids and the subsequent EM data acquisition and analysis were performed by Dr. Paolo Swuec (Università degli Studi di Milano).

- EPR and DEER experiments were performed at the Center of Magnetic Resonance (CERM) of the University of Florence. Dr. Alessio Bonucci (CERM, Florence) recorded the spectra and made the further analysis of the data.

Acknowledgments

Innanzitutto vorrei ringraziare la prof. Anna Moroni per essere stata una guida fondamentale durante il mio dottorato. Grazie, soprattutto, per avermi insegnato cosa significhi essere una ricercatrice determinata e per avermi spronata a dare sempre il meglio. Grazie per avermi sempre aperto le porte del mondo dandomi l'opportunità di confrontarmi con scienziati provenienti da ogni nazione e per aver sempre stimolato la mia curiosità.

Thanks to Professor Gerhard Thiel for have been one of my scientific guides in these years and especially for his humanity. And thank you for letting me be a part of your fantastic Arbeitsgruppe.

I miei ringraziamenti vanno poi al dottor Andrea Saponaro che mi ha guidato sin da quando ho mosso i miei primi passi in laboratorio, insegnandomi a pormi sempre tante domande e, soprattutto, creando insieme a me il progetto della chimera.

My most special acknowledgments go to Oliver that with endless patience helped me during these years and supported me during the process of writing this thesis. I love you.

Infine, vorrei ringraziare con tutto il mio cuore i miei colleghi di laboratorio, nonché amici, che mi hanno accompagnata in questi anni del dottorato: Alessandro Porro, Federica Gasparri, Viviana Prota, Atiye Sharifzadeh, Gerardo Abbandonato, Lorenzo Brocca, Michal Laskowski, Paolo Zuccolini, Sabrina Gazzarrini, Chiara Donadoni, Matteo Pisoni ed Erika Marin.
Questo lavoro è dedicato anche a tutti voi, perché senza il vostro sostegno e senza la complicità che siamo riusciti a creare le giornate passate in laboratorio non sarebbero state le stesse!
And thanks to all the members of the AG Thiel for the beautiful months passed together in Germany.

Chimeric KcsA-HCN4 ion channels to monitor cAMP-induced conformational changes and dynamics

Bianca Introini[1], Andrea Saponaro[1], Alessio Bonucci[2], Oliver Rauh[3], Francesca Cantini[2], Lucia Banci[2], Gerhard Thiel[3] and Anna Moroni[1,*]

[1]Department of Biosciences, University of Milan, Milan, 20133 Italy;
[2]Centro Risonanze Magnetiche (CERM) and Departement of Chemistry, University of Florence, Sesto Fiorentino, 50019 Italy;
[3]Department of Biology, TU-Darmstadt, Darmstadt, 64289 Germany;

* Corresponding Author: anna.moroni@unimi.it

Astract

Hyperpolarization-activated cyclic nucleotide-gated (HCN1-4) channels play a crucial role in the control of cardiac and neuronal pacemaker activity. The direct binding of cAMP to the CNBD domain facilitates channel opening by relieving the tonic inhibition exerted by the latter. However, the molecular mechanism by which cAMP-induced movements propagate through the C-linker leading to the opening of the channel remains poorly understood. In this study, EPR and DEER were used to reveal the cAMP-induced dynamical changes in the structure of a chimeric protein composed by the pore domain of the K^+ channel KcsA and the C-linker/CNBD domain of human HCN4. These spectroscopic experiments revealed that the binding of cAMP to the CNBD domain causes clear conformational changes in the C-terminal region, which transits from a dimer of dimers conformation to a 4-fold symmetrical gating ring.

Introduction

Hyperpolarization-activated cyclic nucleotide-gated (HCN1-4) channels (Gauss et al., 1998; Ludwig et al., 1998; Santoro et al., 1997; Santoro et al., 1998) are the molecular correlate of I_h (or I_f) current, which plays a key role in the control of neuronal and cardiac rhythmicity (Wahl-Schott and Biel, 2008). HCN channels belong to the superfamily of the voltage-gated ion channels (Robinson and Siegelbaum, 2003; Wahl-Schott and Biel, 2008). Four subunits assemble in homo- or hetero- tetramers (Chen et al., 2001; Altomare et al., 2003). One subunit is composed of six-transmembrane segments of which four helices (S1-4) constitute the voltage sensor domain (VSD)

and two helices the pore domain (S5 and S6). In the cytoplasmic C-terminal part of the channel, each monomeric subunit contains a cyclic nucleotide-binding domain (CNBD) which is connected to the pore-forming S6 helix via the C-linker domain (Robinson and Siegelbaum, 2003; Wahl-Schott and Biel, 2008). Moreover, the resolution of the structure of human HCN1 revealed a unique cytoplasmic N-terminal domain, i.e. the HCN domain (HCND) (Lee and MacKinnon, 2017). Particularly, a recent study of our laboratory revealed that the HCND is involved in the voltage-dependent opening of the HCN channels. The HCND, by making contacts with both the VSD and the C-linker domain, is an important coupling and transmission element for the cAMP effect on the channel opening. Indeed, it mechanically connects the conformational changes in the C-linker, which are generated by the binding of cAMP to the CNBD, to the VSD. (Porro et al., submitted).

HCN channels are activated by the hyperpolarization of membrane potential and their opening is further regulated by cAMP, that directly binds to the cytoplasmic CNBD (Wahl-Schott and Biel, 2008). The binding of cAMP causes structural rearrangements that determine the release of the auto-inhibitory action exerted by the CNBD on the pore opening. These cAMP-induced conformational changes propagate from the CNBD to the pore through the C-linker domain and result in an increased open probability of the channel and in speeded activation kinetics (Wainger et al., 2001). cAMP-dependent modulation of HCN channels activity is involved in the fine control of many important physiological functions, such as the regulation of heart rate (DiFrancesco and Tortora, 1991) and, specifically related to neurons, it plays a crucial role in the regulation of working memory networks in pre-frontal cortex (Wahl-Schott and Biel, 2008) and in pain perception (Emery et al., 2012). Thus, a detailed description of the cAMP-induced conformational changes is essential for understanding several physiological processes, as well as diseases affecting cardiac and neuronal functions.

Growing evidences suggest that cAMP action is not limited to the abolishment of the self-inhibitory system controlled by the CNBD. Indeed, the interaction with the cyclic nucleotide seems to play a key role in the control of the symmetrical arrangement of the C-terminal domain of the channel. Moreover, electrophysiological data on the full-length channel (Ulens and Siegelbaum, 2003; Kusch et al., 2012) as well as sedimentation equilibrium data (Lolicato et al., 2011) and MD simulations (VanSchouwen and Melacini 2018) performed on the isolated C-linker/CNBD fragment, indicate that cAMP binding to the CNBD induces the transition of the C-terminal domains from a 2-fold symmetrical dimer of dimers conformation to a 4-fold symmetrical gating

ring conformation and that this dynamical transition is driven by the movements of the C-linker. Yet the molecular mechanism by which ligand binding to the CNBD changes the assembly of the C-terminal domains remains unknown.

Crystallographic and spectroscopic studies on the isolated HCN2 CNBD fragment in the cAMP-free (Saponaro et al. 2014) and -bound (Zagotta et al. 2003) state allowed to describe in detail the conformational changes that characterize the CNBD domain, thus clarifying the starting point of the molecular mechanism that leads to the cAMP-induced opening of HCN channels. However, up to now, there are no structural data available concerning the conformational changes of the C-linker domain caused by the propagation of the cAMP- induced movement of the CNBD through the C-linker itself to the pore. Indeed, the recently solved the cAMP-free and cAMP-bound cryo-EM structures of human HCN1 (Lee and MacKinnon, 2017) did not advance our understanding of the C-linker rearrangements during channel gating. Indeed, the structures were solved at 0 mV, a condition that blocks the VSD in the resting state. In this configuration, the VSD inhibits the movements of both pore and C- linker domains, which are under its allosteric control (Wahl-Schott and Biel, 2008; Lee and MacKinnon, 2017). Previously, the X-ray structures of HCN1/2/4 C-linker/CNBD fragments bound by cAMP, have been solved (Zagotta et al., 2003; Xu et al., 2010; Lolicato et al., 2011). In these crystal structures of the C-terminal domain in the holo state, the C-linker, that is not tethered to the membrane pore, adopts a 4-fold symmetric tetrameric conformation reminiscent of the full-length channel, in which the four monomers interact according to an *elbow on shoulder* arrangement (*elbow of one subunit resting on the shoulder of the neighbour subunit*) (Zagotta et al., 2003). Spectroscopic and electrophysiological studies of the full-length channel indicate that the C-linker undergoes extended conformational changes upon cAMP binding and, actually, the conformation adopted by the C-linker in the crystal structure reflects the resting configuration of this domain (Taraska et al., 2009; Craven and Zagotta, 2008). It is therefore necessary to study the C-linker conformational changes on the full-length protein where the C-linker is properly connected to the pore at the N- terminus and to the CNBD at its C-terminus, respectively. It clearly emerges that acquiring further insight into the dynamical mechanism of regulation of HCN has proven many difficulties.

Thus, in order to overcome these obstacles and investigate the molecular mechanism and the structural dynamics determined by cAMP binding to HCN, we engineered a chimeric protein by fusing the pore domain of the prokaryotic potassium channel KcsA with the regulatory cytoplasmic C-linker/CNBD region of the human HCN4 channel. The well-characterized pore domain of KcsA (Doyle et al., 1998; Chill et al., 2006) revealed to be a stable and functional

building block. Indeed, it has been widely employed in biochemical and structural studies and for the creation of other prokaryotic chimeric channels that, contrary to our chimeric channel, do not have the C-linker domain (Ohndorf and Mackinnon, 2005; McCoy et al., 2014).

In this work, spectroscopic techniques such as EPR and DEER were applied to study dynamic changes in the structure of the purified and labelled chimeric protein. EPR-DEER experiments revealed that the binding of cAMP to the CNBD domain causes clear conformational changes in the C-terminal region, which dynamically transits from a dimer of dimers conformation to a 4-fold symmetrical gating ring. These data confirm previous functional indication obtained on the full-length channel (Ulens and Siegelbaum, 2003; Kusch et al., 2012) and give further details on the direction and the extent of subunit displacement occurring during the conformational transition. The transition of the channel from a dimer of dimer to a tetrameric configuration of the cytosolic domain might reflect a pre-conditioning state for cAMP action on channel gating and partly explains the agonist activity exerted by cAMP on channel kinetics and open probability.

Results

Construction of KcsA-HCN4 chimera

For the creation of the KcsA-HCN4 chimera (hereafter K-H4) the N- and C-terminal cytoplasmic regions of KcsA have been removed and the C-terminal domain was substituted with the C-linker/CNBD of HCN4. The N-terminus was removed in order to increases the thermostability of the channel (Chill et al., 2006). Taking adavantage of a previous work of Ohndorf and MacKinnon where they generated a functional chimeric channel with KcsA pore (Ohndorf and Mackinnon, 2005), we identified the correct attachment site between the two components at the level of G116, which is at the end of the second transmembrane region (M2) of KcsA and glutamine Q518 of hHCN4, which is the first residue of the C-linker domain of HCN4 (Fig. 1A).

The protein was expressed with a N-terminal hexa-histidine tag placed behind a T7 promoter. The purified protein eluted as a single peak on a gel filtration column at a retention volume that corresponds to the molecular weight of the tetramer in both the presence and absence of cAMP, with a yield of ~1.5 mg/L of *E. coli* culture (Fig. 1B). Similar to KcsA, the chimeric channel remains a tetramer when assayed by SDS-PAGE in the absence of heating, suggesting that the C-linker/CNBD do not disrupt the robust KcsA tetramer assembly. Only after boiling the tetrameric assembly completely disassociates into monomers (Fig. 1B).

Functional characterization of K-H4

We investigated the energetics of cAMP binding to the K-H4 chimera using ITC. Thermodynamic cAMP binding assays on full-length HCN channels using ITC have not been reported before. Indeed, cyclic nucleotide binding assays with ITC were performed only on isolated C-linker/CNBD fragments (Lolicato et al., 2011). As shown in figure 2A, the interaction is exothermic. Analysis of the binding curve yields a stoichiometry of n = 0.98 ± 0.01 and a calculated dissociation constant, K_d, of 1.7 ± 0.7 μM (n=2). This value is in agreement with the dissociation constant previously determined for the isolated C-linker/CNBD fragment of hHCN4 when tested for the cyclic nucleotide binding (Lolicato et al., 2011).

In order to further demonstrate that the channel pore of the chimera is able to conduct potassium, a functional complementation assay was conducted using the K^+-uptake deficient *E. coli* strain LB2003 (Epstein and Davies, 1970; Buurman et al., 1995). LB2003 cells were transformed with the WT chimera or with the constitutively open mutant E88A (Cordero-Morales et al., 2007) cloned into an arabinose-inducible vector. The empty vector was used as control. Serial dilution drop test was performed on LB agar plates that differed in their K^+ concentration (i.e. 0 mM, 10 mM and 100 mM), the presence or absence of the inducer L-arabinose (0.2%) and the presence or absence of the K^+ channel blocker $BaCl_2$ (5 mM) (Fig. 2B). Cells transformed with the empty vector were not able to grow on any media with either 0 mM or 10 mM additional KCl, whereas, as expected, they successfully grew on all the three different media containing 100 mM additional KCl. These data confirmed that any effect observed was due to the expression of the chimeric channels. In the absence of inducer, even cells transformed with either WT channel or the open mutant grew only on the plate supplemented with 100 mM KCl confirming that LB2003 is not able to grow in the presence of low potassium concentrations. The expression of both WT and E88A determined the functional complementation of the phenotype under low potassium conditions (i.e. at 10 mM KCl and 0 mM KCl respectively). Particularly, the complementation effect at low K+ concentrations was completely abolished in the presence of 5 mM BaCl2, thus confirming that the pore of the chimeric protein is able to conduct K+ ions.

EPR and DEER experiments

To measure the cAMP-induced conformational changes in the C-linker/CNBD of the chimera, we performed EPR and DEER experiments. Particularly, DEER could help to understand the quaternary organization of the C-terminal domains of K-H4, by measuring the distance distribution between the paramagnetic probes attached at different regions of the protein. Since the chimeric protein has an homotetrameric structure, distance determinations are the result of the geometric interactions between neighboring and diagonally related subunits.

Firstly, pairs of cysteines were introduced into an otherwise cysteine-free protein. A preliminary test showed that the cysteine-free mutant protein can be produced and purified with the same protocols of the WT and that its stability was also preserved (data not shown) Cysteines were placed in the C-linker domain either in the "elbow" (E172C, fig. 3A) or in the "shoulder" (E195C, fig. 3D) to allow to study the active movement of the "elbow on the shoulder". For the achievement of an overview on the dynamics that govern the cytosolic C-terminal regulatory region, the natural cysteine residue (C202, fig. 3G) at the level of the N-terminal helical bundle has been selected. This residue is in a strategical border region that connects the CNBD domain to the C-linker. Thus, its spectroscopic study could help to understand how the conformational changes induced by the binding of the cAMP to the CNBD are transmitted to the C-linker domain. Moreover, as control for the reliability of the movements showed by the chimera, a cysteine residue was introduced at the distal end of the αC-helix of the CNBD domain (R329C, fig. 3J). Indeed, previous spectroscopic studies on the isolated CNBD of HCN2 channel already shed light on the conformational changes that characterize this domain (Puljung et al., 2014; Saponaro et al., 2014). The introduced cysteines were then modified with the nitroxide spin label S-(1-oxyl-2,2,5,5-tetramethyl-2,5- dihydro-1H-pyrrol-3-yl)methyl methanesulfonothioate (MTSL).

In order to analyze the local dynamics of the protein in the regions where the MTSL spin label were attached, the X-band CW-EPR spectra at room temperature of the four different mutants of K-H4 protein were recorded in absence and in presence of cAMP (Fig. 3).

The CW-EPR experiments provided information on the environments surrounding the residue where the paramagnetic tag was grafted and, thus, also about the secondary structure of the protein. Using SimLabel software (GUI of EasySpin), the experimental data were simulated to obtain the spectral components forming the EPR signal and their relative correlational time values (τ_C). The τ_C value reflects the mobility of the MTSL probe (supplementary table 1). The results obtained for all the four mutants revealed that the EPR spectrum is composed by three components with different τ_C (supplementary figure 1) indicating that the protein is present in a multi dynamic states, as previously determined by cryo-EM measurements (data not shown). In particular for E172C-MTSL, E195C-MTSL and C202-MTSL the predominant component (Component 3 ≈76-79% and τ_C = 5.40-5.61 ns, supplementary table1) has a broad lineshape and a high τ_C value, indicating that respectively the "elbow" and the "shoulder" of the C- linker domain and the N-terminal helical bundle have a low degree of flexibility and a compact conformation. On the other hand, CW-EPR spectrum of R329C-MTSL mutant is composed by a less pronounced broad component with a faster tumbling motion of MTSL (component 3 ≈ 55% and τ_C = 3.67 ns,

supplementary table 1). This result clearly indicates that the αC-helix of the CNBD domain is in a more dynamic states and that this region is very flexible compared to the other positions tested. Successively X-band CW-EPR spectra of MTSL-labeled variants were recorded in presence of cAMP. No evident spectral changes and variation on the relative τ_C were observed for E195-MTSL and C202-MTSL samples, indicating that the ligand does not affect the structure of the "shoulder" and N-terminal helical bundle regions. However, E172C-MTSL and R329-MTSL show an EPR broader spectrum when cAMP is present in solution (fig. 3 B, C and K, L), as confirmed by the simulations that present a higher τ_C of ≈ 0.5 ns. These results show that the ligand weakly compromise the dynamic of the protein for the "elbow" and the αC-helix of the CNBD. Particularly, the results obtained for R329C- MTSL are in line with previous EPR data performed on this residue (Puljung et al., 2014; DeBerg et al., 2015).

The distances and distance distributions between the probes were obtained DEER spectroscopy (supplementary table 2). In figure 4 are shown the Q-band background corrected time traces (in the left column) and the resulting distance distributions (in the right column) obtained in the presence and in the absence of cAMP for each different spin-labelled mutant. The inter-spin DEER measurements obtained for both E172C-MTSL and E195C-MTSL in the cAMP-free state (Fig. 4B and D respectively, red signal), revealed that in the absence of the cyclic nucleotide the spin labels explore various inter-spin distances. Indeed, the distance distributions show multiple peaks in the range 1.9-4.1 nm. These data indicate that in the absence of cAMP both the "elbow" and "shoulder" of the C-linker domain are in a multi dynamic state. For both E172C-MTSL and E195C-MTSL samples in the cAMP-bound state was observed a partial variation on echo oscillations (fig. 4A and C respectively). The relative distance distributions for both the MTSL-labeled mutants (Fig. 4 B and D, blue signal) resulted broader and tended to become bimodal, even if the main peaks, i.e. at 2.65 nm for E172C-MTSL and 2.11 nm for E195C-MTSL, that were present also in absence of the ligand, are still present. These results demonstrate that cAMP influences the conformation of the protein in both the elbow and the shoulder regions, leading to a stabilization of the chimera at the level of C-linker.
From the spin-labelled natural cysteine present in the N-terminal helical bundle, i.e. C202-MTSL, Q-band DEER traces were recorded in the absence and in presence of cAMP (fig. 4E). In both the presence and absence of cAMP, the distance distributions show a maximum peak at similar values (fig. 4F). The data indicate an increased structural heterogeneity in this boundary region to which MTSL was attached, suggesting that, even in the absence of cAMP, the protein is able to adopt holo- like conformations.

The DEER experiments performed on R329C-MTSL and the relative distance distributions obtained for the cAMP-free and -bound mutant are shown in figures 4 G and H respectively. Similarly to what was observed in the C-linker domain, the distances explored by R329C-MTSL spread out over a wider distance range in the absence than in the presence of cAMP (fig 4 H, red signal). These results indicate that in the absence of cAMP, the position of the αC- helix is in a multi dynamic state. The conformational space occupied by the αC-helix is then reduced upon cAMP binding as suggested by the bimodal distribution of the distances (Fig. 4H, blue signal). These results are in line with previous spectroscopic studies on the isolated CNBD domain that showed the closing movement of the αC-helix towards the ß roll upon cAMP binding (Puljung et al., 2014; Saponaro et al., 2014; DeBerg et al., 2015). Moreover, the presence of multiple distances explored by the spin labelled residue in the absence of cAMP is due to the fact that the C-terminal region of the αC-helix is known to be unstructured and to become ordered upon cAMP binding (Saponaro et al., 2014; Lee and MacKinnon 2017). Taken together these data confirmed the reliability of the chimeric channel.

The dynamical transition from the dimer of dimers to the tetrameric gating ring

Both EPR and DEER experiments predicted a decrease in the conformational heterogeneity of the C-terminal regulatory domain of HCN4 upon binding to cAMP. This indication emerged especially from the distance distributions obtained from the analysis of the DEER experiments. Particularly, the distributions calculated for both the elbow and the shoulder of the C-linker and the CNBD domain showed multiple distance peaks in the cAMP-free state. The number of the peaks observed, dropped to two in the presence of the ligand. Thus, in order to correlate the distance distributions obtained from the multi-spin interactions and the potential inner symmetries assumed by the C-terminal regulatory domain, we used a reduced geometric model.

First of all, it has to be considered that the number of expected distances and the mathematical relation between them, depend not only on the number of subunits/monomers of the multimeric assembly of interest but also on the symmetrical conformation adopted from the subunits forming the protein. Considering that the chimera K-H4 is a homotetrameric channel, the expected number of distances taken by the MTSL-labelled residues within a tetrameric protein with a 4-fold symmetry is two (fig. 5, D_1 and D_2 in the square). However, this condition, that geometrically corresponds to a square, was observed only for the cAMP-bound protein. In contrast, the number of peaks corresponding to the main distances taken by the probes in the absence of cAMP rises to three. These distances suggest that the spin-labelled residue in the cAMP-free protein are arranged according to a rectangle shape (fig. 5, D_1, D_2 and D_3 in the rectangle).

Thus, the distance distributions obtained from DEER experiments showed that the binding of cAMP to the CNBD domain of the chimera causes relevant conformational changes in the C-terminal regulatory domains of HCN4. Particularly, the geometrical relationship of the distances measured, suggests that both the C-linker and the CNBD domains transit from a 2-fold dimer of dimers conformation to a 4-fold symmetrical gating ring (fig.5).

This peculiar conformational behavior of the cytosolic regulatory domain of HCN channels was already suggested by previous functional and biochemical data (Ulens and Siegelbaum 2003; Zagotta et al., 2003; Lolicato et al., 2011).

Discussion

The creation of the chimera K-H4 was a challenging and arduous goal, as it is the result of the fusion of two evolutionary distant proteins such as the pore of the prokaryotic KcsA channel and the C-linker/CNBD of eukaryotic HCN4. Indeed, finding the correct junction between the two elements have been the major limitation in obtaining a stable and functional chimera. However, we succeeded in engineering a chimeric channel that helped us to describe the dynamics that characterize the propagation of the cAMP-induced movements through the C-linker to the pore. The chimeric channel K-H4 is a stable protein that can be purified in both the cAMP-free and cAMP-bound state. This protein has the advantage that can be produced and easily purified in *E. coli*. Moreover, ITC measurements demonstrated that the purified chimera is able to bind cAMP with a Kd value of 1.7 μM, which agrees with the one previously published for the isolated C-linker/CNBD fragment of HCN4 (Lolicato et al., 2011). Moreover, the rescue of a K^+-uptake deficient *E. coli* strain demonstrated that the chimeric channel is able to conduct a K^+ ions flow. Particularly, the complementation effect at low K+ concentrations was completely abolished in the presence of 5 mM BaCl2, thus confirming that the pore of the chimeric protein is able to conduct K^+ ions.

Structural studies of an active C-linker domain were performed on the purified chimera using Electron Paramagnetic Resonance (EPR) and the Double Electron-Electron Resonance (DEER).

The positioning of the paramagnetic probes along the C-linker/CNBD, i.e. at the level of the "elbow" and the "shoulder" in order to study the active movement of the "elbow on the shoulder", in the N-terminal helical bundle (the border region that connects the CNBD domain to the C-linker) and in the CNBD domain, allowed to have a global view of the movements that characterize the C-terminal regulatory domain of HCN. The results of the EPR-DEER experiments performed on the chimeric channel singularly labelled at the different levels aforementioned, interestingly revealed that the binding of cAMP to the CNBD domain induces a conformational switch in the

C-terminal region of the protein. Indeed, the range of distance distributions obtained suggest that both the C-linker and CNBD domains transit from a 2-fold symmetrical dimer of dimers conformation in the absence of cAMP to a 4-fold symmetrical gating ring upon the binding of the ligand.

These results are in good agreement with previous functional and biochemical studies that have highlighted a key role of the C-linker domain in mediating the formation of the 4-fold symmetrical gating ring in the presence of cAMP (Zagotta et al., 2003). Particularly, fluorometry and electrophysiological data performed on full length HCN channel suggested that, in the absence of cAMP, the four subunits interact as a 2-fold symmetric dimer of dimers (Ulens and Siegelbaum, 2003; Kusch et al., 2012). Notably, the tonic inhibition of the channel in the absence of cAMP is hinted to arise from the 2-fold dimer of dimers symmetry of the C-terminal domains, whose formation is mediated by neighboring C-linkers (Ulens and Siegelbaum, 2003). Moreover, experiments in solution using HCN 2/4 C-linker/CNBD fragments demonstrated that the tetramerization occurs only upon cAMP binding in a C-linker dependent manner (Lolicato et al., 2011). Interestingly, this dynamical transition from dimers of dimers to tetramer was observed for the CNBD of intact Cyclic Nucleotide-Gated (CNG) channels (Higgins et al. 2002).

The transition from a 2-fold symmetrical dimer of dimers conformation to a 4-fold symmetrical gating ring showed by the cytosolic domain of the chimera might reflect a pre-conditioning state necessary for the action of cAMP on channel gating. Accordingly, these alterations in the structural symmetries of the C-terminal region could promote the autoinhibitory action exerted by the CNBD domain on channel opening. Then, the binding of cAMP could disinhibit the channel opening by promoting the assembly of the tetrameric gating ring. Thus, this symmetry change, that previous functional works showed to be C-linker-dependent (Ulens and Siegelbaum, 2003; Lolicato et al., 2011), could partly explains the agonistic activity exerted by cAMP on channel kinetics and open probability.

In support of the eventual autoinhibitory action of the dimer of dimers assembly on the channel opening there are MD simulations for dimer of dimers based on a cAMP-bound hHCN4 C-linker/CNBD crystal structure (VanSchouwen and Melacini 2018). Indeed, MD simulations showed that when the cAMP-induced conformational changes arise from a dimer of dimers assembly of the C-terminal region, the structural rearrangements of the CNBD domain can be transduced to the C-linker domain, avoiding steric clashes and promoting the tetrameric assembly. On the contrary, if the cAMP-induced conformational changes would arise from a tetrameric assembly, this situation would generate steric clashes between the C-linker and the CNBD domain.

Hence, the EPR-DEER structural data obtained in this study suggest that the dynamical assembly of the C-terminal region from dimer of dimers to tetramer could represent a possible mechanism for the removal of the autoinhibition that the CNBD domain exerts on the opening of the channel.

The chimeric channel proved to be a useful tool for enhancing the understanding of the cAMP-dependent regulation of HCN channels. Thereby, the combination of already existing natural systems (i.e. KcsA and HCN4 channels) led to the creation of a synthetic model system that has allowed us to display functions that otherwise would have not been easily accessible to study in the wild type channel. Moreover, the use of the pore of the prokaryotic K^+ channel KcsA proved to be advantageous not only because it promoted the production of the chimera in *E. coli*, but especially because it removed the problem of the Voltage Sensor Domain (VSD). This condition allows the visualization of the conformational changes in the active C-linker.

Moreover, KcsA is a well-characterized protein, whose crystal and NMR structures have been solved (Doyle et al., 1998; Chill et al., 2006) and that has been adopted as a model template for the study of the pore domain of HCN channels (Cheng et al., 2007; Bucchi et al, 2013). Thanks to its versatility, the pore of KcsA has been already employed for the engineering of active chimeric channels (Ohndorf and Mackinnon, 2005; McCoy et al., 2014), demonstrating to be a stable and functional building block. Indeed, once attached to another protein domain such as a CNBD, the pore domain of KcsA does not lose its conductivity (Ohndorf and Mackinnon, 2005; McCoy et al., 2014).

Hence, given these evidences, the use of the pore domain of this prokaryotic channel made it possible to investigate the dynamics behind the cAMP-induced interactions between the C-linker/CNBDs of all the four subunits in a tetrameric assembly. This condition should have promoted to reproduce the physiological condition as close as possible to the wild type channel, thus increasing the reliability of the chimera. Indeed, this investigation would not be possible with neither the soluble C-linker/CNBD fragment nor with the wild type channel.

In conclusion, our attempt to increase the knowledge about the cAMP-induced conformational changes in HCN channels was successful because the data obtained are the first structural evidence that show the transition of the cytosolic domain of HCN channels from a dimer of dimers to a 4-fold symmetrical configuration. Thus, these structural data rationalize the previously obtained functional and electrophysiological data that had already hinted towards this dynamical behavior of the C-linker/CNBD domain (Ulens and Siegelbaum, 2003; Zagotta et al., 2003; Lolicato et al., 2011; Kusch et al., 2012; VanSchouwen and Melacini 2018). Particularly, the chimera has

demonstrated to be a versatile model to study dynamical features otherwise inaccessible with the wild type channel. Such a protein could be used as biological tool for potential future drug screenings in order to find small molecules that antagonize the cAMP-induced transition from a 2-fold symmetrical dimer of dimers conformation to a 4-fold symmetrical gating ring. This will result in the possibility to modulate in an HCN-specific manner the channel activity.

Aknowledgments

Escherichia coli C41(DE3) strain was kindly provided by Sir John Walker (University of Cambridge). pGM930 vector, was kindly provided by Prof. Federica Briani (Università degli Studi di Milano). *E. coli* strain LB2003 was kindly provided by Prof. Gerhard Thiel (TU Darmstadt, Germany).

Author Contributions:

conceptualization, B.I., A.S., A.B., O.R., L.B., G.T. and A.M.; methodology, L.B., G.T., and A.M.; investigation, B.I., A.S., A.B., O.R.; writing original draft preparation, B.I. writing review and editing, A.M, visualization, O.R. and A.M.; supervision, A.M.; funding acquisition, G.T. and A.M.

Declaration of Interests:

The Authors declare no conflict of interest

Figure Titles and Legends

Figure 1: K-H4 is a stable and soluble protein in both cAMP-free and -bound state. *(*A) Schematic representation of one of the four subunits that forms the chimeric channel K-H4. This is a chimeric protein made by the fusion of KcsA pore domain (shown in blue) with the C-linker/CNBD of hHCN4 channel (shown in grey). The hexa-histidine Tag at the N- terminus of KcsA pore allows protein purification on a Nichel affinity column. (B) Superimposed chromatograms of the gel filtration of K-H4 purified with 30 mM n-decylmaltoside (DM) in the absence (bue chromatogram) and in the presence of 200 μM cAMP (red chromatogram). In both conditions K-H4 elutes as a monodisperse peak consistent with the molecular weight of the tetramer. (C) Western Blot analysis of K-H4. The protein is able to maintain the tetrameric state even in denaturing conditions as showed by the high molecular mass band (T, 152 kDa) (lane 1). This stability is typical of a proper pore-forming potassium channel. Upon boiling, K-H4

completely converts to its monomeric state (M) migrating at 38 kDa (lane 2). m: Marker (Novex® Sharp Pre-stained Protein Standards, Invitrogen).

Figure 2: K-H4 is a functional channel able to bind cAMP. (A) ITC measurement showing titration of the chimera K-H4ΔN VG with cAMP. The upper graph shows the raw data. Heat is released upon successive injections of 8 µl of cAMP (200 µM) to the chimeric protein (20 µM). The peaks were integrated, normalized to the cAMP concentration, and plotted against the molar ratio of cAMP to KcsA-HCN4 to obtain the binding curve (lower graph). The solid line represents a nonlinear least-squares fit to a single-site binding model (N=2). (B) Dilutions of transformant cultures harboring the vector pGM930SD either empty or containing the chimeric constructs WT or E88A, were spotted on Luria-Bertani plates. Each plate contains 100µg/mL ampicillin and different additional concentrations of KCl. Some plates contained the inducer 0.2% L-arabinose and eventual 5mM BaCl2. Plates were incubated overnight at 37°C.

Figure 3 X-band CW-EPR spectra. (A), (D), (G) and (J) are schematic representations of the cysteine mutants used for DEER experiments. The residues substituted by cysteine and labeled with MTSL are represented as red spheres. The pore domain of the chimeric channel is represented by blue cylinders. The C-linker/CNBD domains are represented by the corresponding parts of the hHCN1 structure (Lee and MacKinnon, 2017, PDB_ID: 5u6o) lacking the pore domain. The "elbow" of the C-linker domain is colored in green (A) and the "shoulder" in yellow (D). The N-terminal helical bundle is highlighted in cyan (G) and the αC-helix of CNBD is highlighted in blue (J). Room temperature X-band CW-EPR spectra (black) and relative simulations (red) for MTSL attached in the positions shown in the left column. The spectra were recorded in the absence (B,E,H,K) and in presence of 200 µM cAMP (C,F,I,L).

Figure 4: Distance distributions of cAMP-free or -bound MTSL-labelled cysteine mutants using Q-band DEER. Left panel: background subtracted Q-band DEER-refocused echo intensity (black lines) plotted versus dipolar evolution time for each spin-labeled position. The spectra were recorded in the absence and in the presence of cAMP. The signals were fitted using model-free Tikhonov regularization (red lines). Right panel: inter-spin distance distributions obtained from

data in the middle panel. Distances explored by the spin labels in the absence of cAMP are shown in red, whereas blue signals were obtained in the presence of cAMP.

Figure 5: The dynamical transition from the 2-fold symmetrical dimer of dimers to 4-fold symmetrical gating ring. (A) Geometrical shapes for explaining the conformational symmetries taken by the probes within the protein in the cAMP-free and -bound state. D1, D2 and D3 represents the main distances between the spin-labelled residues revealed by DEER experiments. (B)- (D) Model showing that both the C-linker and the CNBD shift between a 2-fold symmetrical dimer of dimers conformation to a 4-fold symmetrical gating ring upon cAMP binding. (B) Schematic representation of the chimeric channel. The pore domain is shown as blue parallelepipeds. The C-linker is schematized as green/orange cylinders (B) and as green/orange circles (C). These two colors respectively represent the "elbow" and the "shoulder" of the cytoplasmic domain. The CNBD domain is shown as blue cylinders (B) and as blue circles (D). The ligand cAMP is represented as a red circle. (C) and (D) depict the structural rearrangements induced in the cytoplasmic regulatory domains of the HCN channels by the binding of the cAMP to the CNBD.

Experimental Procedures

Cloning, expression and purification

The PCR product for the chimera K-H4 consisting of the transmembrane pore of KcsA (L16 to G116) and the C-linker/CNBD domain of human HCN4 (Q518 to H723) was obtained by overlapping PCR strategy (Horton et al., 1993). The fragment was cloned into the pET24b(H3C) vector downstream to an N-terminal hexa-histidine tag, using LIC system (Doyle 2005). *Escherichia coli* C41(DE3) strain was used as host organism for the heterologous expression of the chimera. Cells were grown at 37 °C in LB (10 g/L tryptone, 5 g/L yeast extract, 10 g/L NaCl) to an OD600 of 0.8 and induced with 0.1 mM isopropyl-1-thio-β-D-galactopyranoside (IPTG) overnight at 20 °C. Cells were collected by centrifugation and re- suspended in ice-cold lysis buffer (lysis buffer: 100 mM KCl, 20 mM Tris-HCl (pH 7.6) with the addition of 1 mM β-mercaptoethanol, 10 µg/mL DNase, 0.25 mg/mL lysozyme, 100 µM phenylmethylsulfonyl fluoride, 0.1mg/mL trypsin inhibitor, 1 mM benzamidine, 0.1 mM pefablock (Sigma-Aldrich)). For the purification of the protein in the presence of cAMP, 500 µM of the ligand were added. After a short incubation on ice, cells were mechanically lysed with a high-pressure cell

homogenizer and the lysate was cleared by centrifugation. Cell membranes containing the chimeric protein were isolated by centrifugation of the lysate. The pellet containing the membranes was mechanically resuspended with a buffer supplemented with 30 mM n-decyl-β-D-maltopyranoside (DM, Anatrace, Maumee, OH, USA) (resuspension buffer: 100 mM KCl, 20 mM Tris-HCl (pH 7.6), 1 mM β-mercaptoethanol and 30 mM DM). Chimeric membrane proteins were extracted overnight at 4°C. For the purification of the protein in the presence of cAMP, 500 µM of the ligand were added during the extraction process. the histidine-tagged protein was purified using a nickel affinity column (HiTrap IMAC HP (GE Healthcare)). Once the protein had bound to the nickel resin, the column was washed with 10 column volumes of the following buffer: 100 mM KCl, 20 mM Tris-HCl (pH 7.6), 5mM DM and 40 mM imidazole. The chimera was eluted in the latter buffer supplemented with 300 mM imidazole and successively injected to a HiLoad 16/600 Superdex 200 Prep Grade column (GE Healthcare) equilibrated with buffer containing 100 mM KCl, 20 mM Tris-HCl (pH 7.6) and 5 mM DM. All purification steps were performed at 4 °C and monitored using the AKTApurifier UPC 10 fast protein liquid chromatography system (GE Healthcare). For the purification of the cAMP-bound chimera, each of the aforementioned buffers was supplemented with 200 µM cAMP (Sigma-Aldrich).

The final protein concentration was determined by spectrophotometry using the calculated molecular absorbance coefficient ε= 51,465 M-1 cm-1.

Isothermal Titration Calorimetry

For ITC experiments, the chimeric channels and the ligand cAMP were dissolved in elution buffer (100 mM KCl, 20 mM Tris-HCl (pH 7.6) and 5 mM DM). Measurements were carried out at 20°C using MicroCal VP-ITC microcalorimeter (Malvern Panalytical). The volume of the sample cell was 1.4 mL and the reference cell contained water. The chimera K-H4ΔN VG (20 µM) was titrated with cAMP (200 µM) using injection volumes of 8 µL. Calorimetric data were analyzed with MicroCal Origin software (version 7) using equations described for the single-site binding model (Wiseman et. al, 1989).

Complementation assay

For the complementation assay, pGM930 vector was modified. A double stranded DNA fragment codifying for the ribosomal binding site (Shine-Dalgarno (SD) sequence) was inserted into the linearized vector using the Gibson Assembly Cloning Kit (NEB, Ipswich, MA, USA), following the manufacturer's instructions. The created vector called pGM930$_{SD}$ was generated in order to allow the protein synthesis. The cDNA of K-H4 (i.e. WT, wild type) was cloned into a modified

pGM930$_{SD}$, using the Gibson Assembly Cloning Kit (NEB, Ipswich, MA, USA), following the manufacturer's instructions. Subsequently, the mutation E88A was introduced in this construct by site-directed mutagenesis (QuickChange site-directed mutagenesis kit; Agilent Technologies) following the manufacturer's instructions, for the creation of the open mutant E88A.

The complementation assay was performed using *E. coli* strain LB2003, a derivative of the *E. coli* strain K-12, that lacks the three major K^+ uptake systems, Trk (TrkG and TrkH), Kup (TrkD) and Kdp (Epstein and Davies, 1970). Overnight LB2003 cultures transformed with the aforementioned constructs were diluted with LB medium, not supplemented with KCl but containing 100 µg/mL ampicillin, in order to reach an optical density value (OD_{600}) of 0.1. Starting from the latter, serial dilutions were prepared in the aforementioned K^+-free LB medium (i.e. from 10-1 to 10-4). The different serial dilutions were used to perform a drop test on LB agar plates (10 g/L tryptone, 5 g/L yeast extract, 10 g/L NaCl, 20 g/L agar, pH 6.5 adjusted with 10% (v/v) HCl) containing different additional KCl concentrations (i.e. 0 mM, 10 mM and 100 mM), in the presence or absence of 0.2% (w/v) of the inducer L-arabinose and in the presence or absence of 5 mM BaCl2. Plates were incubated overnight at 37°C.

EPR and DEER experiments

The cysteine-free chimeric channel used for EPR experiments was generated starting from the construct K-H4 cloned in pET24b(H3C) vector. The cysteine-free channel was obtained upon substitution of the cysteine residues of the chimera into serine residues by site-directed mutagenesis (QuickChange site-directed mutagenesis kit; Agilent Technologies) following the manufacturer's instructions.

Each single mutant (i.e. E172C, E195C, C202 and R329C) was purified and successively, each different cysteine mutant was concentrated by Amicon Ultra centrifugal filter (MWCO 100 kDa) to approximately 100 µM. The protein solution was incubated with a 10-fold molar excess of DTT at 4°C in order to reduce the cysteine thiol group. After 30 minutes, the reaction mixture was eluted into a PD-10 desalting column to remove the reducing agent using the buffer containing 100 mM KCl, 20 mM Tris-HCl (pH 7.6) and 5mM DM as mobile phase. Successively S- (1-oxyl-2,2,5,5-tetrmethyl-2,5-dihydro-1H-pyrrol-3yl) methylmethanesulfonothioate (MTSL) was added to the solution with 1:10 protein : label molar ratio. The reaction was kept at 4°C under gentle stirring and in absence of light for at least 16 hours. The unreacted spin label was removed using a PD-10 desalting column and the same buffer applied previously. The fractions containing MTSL-labeled chimeric mutants were checked by recording the relative X-band EPR spectrum and, successively, they were pooled together and concentered using by Amicon Ultra centrifugal filter (MWCO 100

kDa). Half of each sample was supplemented with 200 μM cAMP in order to perform the spectroscopic studies in the presence of the ligand.

The final protein concentration was determined by using the calculated molecular absorbance coefficient ($\varepsilon = 51{,}340\ M^{-1}\ cm^{-1}$) and the labelling yield was estimated.

All CW-EPR spectra were recorded with an ELEXYS E580 spectrometer equipped with a Super High Q resonator operating at X-band (9.9 GHz). The following spectroscopic parameters were used to record every spectrum: microwave power= 10 mW; magnetic field amplitude= 1G; field sweep= 150 G; receiver gain= 60 dB. The labelling yield of each sample was calculated from the double integral of CW-EPR spectrum and comparing it with a calibration curve obtained for free MTSL in water solution at different molar concentrations.

All EPR spectra were simulated with SimLabel software (a GUI of Easyspin software) in order to obtain each spectral component and the relative parameters, such as the g-tensor, the hyperfine constants (A) and the correlational times τc.

All DEER experiments on K-H4ΔN VG spin labeled mutants were performed on Elexys E580 spectrometer coupled with the standard resonator EN5107D2 operating at Q-band (34 GHz). The spectrometer was equipped with an Oxford helium temperature regulation unit and the relative experiments were carried out at cryogenic temperatures (i.e. -200°C). Each spin labeled sample was prepared as described above with a final concentration of ~100 μM, in the absence or in the presence of 200 μM cAMP. Finally, glycerol (10% v/v) was added as cryoprotectant.

DEER experiments were performed using the four-pulse dead-time free DEER sequence with an inversion pulse length of 40 ns. The interpulse t1 was set to 200 ns and the t2 was adjusted basing on the phase memory constant time recorded for each sample. The pump ELDOR pulse (40 ns) was positioned at the center of the MTSL absorption spectrum and the frequency difference between the pump and the observer pulses was 56 MHz. The DEER traces were accumulated at least 14 hours in order to minimize the signal to noise ratio.

DeerAnalysis 2016 software was used to realize the correction of background echo decay and consequently to obtain the inter-spin distances involving the Tikhonov regularization. The regularization factor (α) was used with a value equal to 100, according to L-curve criteria.

Supplemental Information Titles and Legends

Supplementary figure 1: X-band CW-EPR spectra and relative simulations. X-band CW-EPR spectra (black) and relative simulations (red) for E172C-MTSL, E195C-MTSL, C202-MTSL and R329C-MTSL in absence (top panel) and in presence (bottom panel) of cAMP. For each

spectra the relative components constituting the EPR signal are listed below. The simulations were performed after baseline correction usinf SimLabel software (GUI of EasySpin).

Supplementary table 1: Percentage of the components of the X-band CW-EPR spectra and relative correlational time values. Components percentage and relative correlational time values (τ_C) calculated through the simulation, using SimLabel software, of the experimental CW-EPR spectra of K-H4ΔN VG MTSL labeled mutants. Error of ± 1.2% and ± 0.07 ns where estimated respectively for component percentage and correlational times.

Supplementary table 2: **Q-band DEER recorded values.** Values of modulation depth, peak maxima (r_{MAX}), average distance (<r>) and relative standard deviation (σ) through DEERAnalysis2016 software using Tikhonov regularization.

References

Altomare, C., Terragni, B., Brioschi, C., Milanesi, R., Pagliuca, C., Viscomi, C., Moroni, A., Baruscotti, M., DiFrancesco, D., 2003. Heteromeric HCN1-HCN4 channels: a comparison with native pacemaker channels from the rabbit sinoatrial node. J Physiol 549, 347–359. https://doi.org/10.1113/jphysiol.2002.027698

Bucchi, A., Baruscotti, M., Nardini, M., Barbuti, A., Micheloni, S., Bolognesi, M., DiFrancesco, D., 2013. Identification of the molecular site of ivabradine binding to HCN4 channels. PLoS One 8, e53132–e53132. https://doi.org/10.1371/journal.pone.0053132

Buurman, E.T., Kim, K.-T., Epstein, W., 1995. Genetic Evidence for Two Sequentially Occupied K+ Binding Sites in the Kdp Transport ATPase. Journal of Biological Chemistry 270, 6678–6685. https://doi.org/10.1074/jbc.270.12.6678

Chen, S., Wang, J. and Siegelbaum, S.A., 2001. Properties of hyperpolarization- activated pacemaker current defined by coassembly of HCN1 and HCN2 subunits and basal modulation by cyclic nucleotide. J Gen Physiol 117:491–504.

Chill, J.H., Louis, J.M., Miller, C., Bax, A., 2006. NMR study of the tetrameric KcsA potassium channel in detergent micelles. Protein Sci 15, 684–698. https://doi.org/10.1110/ps.051954706

599 Cordero-Morales, J.F., Jogini, V., Lewis, A., Vásquez, V., Cortes, D.M., Roux, B., Perozo, E.,
600 2007. Molecular driving forces determining potassium channel slow inactivation. Nature
601 Structural & Molecular Biology 14, 1062–1069. https://doi.org/10.1038/nsmb1309
602
603 Craven, K.B., Olivier, N.B., Zagotta, W.N., 2008. C-terminal Movement during Gating in Cyclic
604 Nucleotide-modulated Channels. Journal of Biological Chemistry 283, 14728–14738.
605 https://doi.org/10.1074/jbc.M710463200
606
607 DeBerg, H.A., Bankston, J.R., Rosenbaum, J.C., Brzovic, P.S., Zagotta, W.N., Stoll, S., 2015.
608 Structural mechanism for the regulation of HCN ion channels by the accessory protein TRIP8b.
609 Structure 23, 734–744. https://doi.org/10.1016/j.str.2015.02.007
610
611 DiFrancesco, D. and Tortora, P., 1991. Direct activation of cardiac pacemaker channels by
612 intracellular cyclic AMP. Nature 351:145–147.
613
614 Doyle, D.A., Cabral, J.M., Pfuetzner, R.A., Kuo, A., Gulbis, J.M., Cohen, S.L., Chait, B.T.,
615 MacKinnon, R., 1998. The Structure of the Potassium Channel: Molecular Basis of K^+
616 Conduction and Selectivity. Science 280, 69. https://doi.org/10.1126/science.280.5360.69
617
618 Emery, E.C., Young, G.T., McNaughton, P.A., 2012. HCN2 ion channels: an emerging role as
619 the pacemakers of pain. Trends in Pharmacological Sciences 33, 456–463.
620 https://doi.org/10.1016/j.tips.2012.04.004
621
622 Epstein, W., Davies, M., 1970. Potassium-Dependant Mutants of Escherichia coli K-12. J.
623 Bacteriol. 101, 836.
624
625 Gauss, R., Seifert, R., Kaupp, U.B., 1998. Molecular identification of a hyperpolarization-
626 activated channel in sea urchin sperm. Nature 393, 583–587. https://doi.org/10.1038/31248
627
628 Higgins, M.K., Weitz, D., Warne, T., Schertler, G.F.X., Kaupp, U.B., 2002. Molecular
629 architecture of a retinal cGMP-gated channel: the arrangement of the cytoplasmic domains.
630 EMBO J 21, 2087–2094. https://doi.org/10.1093/emboj/21.9.2087
631

Horton, R.M., Ho, S.N., Pullen, J.K., Hunt, H.D., Cai, Z., Pease, L.R., 1993. [17]Gene splicing by overlap extension, in: Methods in Enzymology. Academic Press, pp. 270–279. https://doi.org/10.1016/0076-6879(93)17067-F

Kusch, J., Thon, S., Schulz, E., Biskup, C., Nache, V., Zimmer, T., Seifert, R., Schwede, F., Benndorf, K., 2012. How subunits cooperate in cAMP-induced activation of homotetrameric HCN2 channels. Nature Chemical Biology 8, 162.

Lee, C.-H., MacKinnon, R., 2017. Structures of the Human HCN1 Hyperpolarization-Activated Channel. Cell 168, 111-120.e11. https://doi.org/10.1016/j.cell.2016.12.023

Lolicato, M., Nardini, M., Gazzarrini, S., Möller, S., Bertinetti, D., Herberg, F.W., Bolognesi, M., Martin, H., Fasolini, M., Bertrand, J.A., Arrigoni, C., Thiel, G., Moroni, A., 2011. Tetramerization Dynamics of C-terminal Domain Underlies Isoform-specific cAMP Gating in Hyperpolarization-activated Cyclic Nucleotide-gated Channels. Journal of Biological Chemistry 286, 44811–44820. https://doi.org/10.1074/jbc.M111.297606

Ludwig, A., Zong, X., Jeglitsch, M., Hofmann, F., Biel, M., 1998. A family of hyperpolarization-activated mammalian cation channels. Nature 393, 587–591. https://doi.org/10.1038/31255

McCoy, J.G., Rusinova, R., Kim, D.M., Kowal, J., Banerjee, S., Jaramillo Cartagena, A., Thompson, A.N., Kolmakova-Partensky, L., Stahlberg, H., Andersen, O.S., Nimigean, C.M., 2014. A KcsA/MloK1 chimeric ion channel has lipid-dependent ligand-binding energetics. J Biol Chem 289, 9535–9546. https://doi.org/10.1074/jbc.M113.543389

Ohndorf, U.-M., MacKinnon, R., 2005. Construction of a Cyclic Nucleotide-gated KcsA K+ Channel. Journal of Molecular Biology 350, 857–865. https://doi.org/10.1016/j.jmb.2005.05.050

Porro, A., Saponaro, A., Gasparri, F., Bauer, D., Gross, C., Pisoni, M., Abbandonato, G., Hamacher, K., Santoro, B., Thiel, G., Moroni, A., Submitted to eLIFE. The HCN domain couples voltage gating and cAMP response in Hyperpolarization-activated Cyclic Nucleotide-gated channels.

Puljung, M.C., DeBerg, H.A., Zagotta, W.N., Stoll, S., 2014. Double electron–electron resonance reveals cAMP-induced conformational change in HCN channels. Proc Natl Acad Sci USA 111, 9816. https://doi.org/10.1073/pnas.1405371111

Robinson, R.B., Siegelbaum, S.A., 2003. Hyperpolarization-Activated Cation Currents: From Molecules to Physiological Function. Annu. Rev. Physiol. 65, 453–480. https://doi.org/10.1146/annurev.physiol.65.092101.142734

Santoro, B., Grant, S.G., Bartsch, D., Kandel, E.R., 1997. Interactive cloning with the SH3 domain of N-src identifies a new brain specific ion channel protein, with homology to eag and cyclic nucleotide-gated channels. Proc Natl Acad Sci U S A 94, 14815–14820. https://doi.org/10.1073/pnas.94.26.14815

Santoro, B., Liu, D.T., Yao, H., Bartsch, D., Kandel, E.R., Siegelbaum, S.A., Tibbs, G.R., 1998. Identification of a Gene Encoding a Hyperpolarization-Activated Pacemaker Channel of Brain. Cell 93, 717–729. https://doi.org/10.1016/S0092-8674(00)81434-8

Saponaro, A., Pauleta, S.R., Cantini, F., Matzapetakis, M., Hammann, C., Donadoni, C., Hu, L., Thiel, G., Banci, L., Santoro, B., Moroni, A., 2014. Structural basis for the mutual antagonism of cAMP and TRIP8b in regulating HCN channel function. Proc Natl Acad Sci U S A 111, 14577–14582. https://doi.org/10.1073/pnas.1410389111

Taraska, J.W., Puljung, M.C., Olivier, N.B., Flynn, G. E., and Zagotta, W. N., 2009. Mapping the structure and conformational movements of proteins with transition metal ion FRET. Nat Methods 6:532–537.

Ulens, C., Siegelbaum, S.A., 2003. Regulation of Hyperpolarization-Activated HCN Channels by cAMP through a Gating Switch in Binding Domain Symmetry. Neuron 40, 959–970. https://doi.org/10.1016/S0896-6273(03)00753-0

VanSchouwen, B., Melacini, G., 2018. Role of Dimers in the cAMP-Dependent Activation of Hyperpolarization-Activated Cyclic-Nucleotide-Modulated (HCN) Ion Channels. The Journal of Physical Chemistry B 122, 2177–2190. https://doi.org/DOI: 10.1021/acs.jpcb.7b10125

Wainger BJ, DeGennaro M, Santoro B, Siegelbaum SA, and Tibbs GR (2001) Mo- lecular mechanism of cAMP modulation of HCN pacemaker channels. Nature 411: 805–810.

Wahl-Schott, C., Biel, M., 2008. HCN channels: Structure, cellular regulation and physiological function. Cellular and Molecular Life Sciences 66, 470. https://doi.org/10.1007/s00018-008-8525-0

Wiseman, T., Williston, S., Brandts, J.F., Lin, L.-N., 1989. Rapid measurement of binding constants and heats of binding using a new titration calorimeter. Analytical Biochemistry 179, 131–137. https://doi.org/10.1016/0003-2697(89)90213-3

Xu, X., Vysotskaya, Z.V., Liu, Q., Zhou, L., 2010. Structural Basis for the cAMP-dependent Gating in the Human HCN4 Channel. Journal of Biological Chemistry 285, 37082–37091. https://doi.org/10.1074/jbc.M110.152033

Zagotta, W.N., Olivier, N.B., Black, K.D., Young, E.C., Olson, R., Gouaux, E., 2003. Structural basis for modulation and agonist specificity of HCN pacemaker channels. Nature 425, 200–205. https://doi.org/10.1038/nature01922

Figure 1

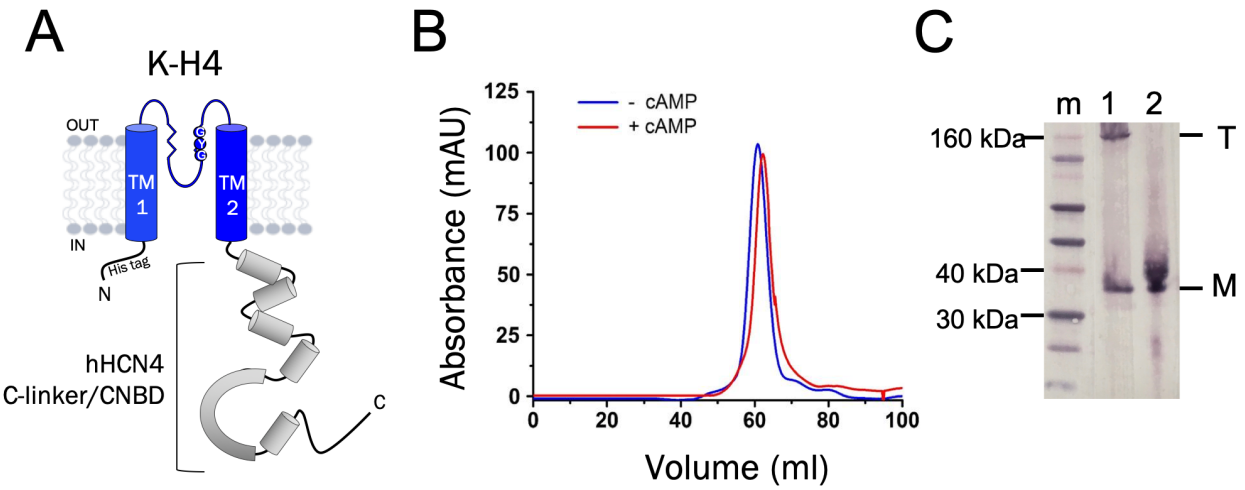
A
K-H4
OUT
TM 1
TM 2
IN
His tag
N
hHCN4
C-linker/CNBD
C
B
- cAMP
+ cAMP
Absorbance (mAU)
125
100
75
50
25
0
0
20
40
60
80
100
Volume (ml)
C
m 1 2
160 kDa
40 kDa
30 kDa
T
M

Figure 2

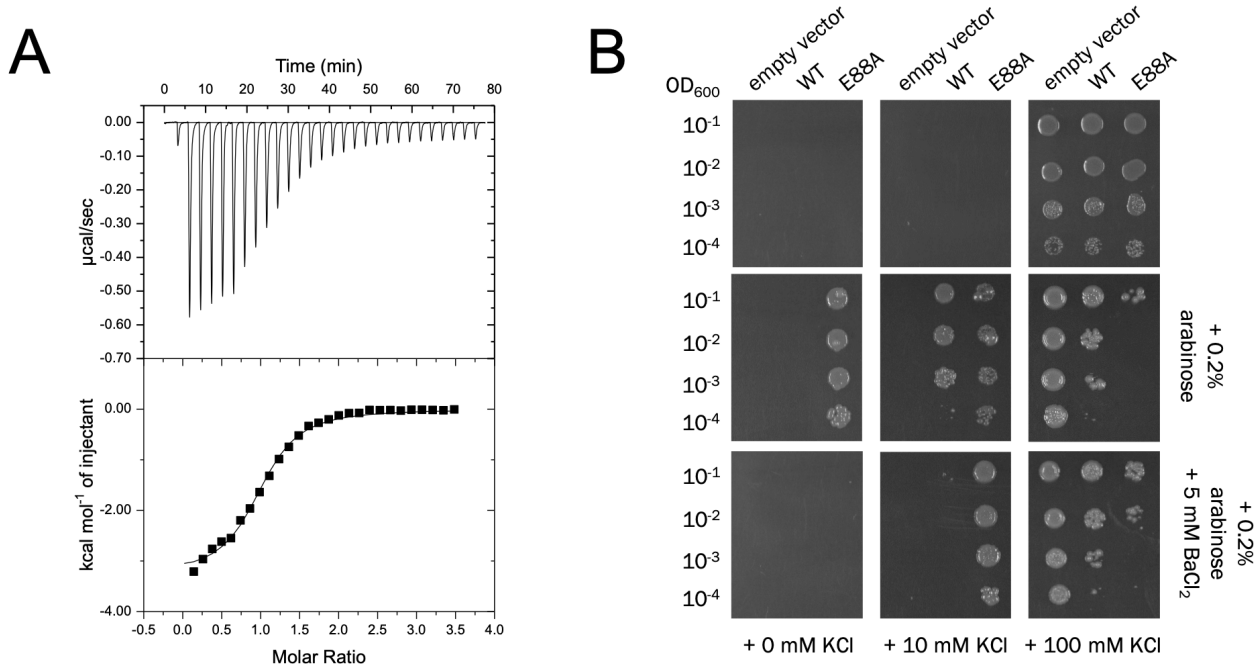
A
Time (min)
0 10 20 30 40 50 60 70 80
µcal/sec
0.00
-0.10
-0.20
-0.30
-0.40
-0.50
-0.60
-0.70
kcal mol-1 of injectant
0.00
-2.00
-4.00
-0.5 0.0 0.5 1.0 1.5 2.0 2.5 3.0 3.5 4.0
Molar Ratio
B
OD600
empty vector
WT
E88A
10-1
10-2
10-3
10-4
+ 0.2% arabinose
+ 0.2% arabinose + 5 mM BaCl2
+ 0 mM KCl
+ 10 mM KCl
+ 100 mM KCl

Figure 3

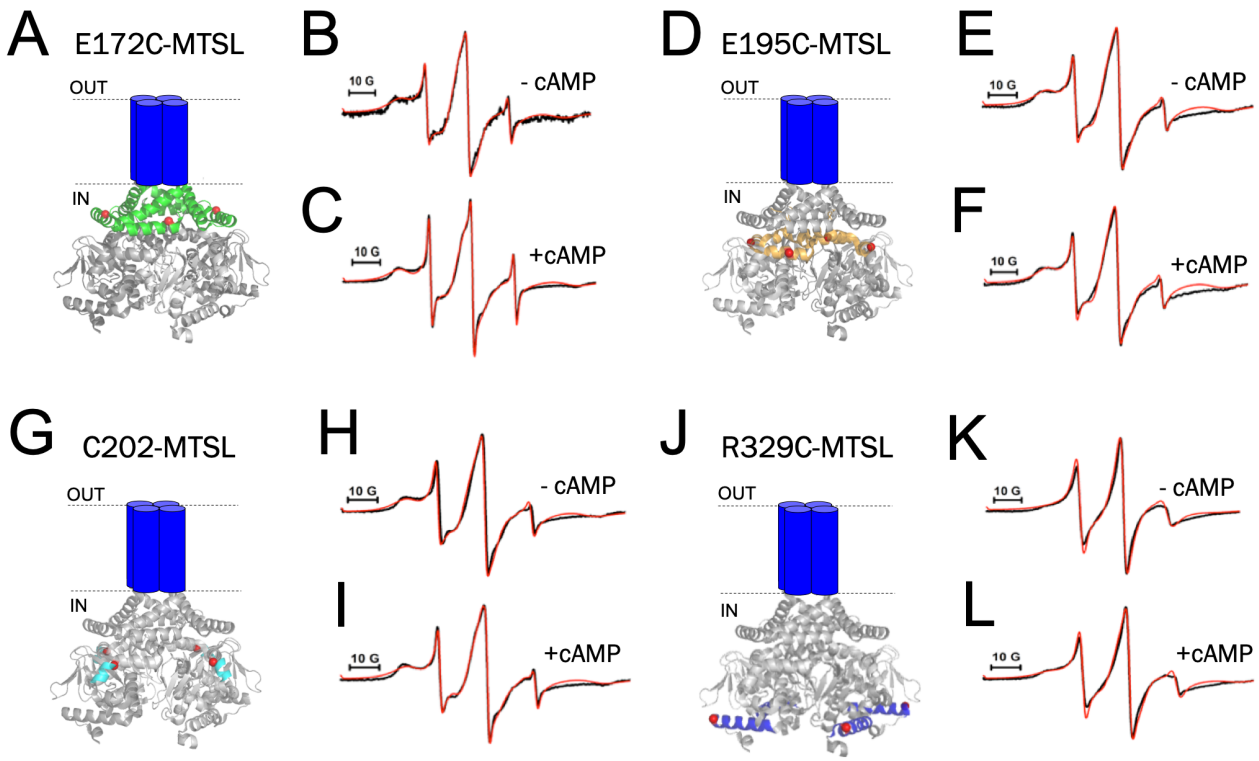
A
E172C-MTSL
OUT
IN
B
10 G
- cAMP
C
10 G
+cAMP
D
E195C-MTSL
OUT
IN
E
10 G
- cAMP
F
10 G
+cAMP
G
C202-MTSL
OUT
IN
H
10 G
- cAMP
I
10 G
+cAMP
J
R329C-MTSL
OUT
IN
K
10 G
- cAMP
L
10 G
+cAMP

Figure 4

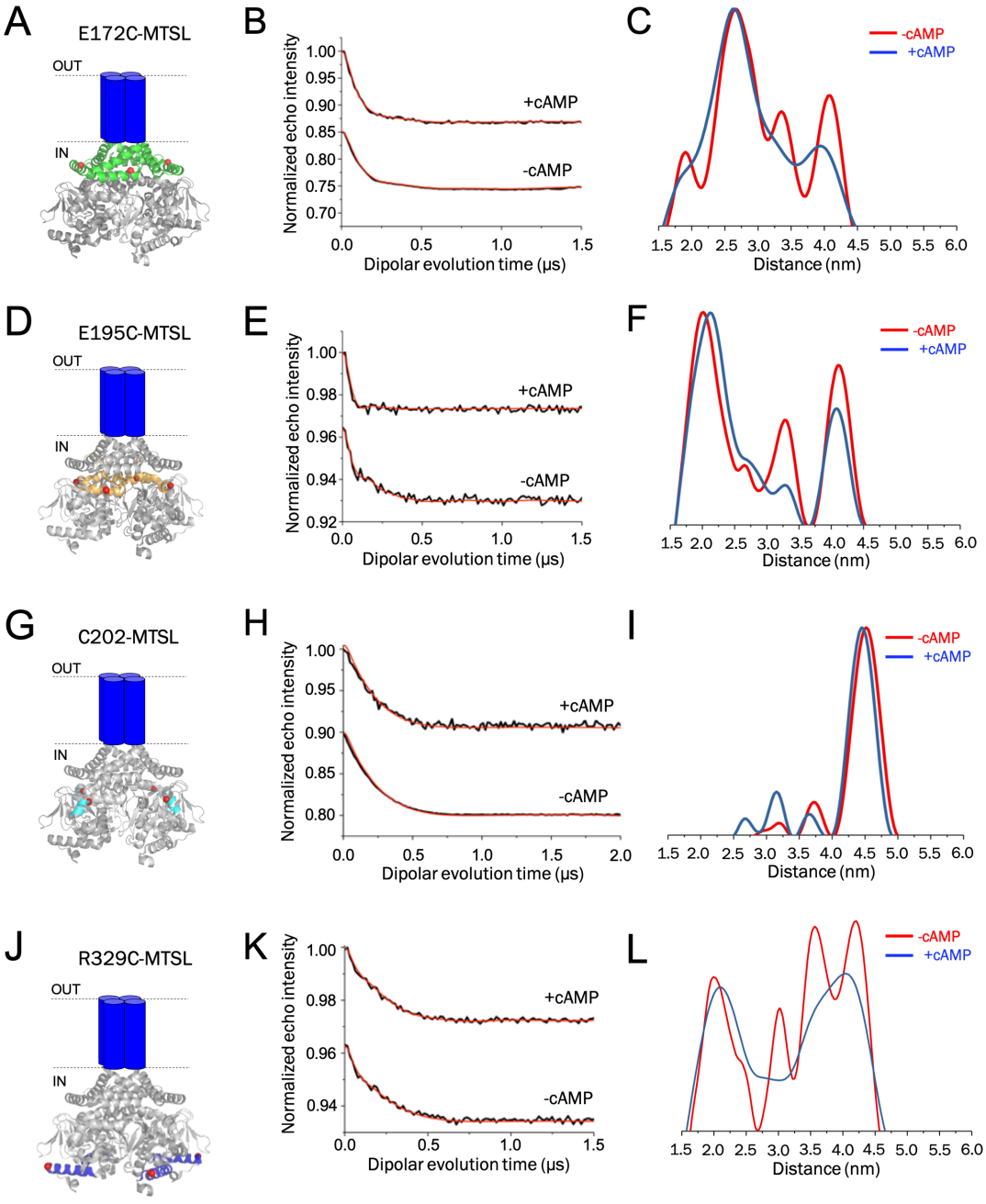
A
E172C-MTSL
OUT
IN
B
Normalized echo intensity
+cAMP
-cAMP
Dipolar evolution time (μs)
C
-cAMP
+cAMP
Distance (nm)
D
E195C-MTSL
OUT
IN
E
Normalized echo intensity
+cAMP
-cAMP
Dipolar evolution time (μs)
F
-cAMP
+cAMP
Distance (nm)
G
C202-MTSL
OUT
IN
H
Normalized echo intensity
+cAMP
-cAMP
Dipolar evolution time (μs)
I
-cAMP
+cAMP
Distance (nm)
J
R329C-MTSL
OUT
IN
K
Normalized echo intensity
+cAMP
-cAMP
Dipolar evolution time (μs)
L
-cAMP
+cAMP
Distance (nm)

Figure 5

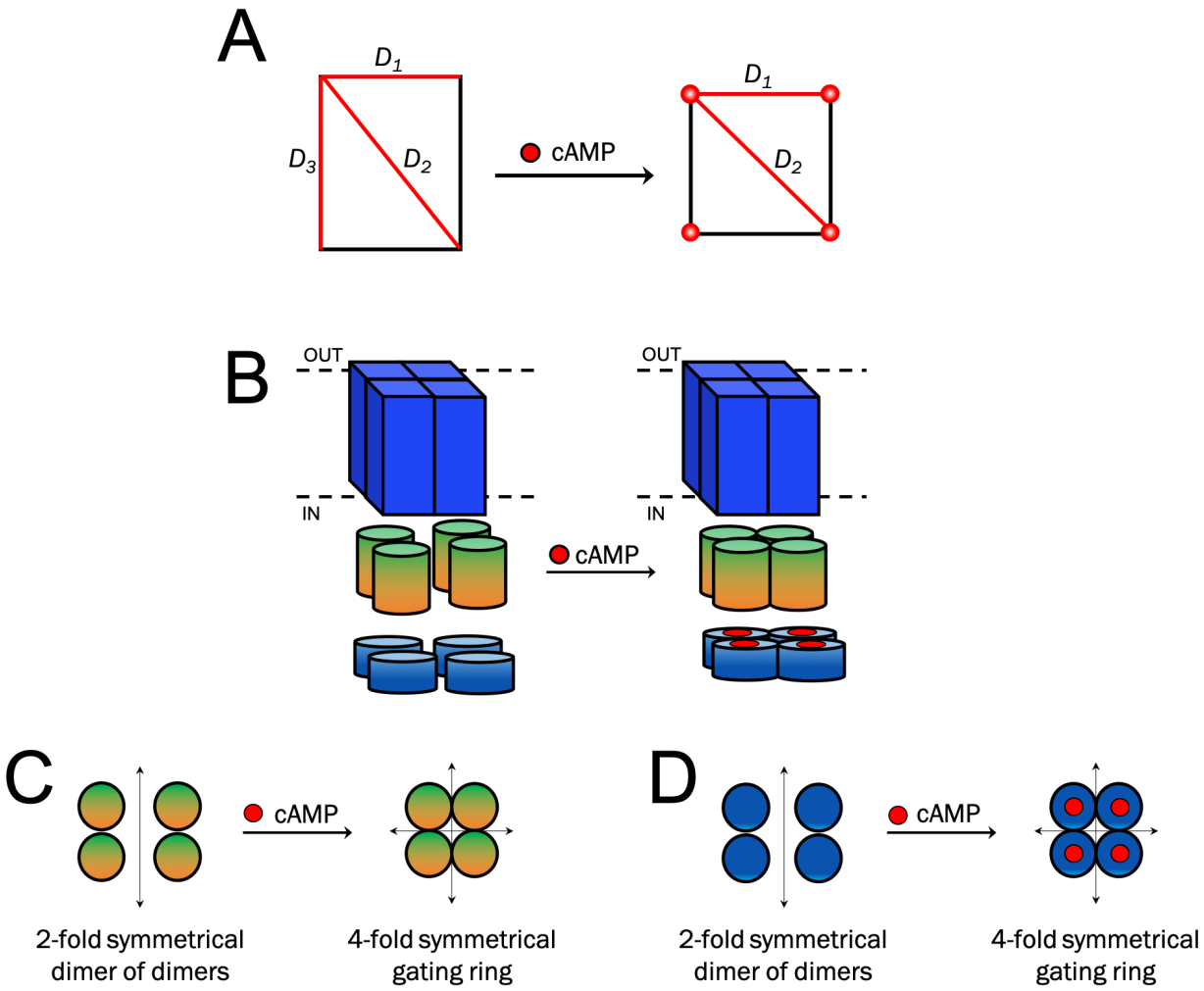
A
D1
D3
D2
cAMP
D1
D2
B
OUT
IN
cAMP
OUT
IN
C
cAMP
2-fold symmetrical
dimer of dimers
4-fold symmetrical
gating ring
D
cAMP
2-fold symmetrical
dimer of dimers
4-fold symmetrical
gating ring

Supplementary figure 1

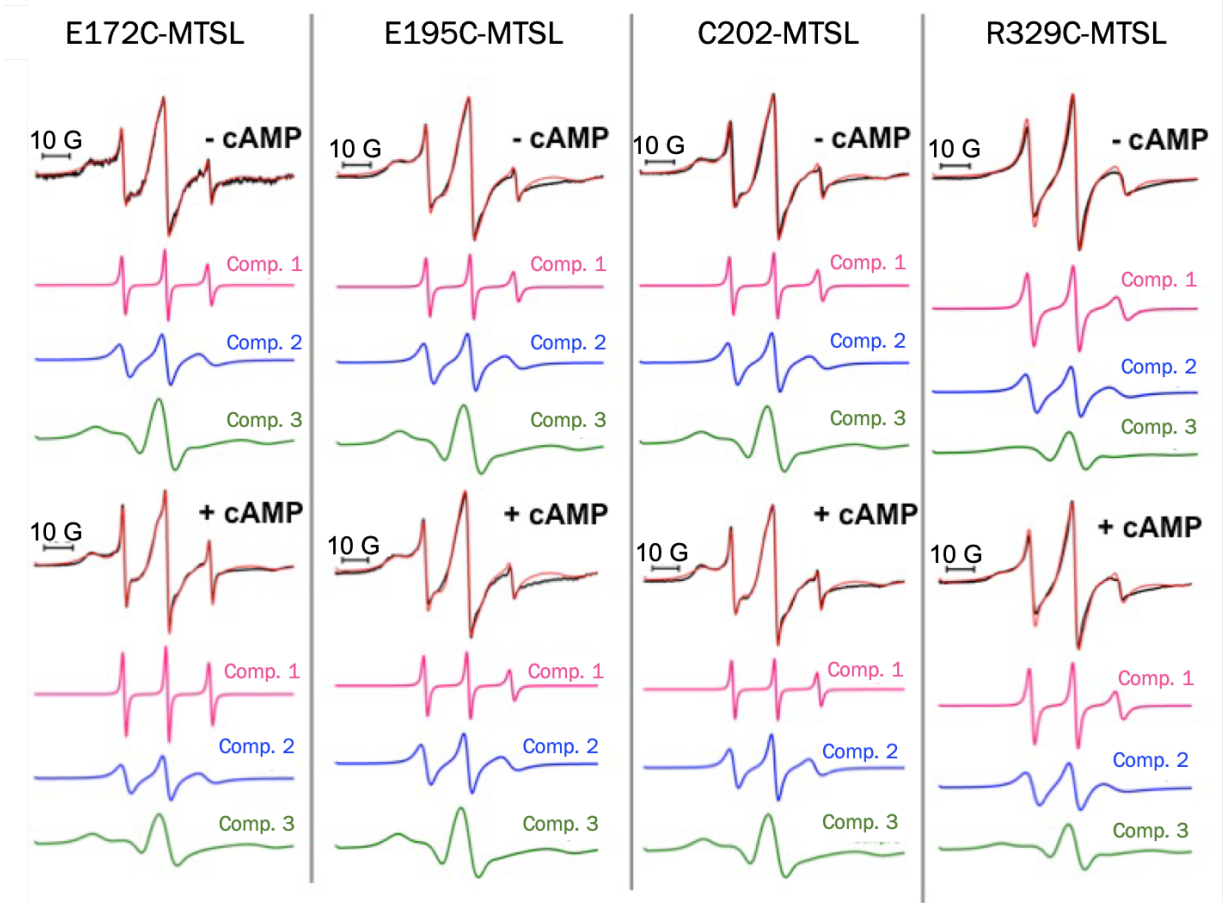

Supplementary table 1

Sample	Comp. 1 (%)	τ_c 1 (ns)	Comp. 2 (%)	τ_c 2 (ns)	Comp. 3 (%)	τ_c 3 (ns)
E172-MTSL	3.0	0.14	18.0	1.30	79.0	5.40
+ cAMP	4.0	0.15	19.0	1.31	79.0	5.90
E195-MTSL	3.0	0.18	19.0	1.25	78.0	5.61
+ cAMP	2.0	0.18	17.0	1.25	81.0	5.61
C202-MTSL	4.0	0.18	20.0	1.23	76	5.61
+ cAMP	2.5	0.12	16.5	1.00	81.0	5.56
R329-MTSL	17.0	0.73	28.0	1.60	55.0	3.67
+ cAMP	10.0	0.51	28.0	1.60	62.0	4.05

Supplementary table 2

Sample	Modulation depth (%)	r_{MAX} (nm)	<r> (nm)	σ (nm)
E172-MTSL	10.4	2.65	3.16	0.58
+ cAMP	13.2	2.64	3.08	0.59
E195-MTSL	4.0	1.99	3.24	0.71
+ cAMP	4.1	2.11	2.95	0.70
C202-MTSL	7.4	4.52	4.74	0.65
+ cAMP	3.8	4.48	4.52	0.72
R329-MTSL	2.4	4.18	3.90	0.81
+ cAMP	2.1	4.02	3.52	0.82